5-2018

New Broadband Common-Mode Filtering Structures Embedded in Differential Coplanar Waveguides for DC to 40 GHz Signal Transmission

Yujie He

New Broadband Common-Mode Filtering Structures Embedded in Differential Coplanar Waveguides for DC to 40 GHz Signal Transmission

A Thesis

Submitted to the Faculty

of

Rose-Hulman Institute of Technology

by

Yujie He

In Partial Fulfillment of the Requirements for the Degree

of

Master of Science in Electrical Engineering

May 2018

ROSE-HULMAN INSTITUTE OF TECHNOLOGY

Final Examination Report

Yujie He — Name

Electrical Engineering — Graduate Major

Thesis Title: New Broadband Common-Mode Filtering Structures Embedded in Differential Coplanar Waveguides for DC to 40 GHz Signal Transmission

DATE OF EXAM: April 18, 2018

EXAMINATION COMMITTEE:

Thesis Advisory Committee		Department
Thesis Advisor:	Edward Wheeler	ECE
	JianJian Song	ECE
	Scott Kirkpatrick	PHOE
	Michael Cracraft	

PASSED X **FAILED** _____

ABSTRACT

He, Yujie

M.S.E.E.

Rose-Hulman Institute of Technology

May 2018

New Broadband Common-Mode Filtering Structures Embedded in Differential Coplanar Waveguides for DC to 40 GHz Signal Transmission

Thesis Advisor: Dr. Edward Wheeler

Coplanar waveguides (CPWs) provide effective transmission with low dispersion into the millimeter-wave frequencies. For high-speed signaling, differential transmission lines display an enhanced immunity to outside interference and are less likely to interfere with other signals, when compared to single-ended transmission lines. Common-mode (CM) conversion from the differential-mode (DM) signal energy can produce unintentional radiation as well as degraded board-level electromagnetic compatibility (EMC) and signal integrity SI environments. Due to the negative effects of CM signals, filtering structures are often used to suppress the propagation of these signals.

The filtering structures introduced in this project all implement the same CM filter design concept. While the concept itself is not new, the physical design of the filter combined with broadside differential CPWs had not been explored at the time of writing this thesis. The CM filtering structures described herein demonstrated to offer broadband CM filtering together with effective DM transmission into millimeter-wave frequencies.

Keywords: Coplanar waveguide, common-mode filtering, electromagnetic compatibility, signal and power integrity

DEDICATION

To my parents. Thank you for your support, love, and understanding.

I am sorry I have not gone home for two years.

ACKNOWLEDGEMENTS

I would like to express my sincere gratitude to my advisor, Dr. Edward Wheeler. His knowledge, patience, guidance, and generosity made this project possible. His encouragements have also made this journey incredible for me.

I would like to thank Dr. Michael Cracraft from IBM, Poughkeepsie, NY. He is the bridge connecting the academic world and the industry world. His expertise helped me overcome many obstacles during this research.

My thanks also go to Dr. Jianjian Song and Dr. Scott Kirkpatrick. Their comments and questions broadened my views from various perspectives.

I would like to offer my special thanks to Joe Faia. He always offered me helpful suggestions and brilliant insights. He has inspired me on many occasions. It is a delight to work with him.

I would like to thank Jack Shrader, Mark Crosby, and Gary Meyer, for their patience and technical support. I am very grateful that they are always there whenever I make a mistake.

I would also like to show my gratitude to Robin J Andrews and her family for treating me like a family member. Life in another country would not be this enjoyable without her family's help.

Last but not the least, I would like to express my appreciation to my family for their support throughout my life.

TABLE OF CONTENTS

LIST OF FIGURES

LIST OF TABLES

LIST OF ABBREVIATIONS

CM – Common Mode

CPW – Coplanar Waveguide

DM – Differential Mode

EMC – Electromagnetic Compatibility

GCPW – Grounded Coplanar Waveguide

GND – Ground

IC – Integrated Circuit

MW – Microwave

PCB – Printed Circuit Board

RF – Radio Frequency

SI – Signal Integrity

LIST OF SYMBOLS

English Symbols

A	Ampere
C	Coulomb
C	Capacitance
Hz	Hertz
V	Voltage
m	Meter
Wb	Weber
Z	Impedance

Greek Symbols

ρ	Electric charge density, in C/m^3.
ω	Frequency, in rad.
ε	Permittivity

Mathematical Symbols

$\bar{B}$	Magnetic flux density vector, in Wb/m^2.
$\bar{D}$	Electric flux density vector, in C/m^2.
$\bar{E}$	Electric field vector, in V/m.
$\bar{H}$	Magnetic field vector, in A/m.
$\bar{J}$	Electric current density vector, in A/m^2.
$\bar{M}$	Magnetic current density vector, in V/ m^2.

GLOSSARY

Common Mode Signal	The half-sum of the differential voltage pair in a differential signaling system.
Common Mode Impedance	Impedance between the differential pair when the transmission line pair is driven by a common source.
Differential Signaling	A signaling method that transmits data and information using a pair of complementary signals, each in its own transmission line. The receiving signal is also called differential mode signal.
Differential Mode Signal	The difference of the differential voltage pair in a differential signaling system.
Differential Mode Impedance	Impedance between the differential pair when the transmission line pair is driven by a differential source.
Even Mode Impedance	Impedance of a single-ended transmission line when the two lines in a differential pair are driven by a common source.
Odd mode Impedance	Impedance of a single-ended transmission line when the two lines in a differential pair are driven by a differential source.

1. INTRODUCTION

The term microwave (MW) is used for electromagnetic waves with frequencies that range from 300 MHz to 300 GHz, which correspond to wavelengths from 1 m to 1 mm in free space. Microwave technology was introduced to commercial communication after its success during World War II. Early in the history of wireless communication, it was found that microwaves cannot be reflected by the ionosphere but are capable of carrying much more information that the lower frequency signals that can be reflected [1]. Nowadays, microwaves are widely used in both wired and wireless systems, in both printed circuit boards (PCB) and integrated circuits (IC).

With each new generation of semiconductor technology that brings more transistors onto chips, computing devices are becoming progressively more powerful. In order to keep up with the increasing speed of computing performance and volume of data transmission, signal communication speed has also been increasing. At lower frequency, most systems can transmit signals with sufficient fidelity over a short range. As communication systems require faster data transmission and higher signal frequencies, the transmitted signals become increasingly vulnerable to attenuation, distortion, noise, and loss. Signal integrity (SI) becomes one of the most concerned topics in the microwave frequency communication industry.

Signal integrity, as well as electromagnetic compatibility (EMC), are properties that play vital roles in communication engineering. SI represents the quality of a transmitted electrical signal, while EMC represents how well the structure can work with other structures as unintentional and unwanted generation, emission, and coupling of electromagnetic energy cause interference. At high frequencies, transmission line effects and impedance mismatch can have negative effects on SI. Ringing, reflections, and ground bounce caused by these effects can hamper the response of the transmitted signal and damage the integrity. Therefore, minimizing these effects is one of the primary goals of SI engineering, particularly with high-speed designs. On the other hand, the study of EMC pursues the prevention of the generated electromagnetic energy by the structure, since the emitted electromagnetic energy can couple to other structures, causing malfunctions and breakdowns of the neighboring designs.

Traditional single-ended signaling is the simplest method to transmit signals. It utilizes two conducting wires to guide the input electric energy. One is the signal trace carrying a varying voltage to transfer data, and the other is usually tied to ground (GND) serving as the reference. The receiving circuit responds to the difference between the transmitted voltage and the reference voltage. Figure 1.1 (a) shows a single-ended signaling scheme implemented on a PCB.

Radiations and electric and magnetic couplings are two major reasons causing the degradation of SI and EMC performances. Any electrically charged structure will emit electromagnetic radiation, and any charged structure will have coupling to its neighboring structure. Assuming

two single-ended wires each carry a signal, as the frequency goes up, each single-ended current will interfere with neighboring circuits due to the increasing electrical and magnetic coupling. Therefore, single-ended systems suffer from poor noise immunity at high frequencies.

Differential signaling is frequently used as an alternative method to transfer data. It typically has a higher noise immunity comparing to single-ended signaling. A differential system, as illustrated in Fig 1.1 (b), consists of a pair of conductors that carries two complementary signals sent from a differential source. The transmitted and received signal of a differential system is the electrical difference between the two conducting traces that carry a pair of complementary signals, which is referred to as a differential mode (DM) signal. The benefits of using differential circuits are that they can theoretically provide much higher noise immunity than single-ended systems. The single-ended signaling and differential signaling differ in how the noise signals affect the received signal. Assuming random noises, V_N, occur along both types of signaling paths. V_N in the single-ended system simply add to the signal voltage and so will be received at the receiving end. On the other hand, V_N in the differential signaling system is common to both traces and can be subtracted away at output. The complementary signals in a differential signaling system result in much lower radiations and couplings. Due to this inherent higher noise immunity, differential signaling is much less of a threat to its neighboring circuits and compatible with lower voltage and/or current signals which can help reduce power levels.

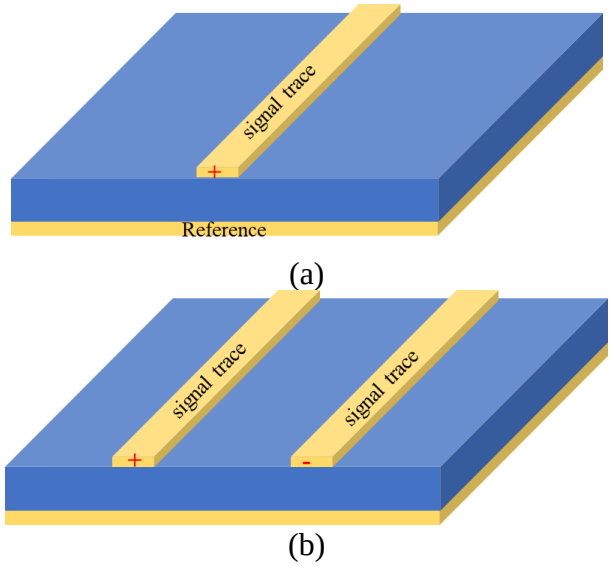

Figure 1.1 Perspective view of (a). a single-ended signaling path; (b). a differential signaling path on a printed circuit board.

However, a design challenge is introduced when using differential signaling. To maintain an ideal differential communication link, both signal traces must have the same electrical lengths and coupling to reference. Unfortunately, this ideal circuit is physically impossible to fabricate. Length differences (skew) is introduced through signal routing paths (e.g., any time the signal is routed around a corner resulting in one trace being electrically longer than the other). Unequal coupling can be introduced when one trace is closer to neighboring circuits than the other (e.g., if the neighboring circuit is on the same layer of metallization, the one trace will necessarily be closer than the other, resulting in the unequal electric field or capacitive coupling). Both skew and unequal coupling in a differential signaling path can result in common-mode (CM) conversion, in which a portion of the DM signal energy is converted to form an unwanted CM signal energy. CM signals share the same magnitude and polarity. Unlike DM signals, CM signals do not carry any important data and will add together instead of canceling each other out

at the receiving end, creating unwanted noise, radiation, and attenuate signals. These CM signals are inevitable in any real circuits. Therefore, the design of CM filtering structures that can suppress the propagation of CM signals while allowing DM signals to propagate is an important part of SI engineering, especially in high-speed and high-performance systems.

Three commonly used transmission line designs for differential signaling are microstrip, stripline, and coplanar waveguide (CPW) structure. A differential microstrip has two conductors on a dielectric substrate and a metallization plane on the other side of the substrate as a reference. For a symmetric stripline structure, which is more widely used than an asymmetric stripline, two conductors are placed in a dielectric with two reference layers placed applied above and below the substrate. The differential transmission line using broadside coupled CPWs consists of two sides, each with a center conducting wire separating two traces acting as a reference. Cross-sections of these three structures are shown in Fig 1.2.

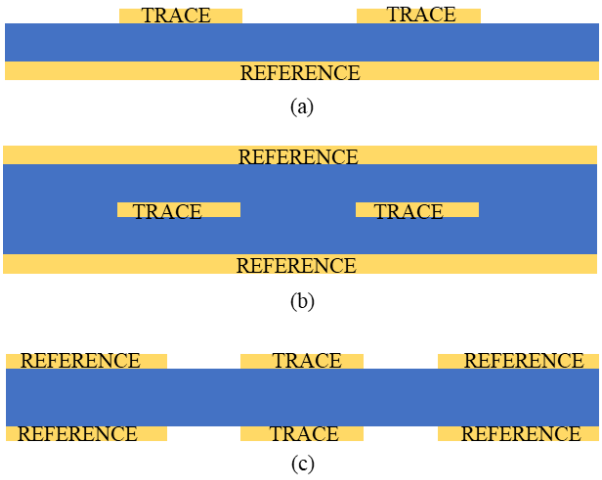

Figure 1.2 Cross-sections of (a). microstrip differential structure, (b). stripline differential structure, and (c). coplanar waveguide differential structure.

Although not much work has been done in CM filtering for CPW differential signaling, many research reports have shown the effective CM filtering using complementary split ring resonator (CSRR) or composite right-/left-handed (CRLH) filtering structures in microstrip transmission lines [2]-[4].

On the other hand, previous works have demonstrated the potential of CPW structures for high-speed signal systems. [5] and [6] show effective characteristics of single-ended CPW transmission lines from DC up to 0.5 THz. When this project first started exploring the possibility of CM filtering using CPW structures (as discussed in section 4.1), simulated DM transmission result seemed too perfect and ideal due to not many related works being found. The publication of [5] and [6] encourages us to keep investigating the potential of CM filtering in CPW transmission lines.

This thesis investigates a unique filtering structure employed in CPW differential signaling structures. Simulations and measurements of bowtie or dipole-like filtering elements are investigated as candidate structures which can be implemented in multilayer PCBs to suppress CM transmission while allowing the propagation of DM signals. It has potential application in high-speed data transmission systems such as cellular systems and computer expansion buses as a means of protecting a PCB's SI performance while enhancing its EMC properties.

2. COMMON-MODE FILTERING AND S-PARAMETER MEASUREMENTS

To understand the proposed CM filtering concept, we need to know how to analyze the differential CPW structure and how the wave travels in it. In addition to that, we also need to understand what parameter and measuring technique can help us verify our simulated and fabricated model. For a differential CPW structure, true transverse electromagnetic mode does not exist. To find the best location to place our filtering elements, we will need the help of even and odd mode, and differential and common mode analyses. As for measurement, scattering parameters are used to measure the power waves being transmitted and reflected at each port of the device. In the following section, we will explain each term to help readers understand how we came up with our filtering designs.

2.1 Electromagnetic Waves and Transverse Electromagnetic Mode

Electromagnetic energy transmits in the form of waves. The directions of electric and magnetic fields of wave transmission can have different orientations to the direction of the traveling wave, depending on the propagation mode. It's possible that many field configurations exist for a given electromagnetic boundary value problem. A transverse electromagnetic mode (*TEM mode*) is one of these configurations whose both electric and magnetic fields are restricted to directions perpendicular (transverse) to the wave's propagation direction.

Maxwell's equations are needed to demonstrate TEM mode. Maxwell's equations are a set of four differential equations that describe how electric and magnetic fields propagate and interact. The general form of Maxwell's equations can be written as:

$$\nabla \times \bar{E} = -j\omega\mu\bar{H}, \quad \textit{(Equation 2-1)}$$

$$\nabla \times \bar{H} = j\omega\varepsilon\bar{E}, \quad \textit{(Equation 2-2)}$$

$$\nabla \cdot \bar{D} = \rho, \quad \textit{(Equation 2-3)}$$

$$\nabla \cdot \bar{B} = 0. \quad \textit{(Equation 2-4)}$$

The script quantities are defined below:

$\bar{E}$ is the electric field vector, in V/m.

$\bar{H}$ is the magnetic field vector, in A/m.

$\bar{B}$ is the magnetic flux density vector, in Wb/m^2.

$\bar{D}$ is the electric flux density vector, in C/m^2.

$\bar{M}$ is the magnetic current density vector, in V/ m^2.

$\bar{J}$ is the electric current density vector, in A/m^2.

ρ is the electric charge density, in C/m^3.

ω is the frequency, in rad.

It is worth mentioning that magnetic current is often used for mathematical convenience and completeness since magnetic charge or the magnetic monopole is not known to exist. A loop of electric current or a magnetic dipole is the true source of magnetic current. Assuming the wave is

a uniform plane wave traveling in the $\hat{a}_z$ direction, the electric filed and magnetic field have only x and y components, respectively.

Differential transmission lines, for example, striplines, are usually able to support TEM waves since they consist of two conductors in a homogeneous dielectric and have zero longitudinal field components. But transmission lines in CPW structures without cover plates, as seen in Fig 1.2 (c), are surrounded by more than one medium. A portion of the signal waves can transmit in free space. Consequently, a very small longitudinal component can be found, and true TEM mode does not present. This approximation of TEM mode is called *quasi-TEM mode*. Because of this, the effective permittivity of the dielectric can be different than the labeled material permittivity.

2.2 Even Mode Analysis and Odd Mode Analysis

Most differential signaling designs in microwave engineering involve symmetric transmission lines. When two transmission lines are placed closely, their fields and power can be coupled from one conductor to the other. The amount of coupling usually depends on the distance between transmission lines and signal frequencies. Figure 2.1 shows a broadside coupled coplanar waveguide, whose cross-section also appeared in Fig 1.2 (c). Using superposition, any arbitrary excitation of this CPW structure can be considered as a combination of two modes: even and odd. Both excitation modes are illustrated in Fig 2.2, where the red lines represent electric flux.

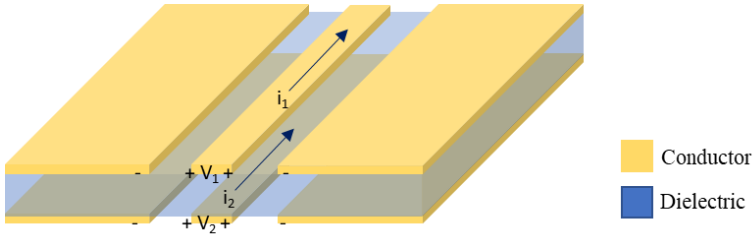

Figure 2.1 Schematic of a coupled coplanar waveguide

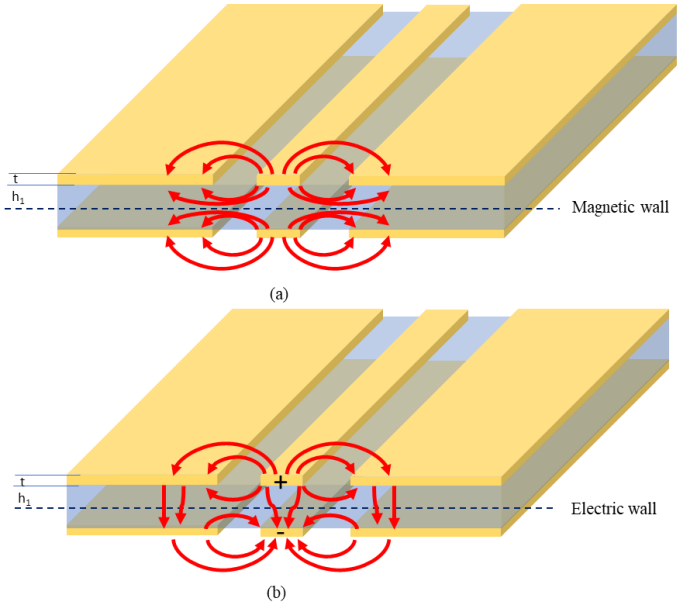

Figure 2.2 Transversal electrical field of a coupled CPW under (a). even mode excitation; (b). odd mode excitation

2.2.1 Even Mode

For even mode analysis, a magnetic wall is placed along the plane of symmetry to restrict the analysis to either the top or bottom half of the structure. The total capacitance then is expressed as C_e, where the capacitance per unit length is contributed by half of the substrate, h_1. C_e can be calculated using

$$C_e = 2\varepsilon_0\varepsilon_r \frac{K(k_e)}{K(k\prime_e)}, \quad \textit{(Equation 2-5)}$$

$$and\ k_e = \frac{sinh(\frac{\pi W}{4h_1})}{sinh(\frac{\pi(W+2S)}{4h_1})}, \quad \textit{(Equation 2-6)}$$

where W is the width of the conductor and S is the gap between the conductor and GND reference trace. $K(k_e)$ and $K(k'_e)$ are the complete elliptic integral of the first kind and its complement [8].

The effective dielectric constant for even mode is defined using C_e and the even mode capacitance per unit length with air as the dielectric can be expressed as:

$$C_{e-air} = 2\varepsilon_0 \frac{K(k_e)}{K(k\prime_e)}, \quad \textit{(Equation 2-7)}$$

$$\varepsilon_{eff-even} = \frac{C_e}{C_{e-air}}. \quad \textit{(Equation 2-8)}$$

Hence, the even mode characteristic impedance $Z_{0,e}$ can be expressed as:

$$Z_{0,e} = \frac{1}{c\sqrt{C_e C_{e-air}}}, \quad \textit{(Equation 2-9)}$$

where c is the speed of light in free space [8].

2.2.2 Odd Mode

Similar to even mode analysis, an electric wall is placed along the plane of symmetry for odd mode analysis to simplify calculation to either top or bottom half of the structure. The total capacitance then is expressed as C_o, where the capacitance per unit length is contributed by half of the substrate, h_1.

$$C_o = 2\varepsilon_0\varepsilon_r \frac{K(k_o)}{K(k\prime_o)}, \quad \textit{(Equation 2-10)}$$

$$and\ k_o = \frac{tanh(\frac{\pi W}{4h_1})}{tanh(\frac{\pi(W+2S)}{4h1})}, \qquad \textit{(Equation 2-11)}$$

where W is the width of the conductor and S is the gap between the conductor and GND reference trace. $K(k_o)$ and $K(k'_o)$ are the complete elliptic integral of the first kind and its complement [8].

The effective dielectric constant for even mode is defined using C_e and the odd mode capacitance per unit length with air as dielectric:

$$C_{o-air} = 2\varepsilon_0 \frac{K(k_o)}{K(k'_o)}, \quad \textit{(Equation 2-12)}$$

$$\varepsilon_{eff-odd} = \frac{C_o}{C_{o-air}}. \quad \textit{(Equation 2-13)}$$

The odd mode characteristic impedance $Z_{0,o}$ can be expressed as

$$Z_{0,o} = \frac{1}{c\sqrt{C_o C_{o-air}}}. \quad \textit{(Equation 2-14)}$$

where c is the speed of light in free space [8].

The characteristic impedance, Z_c or Z_0, of a single-ended transmission line can be expressed as

$$Z_c = Z_0 = \sqrt{Z_{0,o} Z_{0,e}} \qquad \textit{(Equation 2-15)}$$

2.2.3 Differential Mode and Common Mode

As seen in Fig 2.1, V_1 and V_2 is the differential voltage pair sent to the transmission lines. Using even mode voltage V_e and odd mode voltage V_o, V_1 and V_2 are defined as

$$V_1 = V_e^+ e^{-\gamma_e z} + V_e^- e^{\gamma_e z} + V_o^+ e^{-\gamma_o z} + V_o^- e^{\gamma_o z}, \qquad \textit{(Equation 2-16)}$$

$$V_2 = V_e^+ e^{-\gamma_e z} + V_e^- e^{\gamma_e z} - V_o^+ e^{-\gamma_o z} - V_o^- e^{\gamma_o z}, \qquad \textit{(Equation 2-17)}$$

since $V_e = \frac{V_1+V_2}{2}$ and $V_o = \frac{V_1-V_2}{2}$.

Therefore, the resulting currents i_1 and i_2 are:

$$i_1 = \frac{1}{Z_{0,e}}(V_e^+ e^{-\gamma_e z} - V_e^- e^{\gamma_e z}) + \frac{1}{Z_{0,o}}(V_o^+ e^{-\gamma_o z} - V_o^- e^{\gamma_o z}), \qquad \textit{(Equation 2-18)}$$

$$i_2 = \frac{1}{Z_{0,e}}(V_e^+ e^{-\gamma_e z} - V_e^- e^{\gamma_e z}) + \frac{1}{Z_{0,o}}(-V_o^+ e^{-\gamma_o z} + V_o^- e^{\gamma_o z}). \qquad \textit{(Equation 2-19)}$$

Define differential mode (V_d) and common mode (V_c) voltages and currents (i_d and i_c) as:

$$V_d = V_1 - V_2, \qquad \textit{(Equation 2-20)}$$

$$V_c = \frac{V_1+V_2}{2}, \qquad \textit{(Equation 2-21)}$$

$$i_d = \frac{i_1+i_2}{2}, \qquad \textit{(Equation 2-22)}$$

$$i_c = i_1 + i_2. \qquad \textit{(Equation 2-23)}$$

Substitute V_1 and V_2, i_1 and i_2:

$$V_d = 2(V_o^+ e^{-\gamma_e z} + V_o^- e^{\gamma_o z}), \qquad \textit{(Equation 2-24)}$$

$$V_c = V_e^+ e^{-\gamma_e z} + V_e^- e^{\gamma_e z}, \qquad \textit{(Equation 2-25)}$$

$$i_d = \frac{V_o^+ e^{-\gamma_e z} - V_o^- e^{\gamma_o z}}{Z_{0,o}}, \qquad \textit{(Equation 2-26)}$$

$$i_c = \frac{2(V_e^+ e^{-\gamma_e z} - V_e^- e^{\gamma_e z})}{Z_{0,e}}. \qquad \textit{(Equation 2-27)}$$

When only considering the positive differential voltages and currents, the differential mode characteristic impedance Z_d and common mode characteristic impedance Z_c for a symmetric CPW differential signaling system in Fig 2.1 can be expressed as:

$$Z_d = \frac{V_d^+}{i_d^+} = 2Z_{0,o}, \qquad \textit{(Equation 2-28)}$$

$$Z_c = \frac{V_c^+}{i_c^+} = \frac{Z_{0,e}}{2}. \qquad \textit{(Equation 2-29)}$$

2.3 S parameters and Vector Network Analyzer (VNA) Measurement

A simplified model of a coupled differential signaling system is shown in Fig 2.3, assuming port 1 and 3 are the system inputs, and port 2 and 4 are the outputs. Under perfect circumstances, all signals incident in port 1 should transmit to port 2, and none should be received at port 4. The same applies to signals sent from port 3.

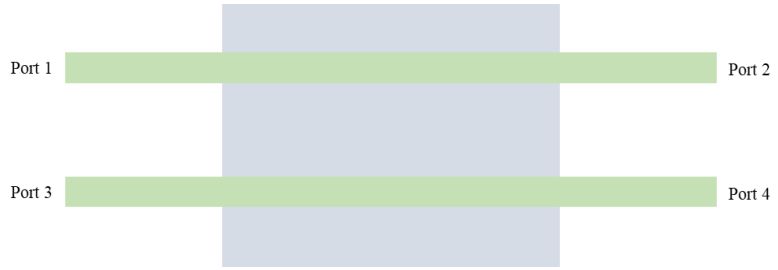

Figure 2.3 Simplified model of a 4-port differential signaling system.

In microwave and millimeter-wave engineering, various parameters are used to describe electrical behaviors of linear electrical networks. Parameters like admittance parameters (Y parameters) and impedance parameters (Z parameters) are useful in many circumstances. Direct measurements of these parameters are difficult since equipment that can measure voltage and current at MW frequencies is simply not available. Thus, scattering parameters (S parameters) are required to characterize system performance at high frequencies. The magnitude of S parameters are ratios of power waves which are proportional to the square root of a wave's power being transmitted and reflected. Therefore, they do not require open or short circuit

conditions like Y and Z parameters. Instead, matched loads (reference impedance) are used to characterize linear electrical networks.

Each port combination in a linear network has its own associated S parameter, which is defined in terms of incident and reflected powers. The quantity a_n is used to represent a wave incident to port n and b_n is used to represent a wave reflected from port n. For the 4-port network that's illustrated in Fig 2.3, the single-ended S parameter matrix is:

$$\begin{pmatrix} S_{11} & S_{12} & S_{13} & S_{14} \\ S_{21} & S_{22} & S_{23} & S_{24} \\ S_{31} & S_{32} & S_{33} & S_{34} \\ S_{41} & S_{42} & S_{43} & S_{44} \end{pmatrix},$$

where

$$\begin{pmatrix} b_1 \\ b_2 \\ b_3 \\ b_4 \end{pmatrix} = \begin{pmatrix} S_{11} & S_{12} & S_{13} & S_{14} \\ S_{21} & S_{22} & S_{23} & S_{24} \\ S_{31} & S_{32} & S_{33} & S_{34} \\ S_{41} & S_{42} & S_{43} & S_{44} \end{pmatrix} \begin{pmatrix} a_1 \\ a_2 \\ a_3 \\ a_4 \end{pmatrix}. \textit{(Equation 2-30)}$$

Due to it being passive and reciprocal, the network's S parameter is equal to its transpose, which means $S_{mn} = S_{nm}$. $S_{11}$and $S_{33}$are the forward reflection coefficients, when S_{22} and S_{44} are the reverse reflection coefficients. S_{21} and S_{43} are the forward gains with a source (usually 50 Ω in practice) and matching loads, and S_{12} and S_{34} are the reverse gains of the network under the same condition. For an ideal transmission line, magnitudes of S_{11}, S_{33}, S_{22}, and S_{44} should equal to 0, representing zero reflection, and the magnitudes of S_{21} and S_{43} should be 1, representing zero loss.

In addition to the 4-port single-ended S parameter matrix, a mixed mode S parameter matrix is used to characterize the network in terms of differential and common mode signals:

$$\begin{pmatrix} b_{d1} \\ b_{d2} \\ b_{c1} \\ b_{c2} \end{pmatrix} = \begin{pmatrix} S_{dd11} & S_{dd12} & S_{dc11} & S_{dc14} \\ S_{dd21} & S_{dd22} & S_{dc21} & S_{dc24} \\ S_{cd11} & S_{cd12} & S_{cc11} & S_{cc34} \\ S_{cd21} & S_{cd22} & S_{cc21} & S_{cc44} \end{pmatrix} \begin{pmatrix} a_{d1} \\ a_{d2} \\ a_{c1} \\ a_{c2} \end{pmatrix}. \textit{(Equation 2-31)}$$

S_{dd21} is the input differential insertion loss. $S_{cc21}$is the common mode rejection. $S_{cd21}$is the differential to common mode conversion from port 1 to port 2. To limit CM transmission and conversion, S_{cc21} and S_{cd21} should be minimal. To calculate S_{dd21} and S_{cc21} from VNA measurements, S_{dd21} and S_{cc21} can be rewritten as:

$$S_{dd21} = 0.5 \times (S_{21} - S_{23} - S_{41} + S_{43}), \textit{(Equation 2-32)}$$

$$S_{cc21} = 0.5 \times (S_{21} + S_{23} + S_{41} + S_{43}), \textit{(Equation 2-33)}$$

$$S_{cd21} = 0.5 \times (S_{21} - S_{23} + S_{41} - S_{43}). \textit{(Equation 2-34)}$$

In addition, the forward differential return loss (port 1 reflection) S_{dd11} and reverse differential return loss (port 2 reflection) S_{dd22} can be rewritten as:

$$S_{dd11} = 0.5 \times (S_{11} - S_{13} - S_{31} + S_{33}), \textit{(Equation 2-35)}$$

$$S_{dd22} = 0.5 \times (S_{22} - S_{24} - S_{42} + S_{44}) . \textit{(Equation 2-36)}$$

For ideal transmission, they should also be kept minimal.

2.4 Common Mode Filtering

To effectively eliminate common mode noise, the filter structure should affect either the CM electric or magnetic field between the transmission line conductors. In this thesis, a metallization plane that is tied to the reference is placed in the horizontal plane of symmetry to act as an electric wall and achieve effective CM filtering results. Illustrations of the electric flux for a differential CPW under DM and CM are shown below in Fig 2.4 (a) and (b), respectively. Figure 2.4 (c) and (d) demonstrate how a GND conductor plane in the substrate can affect CM signals but not DM signals.

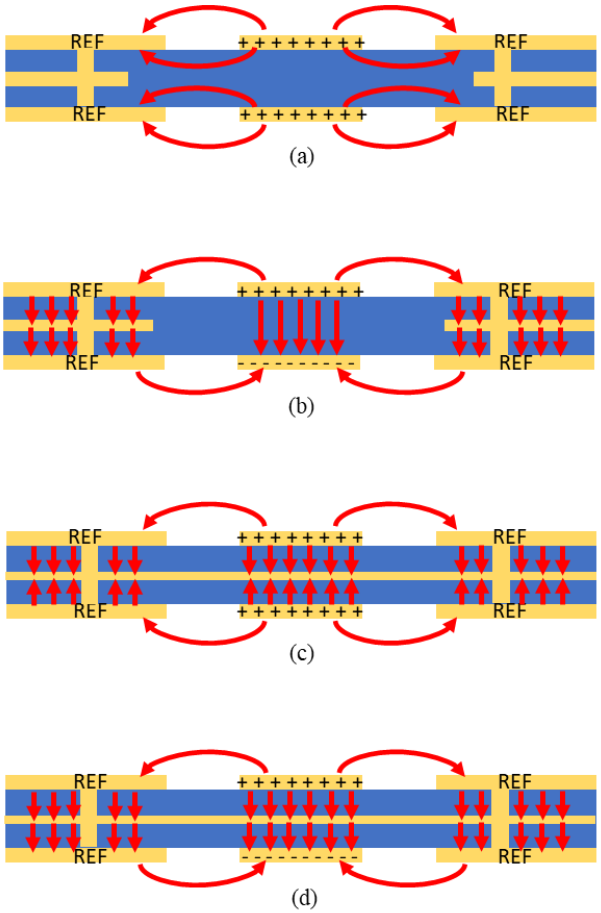

Figure 2.4 Electric field of a differential CPW structure (a). under DM signals; (b). under CM signals; (c). under CM with CM filtering elements presenting; (d). under DM with CM filtering elements presenting.

3. DESIGN OF THE COMMON MODE FILTERING STRUCTURE

3.1 Original Design and Simulation

The original CPW CM filter design, as shown in Fig 3.1 (a), consists of only simple rectangular cutouts in the middle metallization plane. The metal in the simulated model is lossy copper with 0.035mm thickness, and the dielectric is MEGTRON 6. The simulation results, as seen in Fig. 3.1 (b), show outstanding DM transmission and CM filtering up to 100 GHz, where S2(1),1(1) represent the DM transmission and S2(2),1(2) represent the CM transmission. The original design model and simulated data were lost due to an unfortunate hacking. Therefore, we are unable to show the exact dimensions of the simulated model.

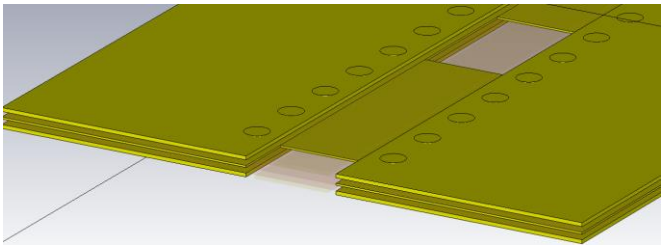

(a)

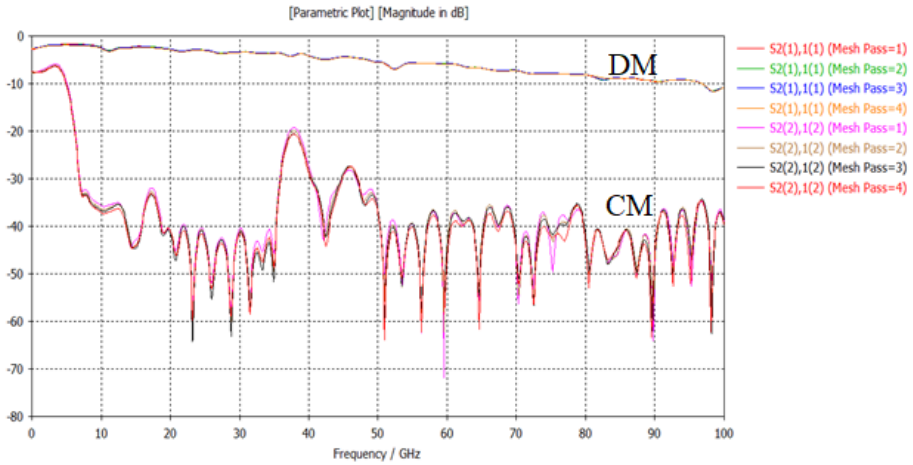

(b)

Figure 3.1 (a). Filter layer view of the original design; (b) Simulated DM and CM transmission of the original design.

3.2 Improved Design

3.2.1. Single Filter Design

I. Filter Design Concept

The improved CPW CM filter design uses the same stack up as the design shown in the previous section. As before, it acts as a half-wavelength resonator but consists of a rectangular metal patch placed in the middle metallization layer, as shown in Fig. 3.2 (a), with two stubs connecting the structure to the surrounding reference plane. Figure 3.2 (b) shows the details of this proposed design with all parameters labeled, where *fl* is the filter length, *fw* is the filter width, *sl* is the stub length and *sw* is the stub width. With every dimension of the filter parameterized, the relationship between the physical structure of a filter and its effective length in a differential CPW environment can be readily explored.

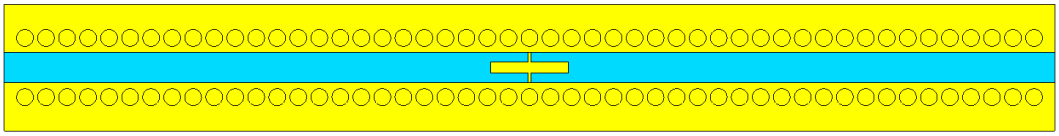

(a)

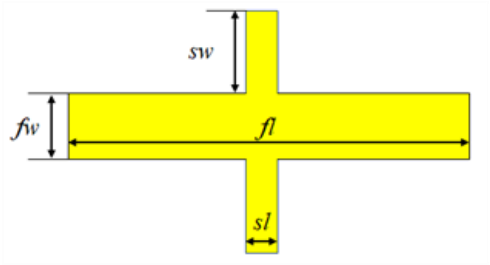

(b)

Figure 3.2 (a) Top view of the filter layer of the original single filter design, (b) close-up view of a single filter with all dimensions labeled.

II. Filter Effective Length

The physical length of a filter in a PCB is not typically its effective filter length due to parasitic elements and/or fringing capacitance. Because of this, finding the effective length is important for our filter design. A correct approximation can help engineers design the filter to target CM signals at the required frequency correctly. To help us obtain a better understanding of the filtering behavior of this half-wavelength resonator design, we modeled two filters that are aimed at 10 GHz ($\lambda/2$ = 8.8 mm) and 20 GHz ($\lambda/2$ = 4.4 mm), respectively, for two models. From the simulation results shown in Fig. 3.3, it is clear that the simulated CM filtering frequencies are lower than what we initially designed for, even though the -10 dB filtering bandwidth covers the targeted frequency for each case. The simulated filtering frequency for the 10 GHz filter is 9.275 GHz, and the simulated filtering frequency for the 20 GHz filter turns out to be 16.73 GHz.

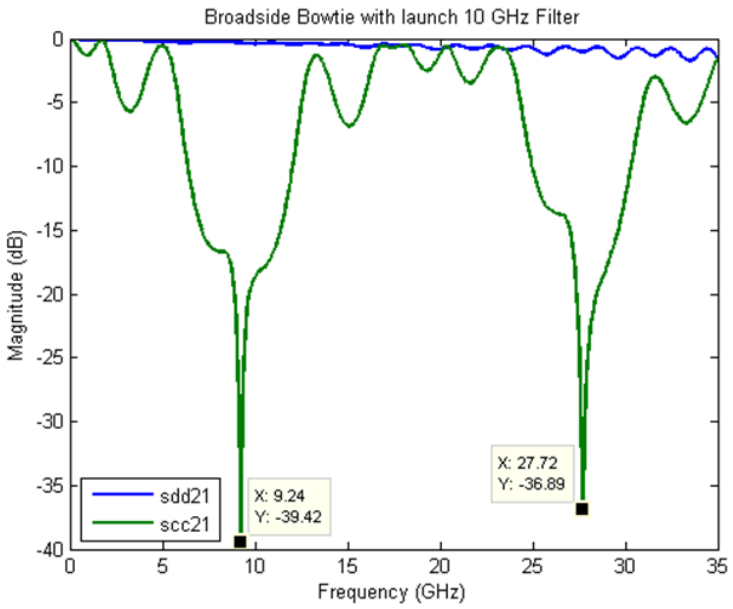

(a)

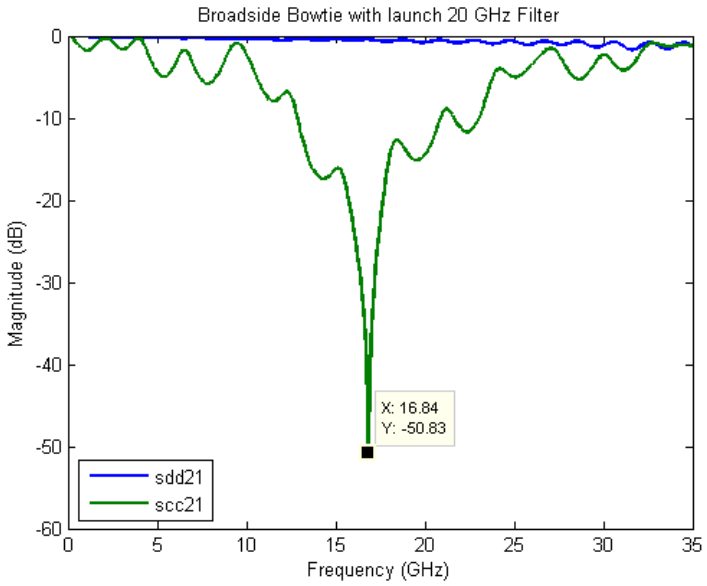

(b)

Figure 3.3 Simulated DM and CM transmission of a CPW board with (a) a 10 GHz filter, and (b) a 20 GHz filter.

The first approach we take to find the effective length is inspired by the microstrip model introduced by E.O Hammerstad and F. Bekkadal [7]. The length extension, Δl, of a microstrip line can be approximated with

$$\Delta l = 0.412d\left(\frac{\varepsilon_{eff}+0.3}{\varepsilon_{eff}-0.258}\right)\left(\frac{w+0.262d}{w+0.813d}\right),$$

where *d* is substrate thickness, *w* is the transmission line width, and ε_{eff} is the effective permittivity. The extended length is physically due to fringing flux which does not immediately go to zero at the end of the conductor. Even when the filtering element is essentially a stripline structure, this equation can be employed to obtain a first estimate of the length extension of a filter. The calculated length extension is around 0.0524 mm for each filter. Unfortunately, applying this answer did not give us satisfying results as the expected filtering frequencies are

calculated to be 9.824 GHz and 19.420 GHz instead of the 9.275 GHz and 16.73 GHz we have from the simulation.

The second approach taken is to use the open circuit and short circuit models of a CPW structure. This method is inspired by the design rule mentioned in R.N. Simons' work [8]. The filter structure can be seen as either an open circuit model or a short circuit model, depending on the location of the observation as demonstrated in Fig. 3.4.

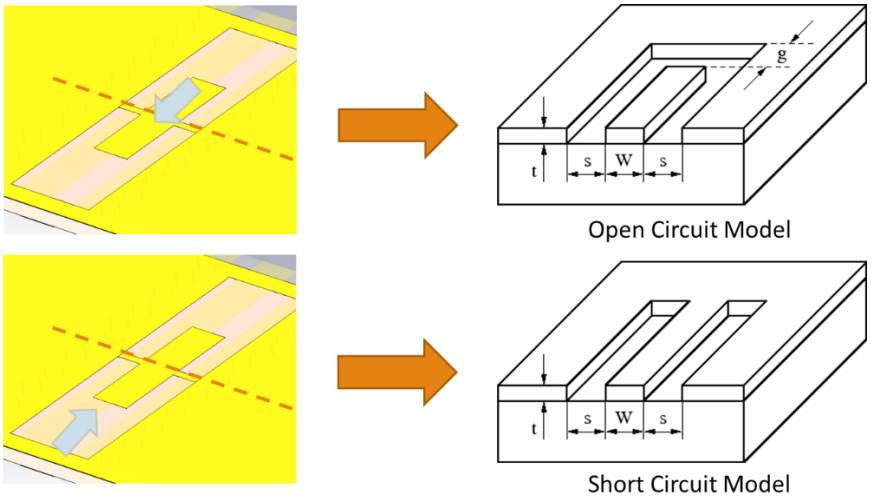

Figure 3.4 Open circuit and short circuit models of the CM filtering element.

The length extension, Δl_{open}, of an open circuit model can be expressed as

$$\Delta l_{open} = \frac{C_{open}}{C'} \approx \frac{W + 2S}{4}$$

Since the gap, g, is usually much larger than $W + 2S$ for the filter design, and the length extension, Δl_{short}, of a short circuit model can be expressed as

$$\Delta l_{short} = \frac{L_{open}}{L'} \approx \frac{W + 2s}{8}$$

In both assumptions, length extensions are considered as frequency independent since the effective permittivity of the dielectric is fairly consistent over a wide range of frequencies. Therefore, we can find $\Delta l_{open} = 0.1778\ mm$ and $\Delta l_{short} = 0.0889\ mm$ with the help of these equations. The filtering frequencies are expected to be 9.555 GHz for the 10 GHz filter and 18.396 GHz for the 20 GHz filter with the length extension of an open circuit, adding the short circuit length extension to the 10 GHz and 20 GHz filters moves the expected filtering frequencies to 9.744 GHz and 19.110 GHz. All results are far from the simulated CM filtering frequencies. The length extensions due to fringing are much smaller than the physical lengths of the filter, and so would result in only minor adjustments in any case.

After several unsuccessful attempts at estimating the effective half-wavelength resonator length, another effective length model is suggested. The assumed effective length of a filter, l_{eff}, includes the stub length and half of the width of the metal patch so that the half-wavelength of the target frequency would be estimated using

$$l_{eff} = 2(\frac{fl}{2} + \frac{fw}{2} + sw),$$

where resonances are expected to occur at $l_{eff} = n\,\lambda/2$, where n = 1, 3…. Since the filter width *fw* is 0.3048mm and the stub width *sw* is 0.2032 mm, the approximated effective filter length is 9.6702 mm for the 10 GHz filter and 5.3702 mm for the 20 GHz filter, which gives expected filtering frequencies at 9.0465 GHz and 16.290 GHz, respectively. Both answers are very close to the simulated 9.275 GHz and 16.73 GHz in Fig. 3.3.

To validate this effective length approximation, we built two additional CPW models with different CM filtering structures. One has an 8 GHz filter that actually filters at 7.5 GHz in simulation, and the other has a 35 GHz filter that only filters at 27.25 GHz in simulation due to the more serious impact caused by fringing capacitance. The expected filtering frequencies calculated by implementing this method give 7.41 GHz and 25.97 GHz for these two cases, which again shows that this estimation is decent enough for our filter design.

III. PCB Stack-up

To manufacture a test board for this project, a special board stack-up is needed since this differential CPW structure requires odd-layered board while even-layered stack-ups are more commonly used in the industry. After consulting PCB manufacturer, the final stack-up of our PCB is shown in Fig. 3.5. The dielectric used for this PCB is Rogers RO4350B which has a relative permittivity of 3.48. To maintain symmetry, both top and bottom CPW transmission lines share the same dimensions, as shown in Fig. 3.5 (a) and (b). A thin layer of Rogers RO4450F film, with a designed permittivity of 3.52, is used for bonding in the manufacture and is included in our simulation models as seen in Fig. 3.5 (c). Via fences are implemented along the CPW transmission line to prevent filtered CM energy from exciting parallel-plane waveguide modes.

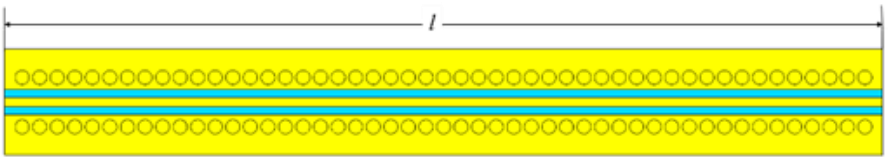

(a)

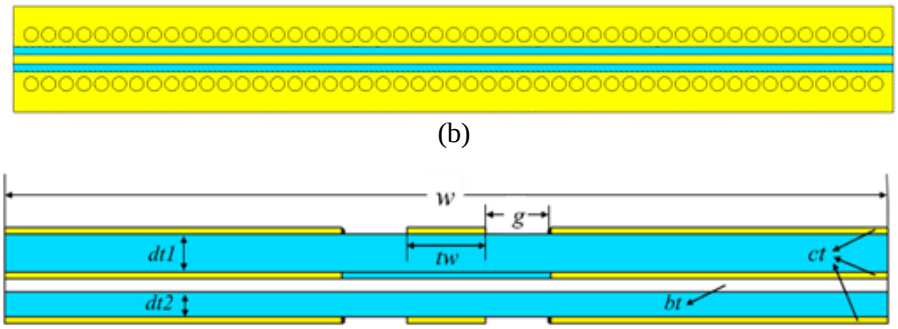

(b)

(c)

Figure 3.5 (a) Top view, (b) bottom view and (c) cross-section view of the new stack-up of the PCB.

IV. Single Filter Design

To verify our filter concept, a differential CPW structure with a single 16 GHz filter element is modeled and simulated. Table 3.1 shows all labeled dimensions for this CPW board with a CM filtering element that target at 16 GHz. *ct*, *dt1*, and *dt2* represent the thickness of the metallization layer, top and bottom dielectric layers. The thickness of the bonding film is *bt* with the board width and length labeled as *w* and *l*, respectively. Simulation results for this model can be found in section 4.1.1.

Table 3-1 Dimensions of a 16 GHz CM Filtering CPW Design Shown in Fig. 3 and 4

Parameters	Value	Parameters	Value
ct	0.0432 mm	*tw*	0.5360 mm
dt1	0.2540 mm	*g*	0.4432 mm
dt2	0.1676 mm	*fw*	0.5360 mm
bt	0.0963 mm	*fl*	3.6981 mm
w	6.0000 mm	*sw*	0.4432 mm
l	50.000 mm	*sl*	0.1250 mm

Based on this design, two other single filter structures that can filter at 8 GHz and 11 GHz were also made. Their dimensions are recorded in Table 4.2.

Table 3-2 Dimensions of the 8 GHz and 11 GHz CM Filtering CPW Designs

8 GHZ FILTER			
Parameters	**Value**	**Parameters**	**Value**
ct	0.0432 mm	*tw*	0.5360 mm
dt1	0.2540 mm	*g*	0.4432 mm
dt2	0.1676 mm	*fw*	0.5360 mm
bt	0.0963 mm	*fl*	4.3100 mm
w	6.0000 mm	*sw*	0.4432 mm
l	50.000 mm	*sl*	0.1250 mm
11 GHZ FILTER			
Parameters	**Value**	**Parameters**	**Value**
ct	0.0432 mm	*tw*	0.5360 mm
dt1	0.2540 mm	*g*	0.4432 mm
dt2	0.1676 mm	*fw*	0.5360 mm
bt	0.0963 mm	*fl*	2.9336 mm
w	6.0000 mm	*sw*	0.4432 mm
l	50.000 mm	*sl*	0.1250 mm

3.2.2. Cascaded Filter Design

In the previous section, we can only expect each filter design will only work for one frequency and its odd harmonics due to the filter acting as a frequency resonator. In order to achieve filtering at multiple fundamental frequencies, we can cascade multiple different filtering elements with varying lengths. Therefore, for this section, we will place all three filters that are mentioned before to target CM filtering at 8, 11 and 16 GHz. Figure 3.6 shows the placement of these three filters. The simulation result for this cascaded structure is shown in section 4.1.2.

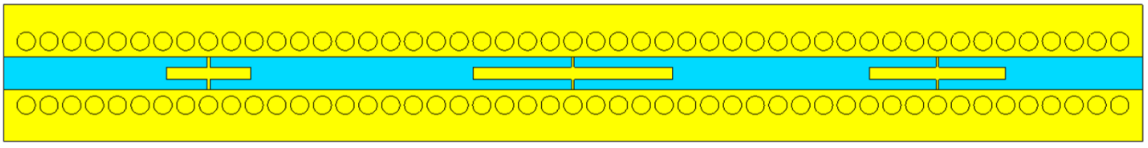

Figure 3.6 Filter layer view of the cascaded 8, 11 and 16 GHz filter design.

3.2.3. Centered and Off-Centered Stub Filter Designs

We can expect multi-frequency filtering with the cascaded filtering elements described in the previous section. But having multiple filters on the same layer also increases the size of the device. The original filter discussed in section 3.2.1 is a half-wavelength resonator. At the same time, it can also be considered as a combination of two quarter-wavelength resonators for the same frequency. To achieve a more compact system design and still filter at multiple frequencies, we take the approach of adjusting the location of the patch-to-reference stub to create a single structure providing filtering at two different frequencies.

To verify this concept, we choose to look at frequencies such as 16 GHz and 32 GHz. Two models are built and simulated for the purpose of comparison. The first model, which draws direct inspiration from Section 3.2.1 and 3.2.2, has two filters, one for 16 GHz and one for 32 GHz. Both filters have the centered stub design. The second model takes half of each filter in the first model to create a single filtering element with an off-centered stub. Each model is displayed in Fig. 3.7, and 3.8, respectively. Simulation results of this model are discussed in Section 4.2.3.

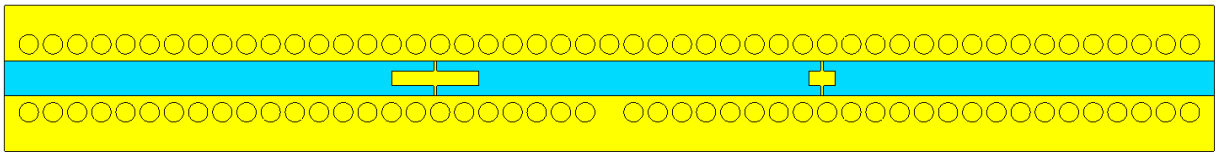

Figure 3.7 Filter layer view of the cascaded 16 and 32 GHz filter design with centered reference stub.

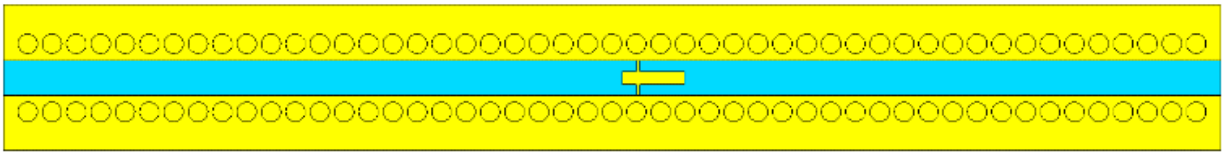

Figure 3.8 Filter layer view of the single filter design with off-centered reference stub.

3.3 Simple RF Launch Design and Simulation

To ease the design of signal launch while effectively avoiding skew, radio frequency (RF) probe launch structures were placed symmetrically on each side of the PCB. The launch structure consists of 50 Ω CPW RF probe launch pads and a short taper for transmission line impedance matching. A close-up view is shown in Fig. 3.9, where S is the trace to reference separation, W is the width of the transmission line, TL is the length of the taper, WL is the width of the signal launch pad, and SL is the separation between the launch pad and the reference metal. The pitch from the center of the signal pad to the center of the GND pad is 500 µm.

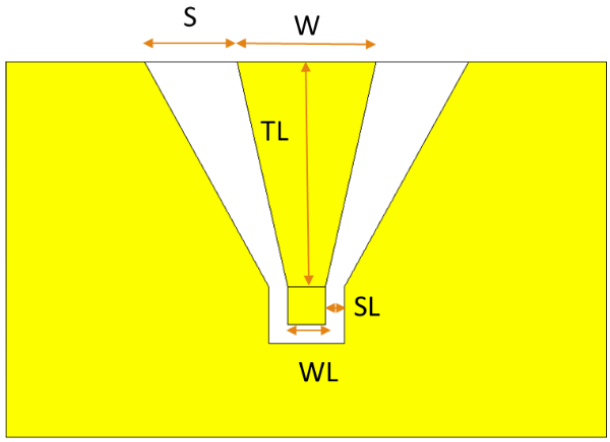

(a)

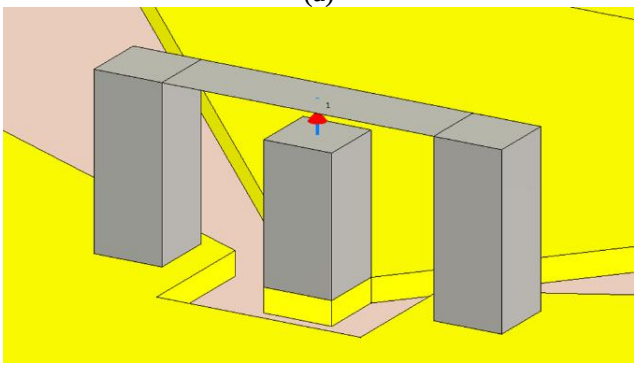

(b)

Figure 3.9 (a) Top view of the originally proposed RF launch structure; (b) Port model of the proposed RF launch structure. The PEC columns represent the locations of the two ground pads and the center signal pad.

When comparing the simulation results in Fig 3.10 (b) to Fig 3.11, which shows the simulated transmissions without the proposed RF launch model, it is clear that unwanted attenuation is introduced by this launch design. After placing surface current monitor at different frequencies, we found out that power leakage exists in this model since no via fence is present to help confine the signal in the launch structure so that it adequately matches that of the remaining TL structure. As seen in Fig. 3.12, the performance is much improved after adding via fences around the launch structure.

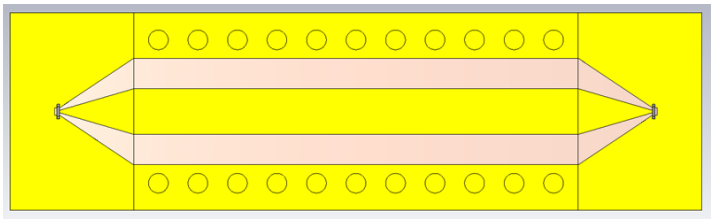

(a)

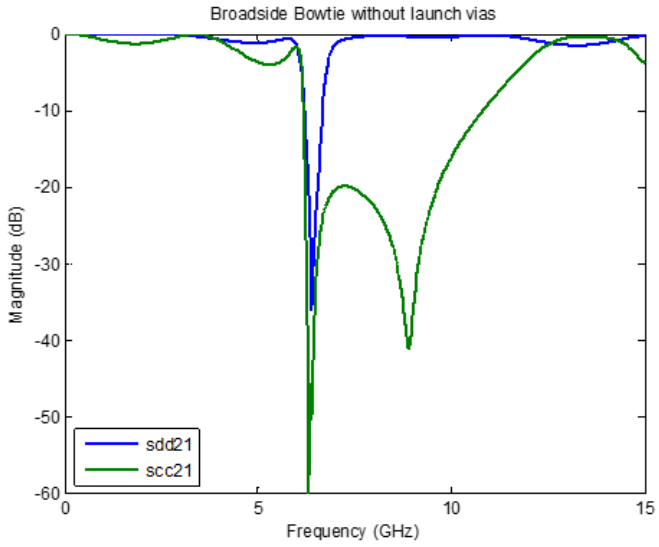

(b)

Figure 3.10 (a) Top view of the board design with the original RF launch attached. It is worth mentioning for this model, the filter is designed to attenuate CM signals at 8 GHz; (b) Simulation results of this structure with this proposed RF launch.

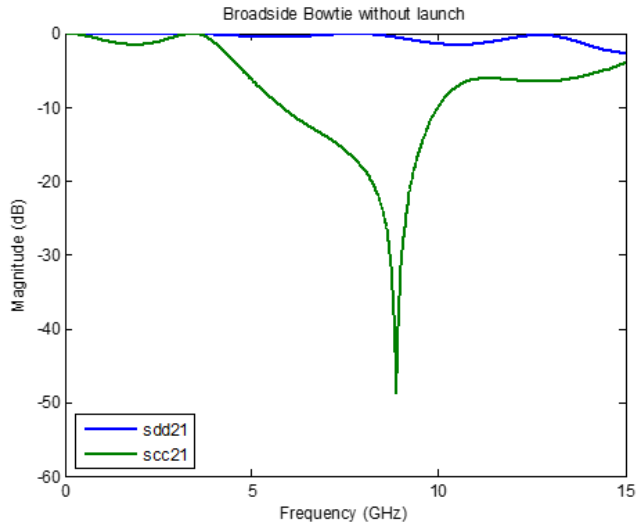

Figure 3.11 Simulated DM and CM transmissions of the board in Fig. 3.9 (a) without the proposed RF launch model.

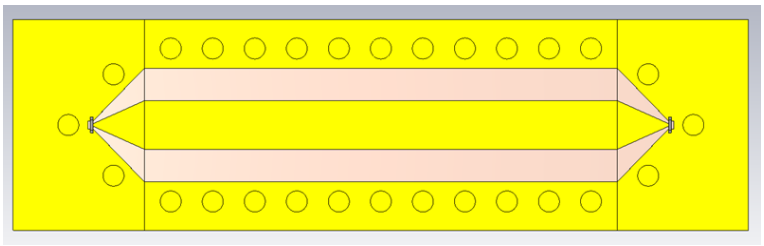

(a)

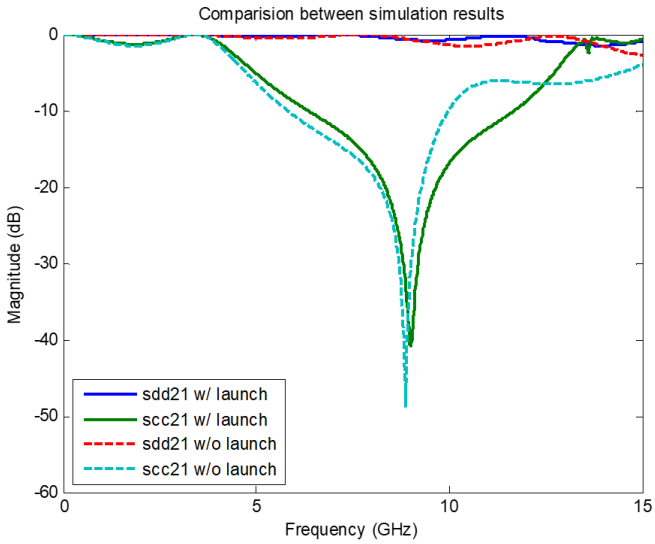

(b)

Figure 3.12 (a) Top view of the board design with the RF launch and via fence. (b) Comparison between the simulation results of this structure with and without the proposed RF launch with via fence.

To ensure the performance of our connector model, simulations of a THRU model is conducted. The THRU model consists of two launch structures connecting directly to each other with no transmission line presents, as seen in Fig. 3.13. Simulation results, as shown in Fig. 3.14, verify that our RF launch model does not significantly interfere with the transmission as both DM and CM insertion losses are quite low.

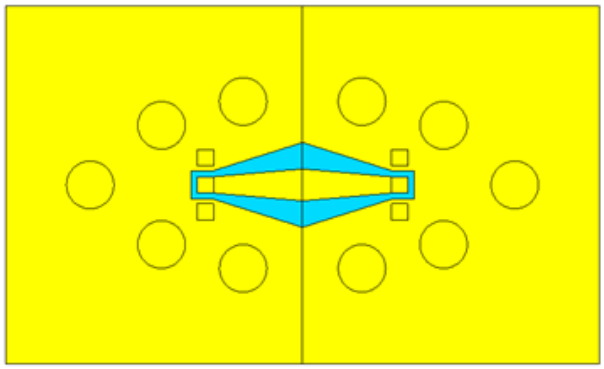

Figure 3.13 Thru model of the proposed RF launch model.

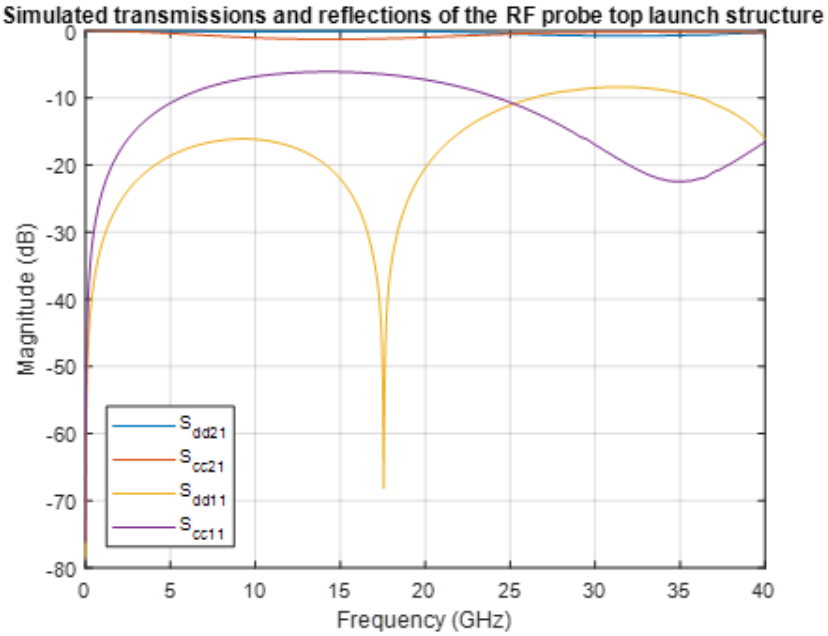

Figure 3.14 Simulated transmission and reflection results of this proposed model.

3.4 Sensitivity and Registration Study

In a multilayer PCB fabrication process, the sensitivity to layer-to-layer misregistration is of vital importance since it can have a serious impact on the system performance. Previous studies have also observed that misregistration can significantly increase layer-to-layer DM to CM conversion [9].

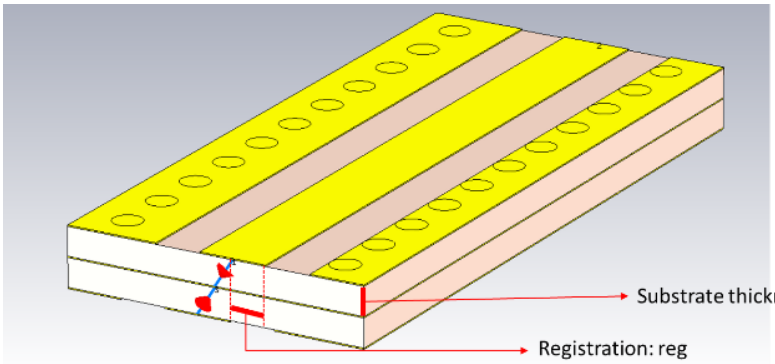

Figure 3.15 Simulation model, with each parameter labeled, for the two cases in sensitivity study.

Two sensitivity studies, limited at this stage to simulation only, were conducted to help understand the sensitivity of our structures to substrate thickness and transmission line misalignment. For the first case, the thickness of the top and bottom dielectric board is parameterized as "*h*" and swept from 0.127 mm to 0.77 mm. Figure 3.16 shows that the changing substrate thickness does affect the DM and CM transmissions. As the substrate thickness increases, the effective dielectric constant decreases and the impedance of the transmission line increases, resulting the shifting of CM filtering frequency. To confirm this behavior, the DM and CM impedances were found for the design using 2-D cross-section analysis tool FEMAS. In this simulation, two different dielectric thicknesses are simulated, and the characteristic impedance of

the transmission line in each case is kept as 50 Ω as seen in Fig. 3.17. The simulated results are recorded in Table. 3.4.

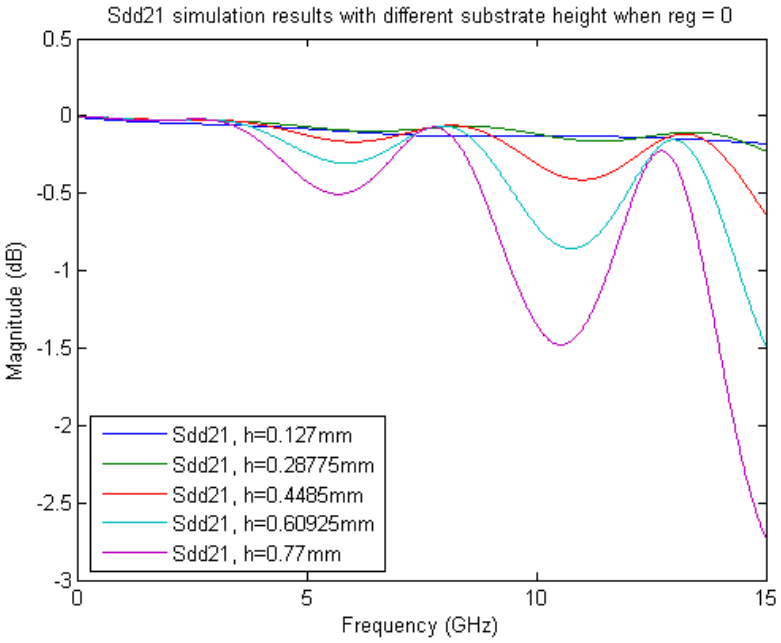

(a)

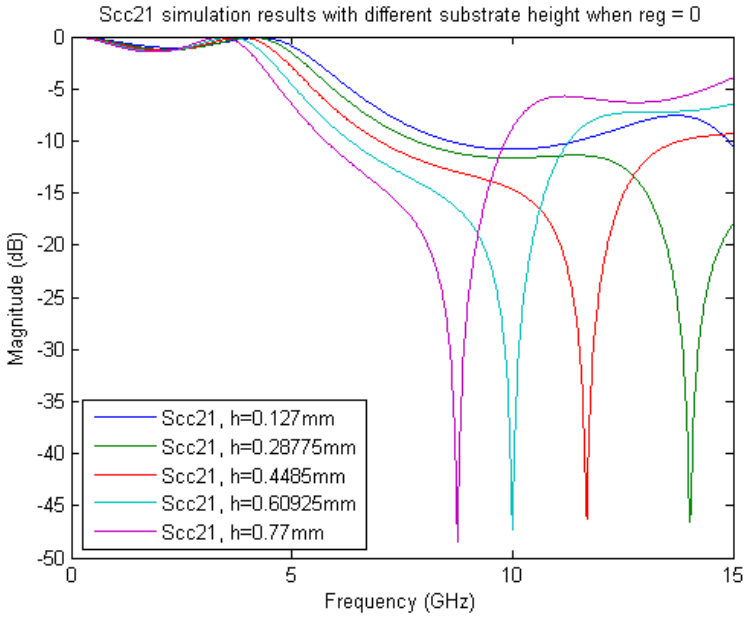

(b)

Figure 3.16 Simulated (a) DM transmission and (b) CM transmission of the structure shown in Fig. 4.13 in a substrate sensitivity test.

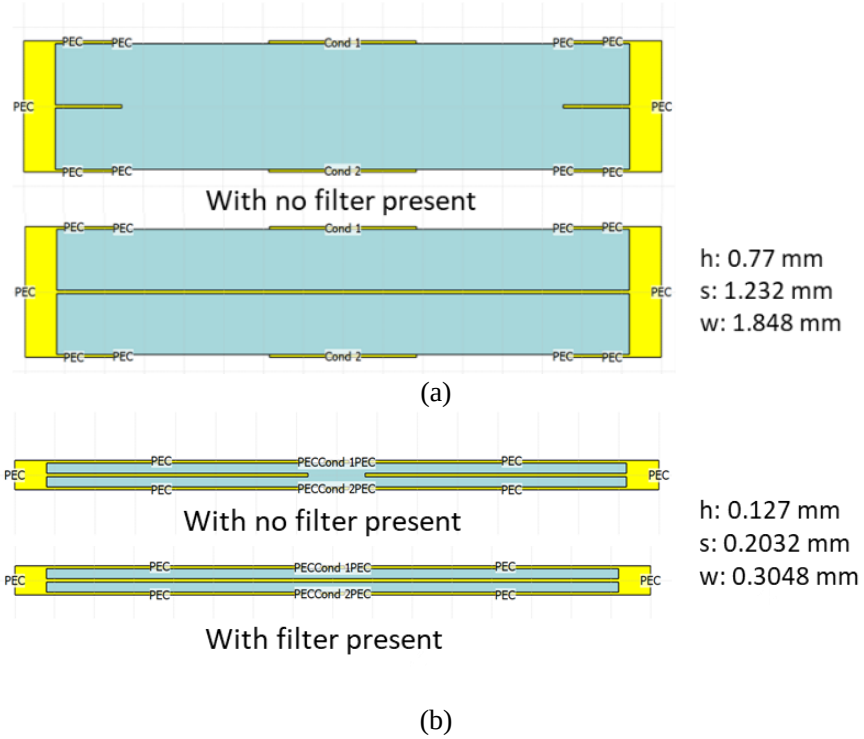

Figure 3.17 Cross-section model of (a) a board with substrate thickness of 0.77 mm, trace width of 1.848 mm, and gap width of 1.232 mm, and (b) a board with substrate thickness of 0.127 mm, trace width of 0.3048 mm, and gap width of 0.2032 mm in FEMAS.

Table 3-3 Simulated DM and CM Impedances of the Two Structures Shown in Fig. 3.15

STRUCTURE	Z_c	Z_d
With no Filter (h = 0.77mm)	96.134	114.541
With Filter (h = 0.77mm)	21.9748	87.8958
With no Filter (h = 0.127mm)	46.593	100.343
With Filter (h = 0.127mm)	18.4433	73.7727

In the second case, the distance from the center of the transmission line to the vertical center axis of the board is parameterized as "*reg*" and swept from 0mm to 5 mils. With each simulated value of *reg*, both top and bottom signal lines move away from the center in opposite directions. Thus, the actual trace-to-trace misregistration, or reg_{abs}, is twice the value of *reg*. To fully explore the effect of misregistration, we used the cascaded model from section 3.2.2 and extended the simulation frequency to 50 GHz. The plots in Fig. 3.18 show that our signaling and

filter designs are still able to maintain performance even when the trace-to-trace misregistration reaches 10 mils (5-mil single layer misregistration).

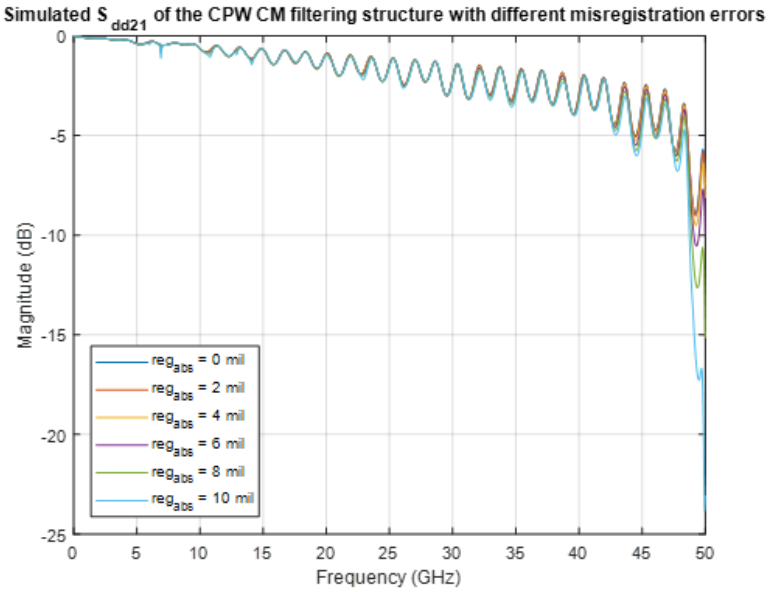

(a)

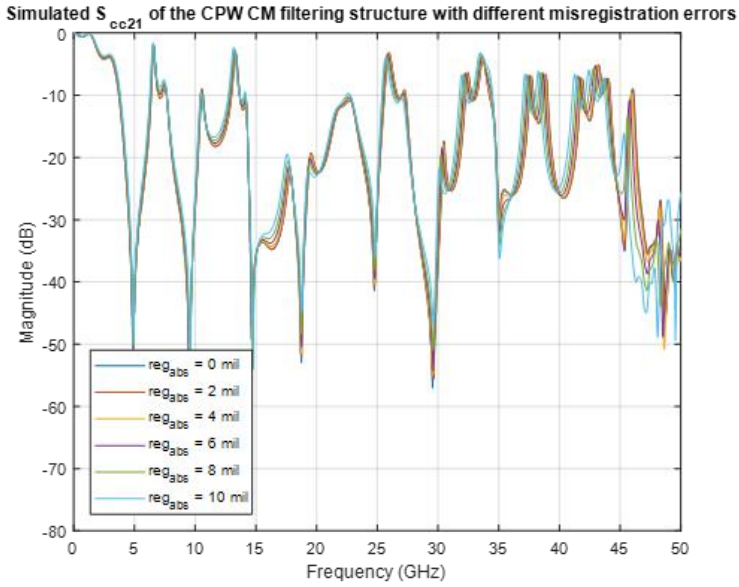

(b)

Figure 3.18 Simulated results of the registration study: (a). differential mode signal transmission; (b). common mode signal transmission.

4. SIMULATION RESULTS

The proposed filter structure, when excited by CM signals at resonance, strongly couples the transmission lines to the reference plane thus providing significant CM filtering at resonance. Away from resonance, the filtering element affects the electrical flux lines of CM signals to a higher degree than the electrical flux lines of DM signals thus altering the CM impedance while keeping DM impedance almost untouched. Therefore, the structure is able to eliminate CM signals over a wide band and keep the SI of DM signals. To demonstrate this and further prove the concept discussed in section 2.4, Fig. 4.1 shows additional simulations of the electrical flux lines of our PCB design under both CM and DM excitations with comparisons when no filter is presented.

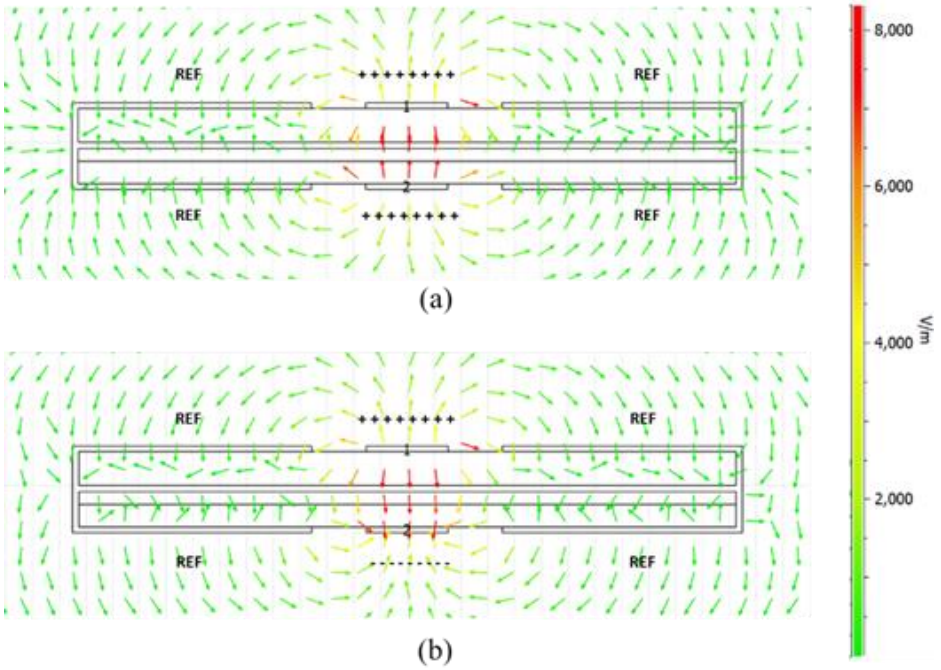

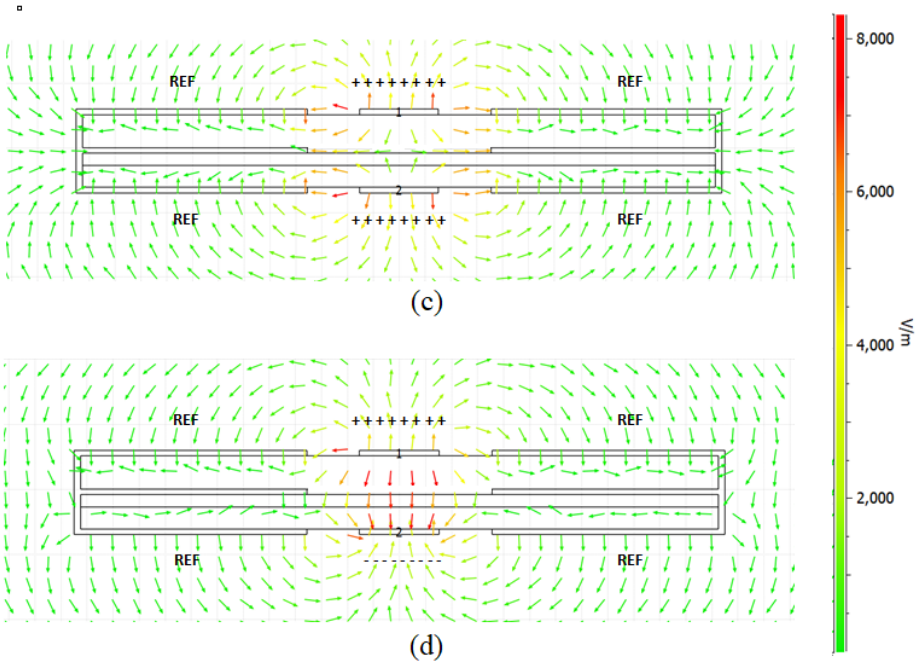

Figure 4.1 Cross-section view of the simulated electrical flux lines of a differential CPW structure with (a). the proposed filter structure shown in Fig. 3 and 4 under CM signals; (b). the same structure under DM signals; (c). a differential CPW structure without any filter structure under CM signals; (d). the same structure under DM signals.

As we mentioned in the previous section, our transmission line models were initially built without any launch structure. In the following sections, we will show the simulations with and without the RF launch separately and discuss possible optimization for the RF launch.

4.1 Simulation Results for Each Filter Design without RF Launch Structure

4.1.1. Single Filter Design

Figure 4.2 shows the simulated differential and common mode transmissions for this single filter model. The -10-dB percent bandwidth is 40% and centered at 15 GHz, demonstrating the

strong broadband CM filtering capability of this design at a single frequency. DM signal also stays above -3 dB over the whole frequency spectrum. Similar results also appear when the filtering frequency is changed to 8 or 11 GHz.

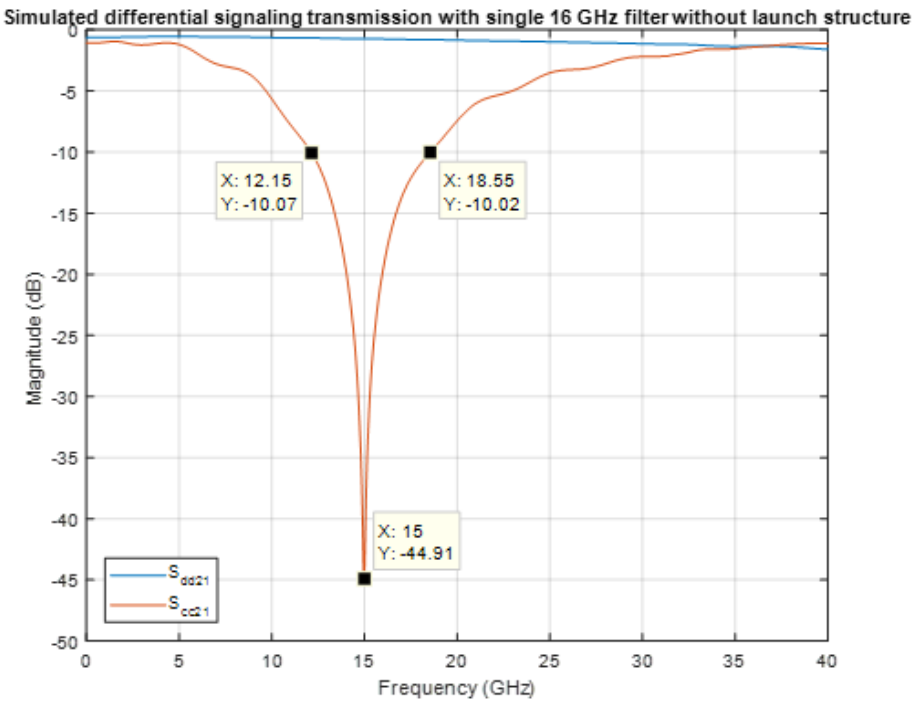

Figure 4.2 Simulated transmission results of a differential CPW structure with a 16 GHz CM filter.

4.1.2. Cascaded Filter Design

Simulation results in Fig. 4.3 demonstrate impressive broadband CM filtering around each target frequency and its harmonics. The green dash line indicates the locations of each -10 dB band. DM signal, on the other hand, still shows less than 3 dB attenuation all the way from DC to 40 GHz.

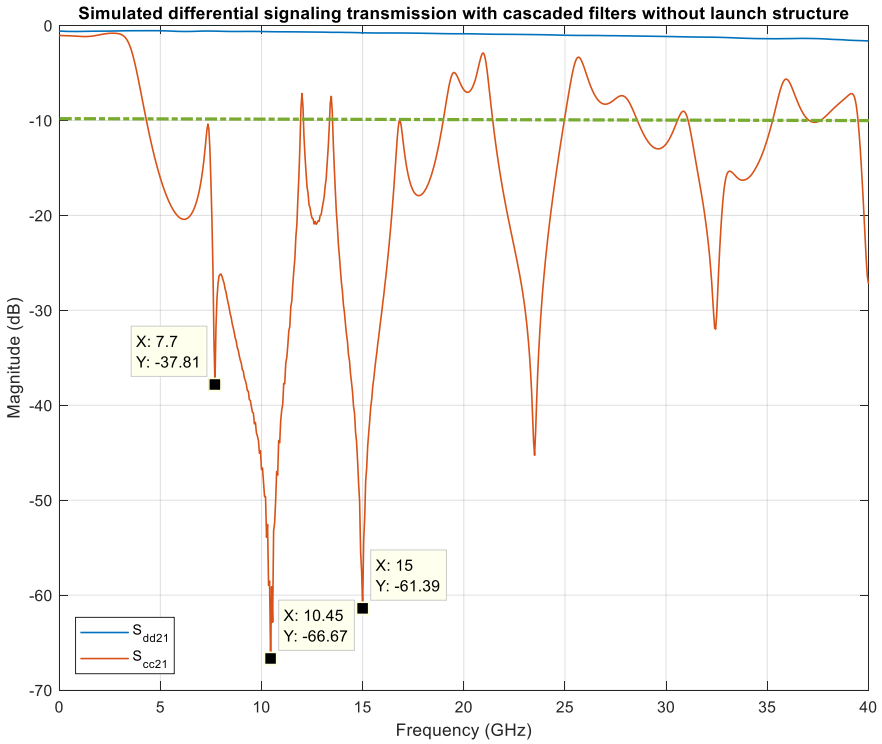

Figure 4.3 Simulated results of a differential CPW structure with cascaded 8, 11 and 16 GHz CM filters. The olive-green dashed line signifies where all -10 dB bandwidths are located.

4.1.3. Centered and Off-Centered Stub Filter Designs

Figure 4.4 shows simulated DM and CM transmission results for both models we mentioned in section 3.2.3. DM signals for both models keep their excellent performance, both having less than -3dB of loss over the whole frequency range. CM propagation is suppressed significantly; However, we see that simply merging two quarter-wavelength resonators together shifts the CM filtering effect to higher frequencies, a significant effect for the shorter filtering element.

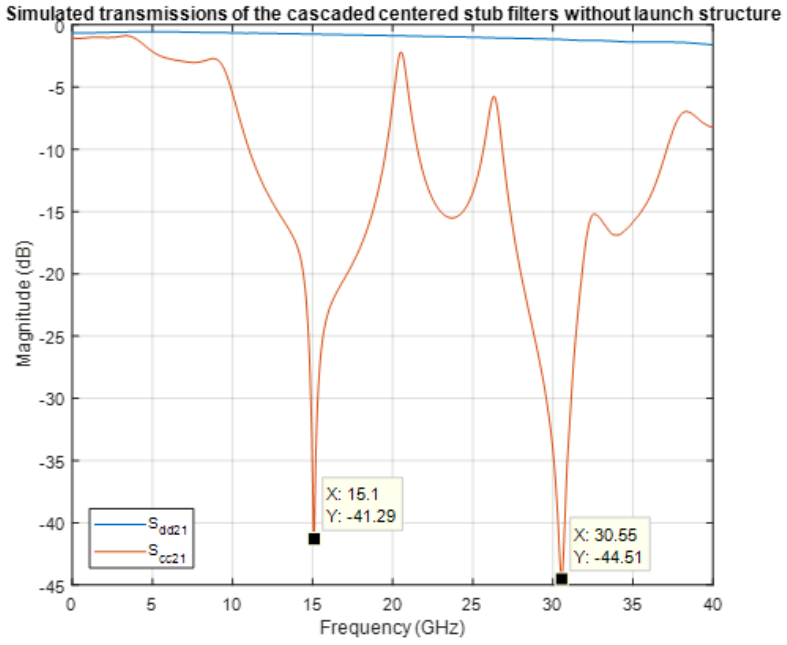

(a)

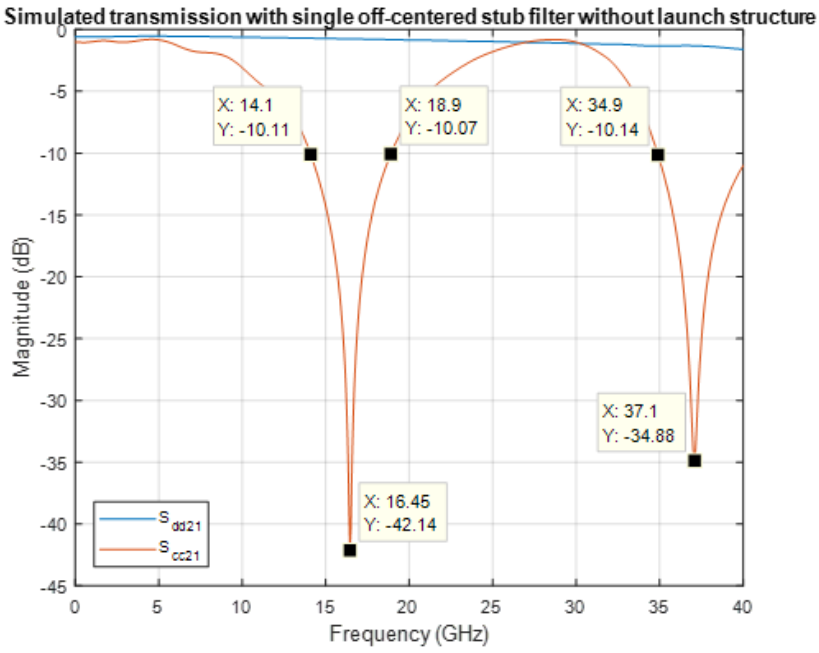

(b)

Figure 4.4 Simulated differential signaling transmissions of (a) cascaded 16 GHz and 32 GHz filters with centered filter-to-reference stub and (b) single filter with off-centered filter-to-reference stub achieving multi-frequency filtering.

4.2 Simulation Results for Each Filter Design with RF Launch Structure

To appreciate the effect of signal launch structures, we reran all simulations from section 4.1 with the launch model proposed in section 3.3. Section 4.2.1 to 4.2.3 are simulated results of all models that have been presented previously. At the same time, we also plotted results when no launch structure is attached to the filtering structure so the effect of the RF launch on the system is more distinguishable.

4.2.1. Single Filter Design

Figure 4.5 compares simulated results of the 16 GHz filter with the RF launch with the simulated results of the structure without the RF launch. From this comparison, we can tell that the filtering frequency does not change with the presence of the launch structure; However, ripples in both DM and CM transmissions do suggest slight impedance mismatching from the launch to the transmission line.

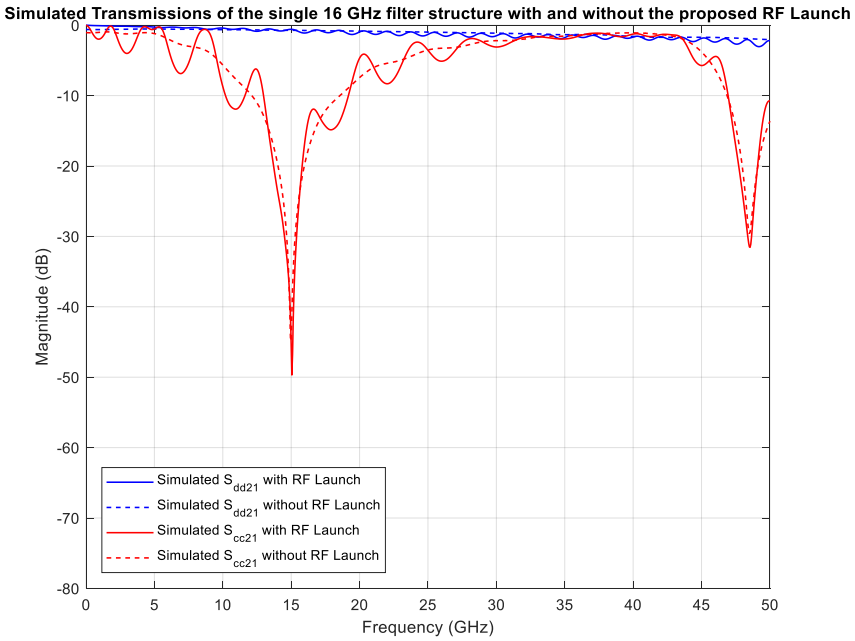

Figure 4.5 Simulated transmission results of a differential CPW structure with a single 16 GHz filter with and without the proposed launch structure.

4.2.2. Cascaded Filter Design

Figure 4.6 compares simulated results of the cascaded 8, 11 and 16 GHz filters with the RF launch with the simulated results of the same structure without the RF launch. Similar to the results in section 5.2-A, we can tell that the filtering frequency does not change with the presence of the launch structure. But ripples in both DM and CM transmissions still suggest slight impedance mismatch from the launch to the transmission line.

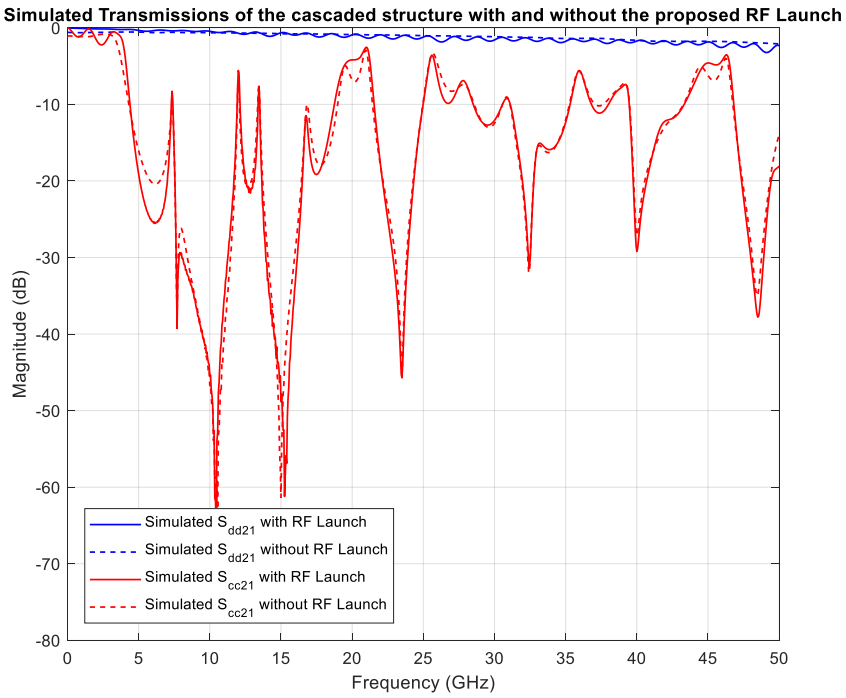

Figure 4.6 Simulated transmission results of a differential CPW structure with cascaded 8, 11 and 16 GHz filters with and without the proposed launch structure.

4.2.3. Off-center Stub Filter Design

Figure 4.7 compares simulated results of the cascaded 16 and 32 GHz filters with a centered filter-to-reference stub (symmetric filter design) with the RF launch to the simulated results of the same structure without the RF launch. The results in Fig. 4.8 compares simulated results of the a single 16-and-32-GHz filter with off-centered filter-to-reference stub (asymmetric filter design) with the RF launch with the simulated results of the same structure without the RF launch. Similar to the results in Section 4.2.1 and 4.2.2, the filtering frequencies for both cases do not shift with the launch structure attached. On the other hand, ripples still exist in both DM and CM transmissions suggesting an impedance mismatch from the launch structure to the transmission line.

Figure 4.7 Simulated transmission results of a differential CPW structure with cascaded 16 GHz and 32 GHz filters with centered filter-to-reference stub with and without the proposed launch structure.

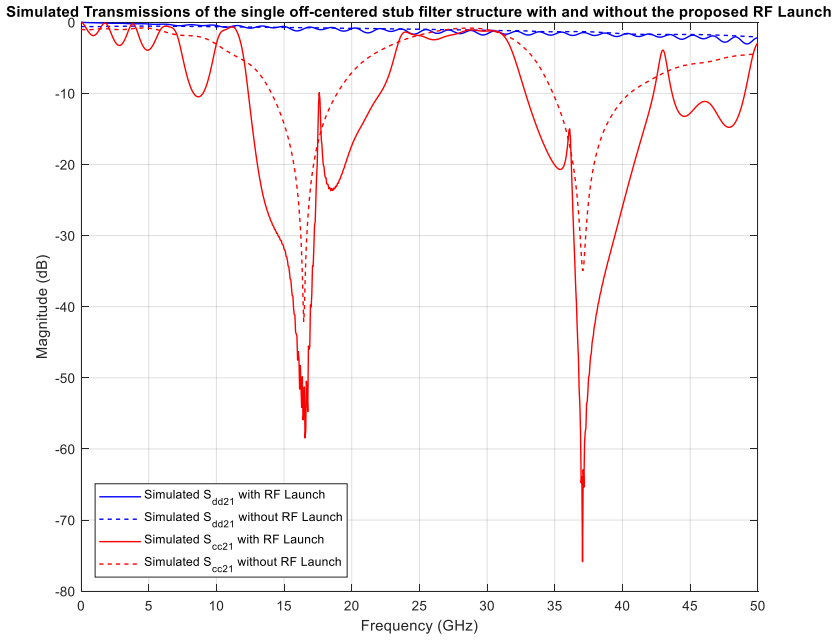

Figure 4.8 Simulated transmission results of a differential CPW structure with a single filter with off-centered filter-to-reference stub with and without the proposed launch structure.

4.2.4. Refinement of the RF Launch Design

As the plots show in Fig. 4.5, 4.6, 4.7 and 4.8, the performance of each CM filtering structure is not influenced by the launch structure; however, the ringing effect of DM transmission at higher frequencies introduces concerns over the signal integrity of the system and suggest a modest impedance mismatch from launch to transmission line.

To find a potential solution to this problem, we first kept the RF launch model unchanged and extended the transmission line model. Fig. 4.9 shows the top view of the structure with cascaded 8, 11 and 16 GHz filters and the extended transmission line model with the same filter design. The longer transmission line should not affect the matching but should introduce added phase progression. Simulation results in Fig. 4.10 are consistent with this hypothesis.

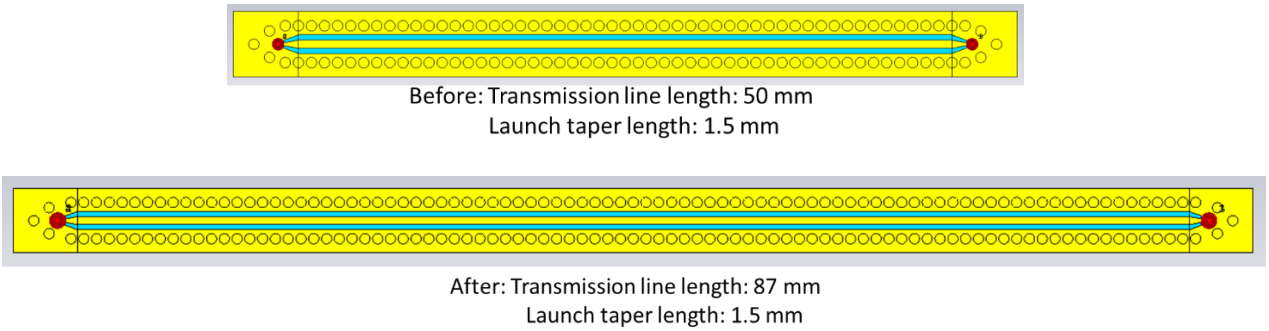

Figure 4.9 Two different transmission line models for the RF launch study.

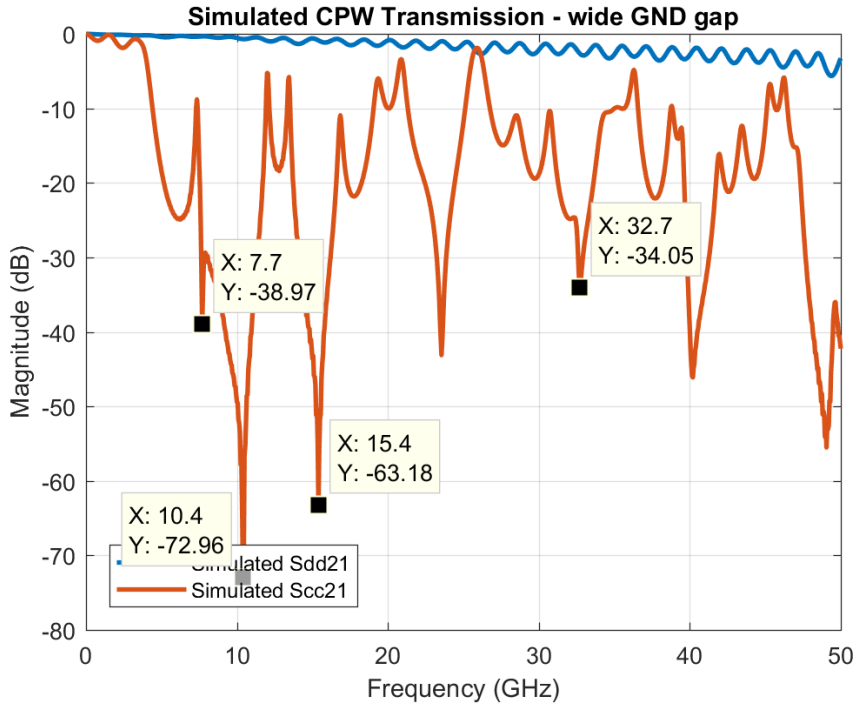

(a)

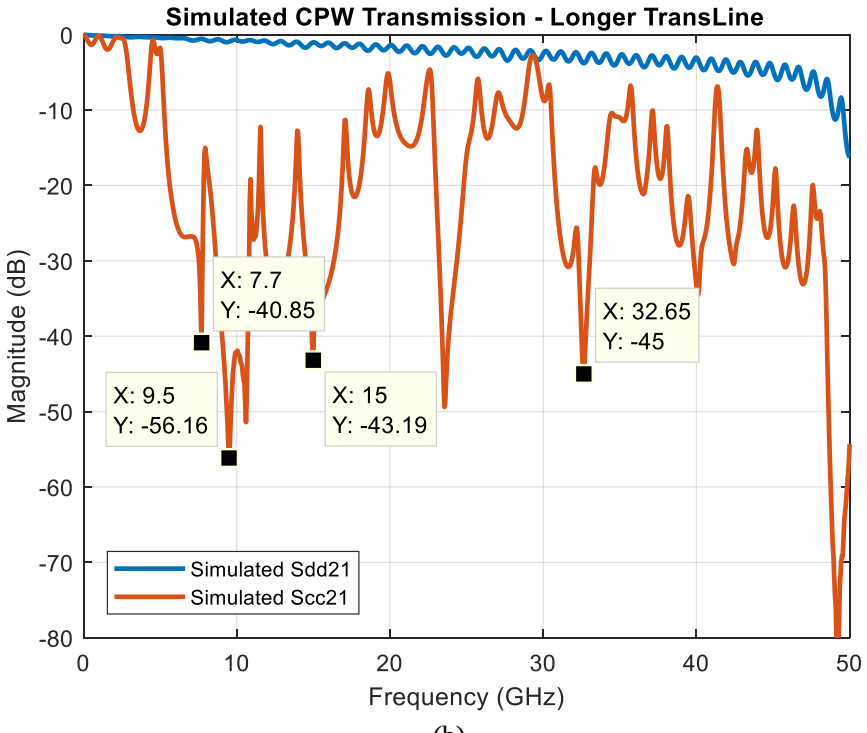

(b)

Figure 4.10 Simulated results of (a). a CPW structure with 8, 11, and 16 GHz filter with 50 mm transmission line and (b). a CPW structure with 8, 11, and 16 GHz filter with 87 mm transmission line.

We next kept the length of the transmission line unchanged and extended the taper length in the RF launch model. Figure 4.11 shows the top view of the structure with cascaded 8, 11 and 16 GHz filters and the extended taper model with the same filter design. A longer taper from the launch pad should give better impedance matching, and simulation results in Fig. 4.12 show that the mismatching is indeed reduced when a longer taper is introduced as the ripple in DM transmission is significantly reduced.

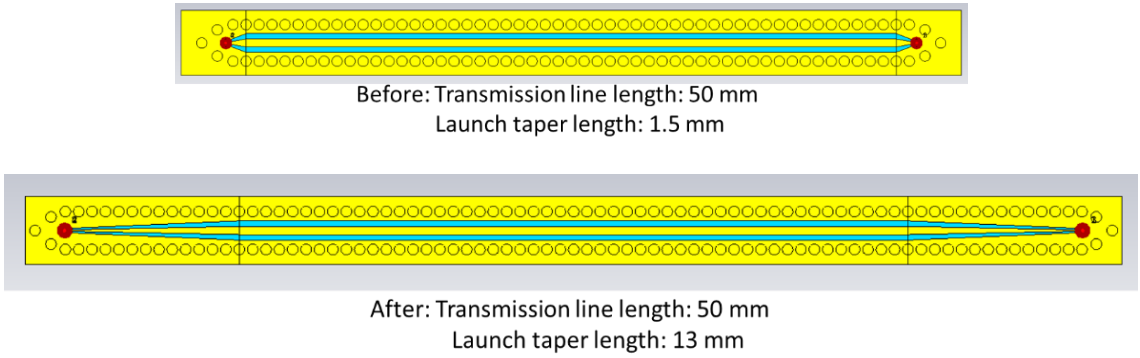

Figure 4.11 Two different taper models for the RF launch study.

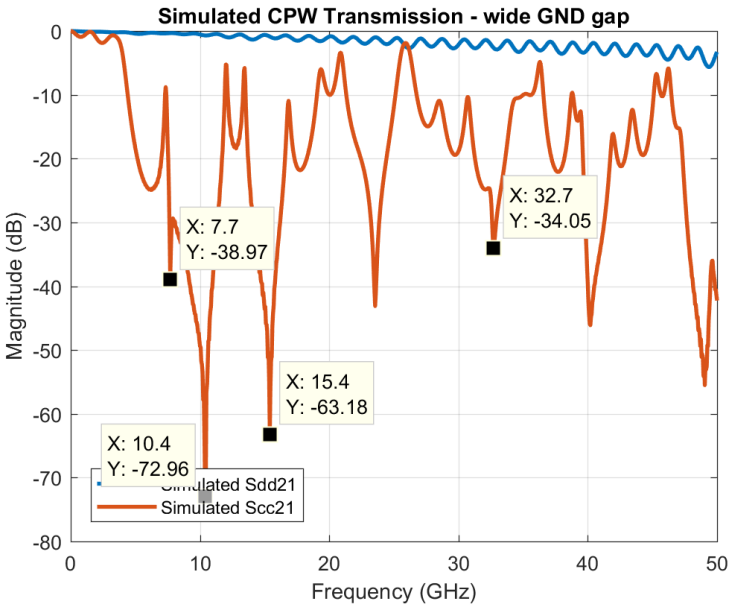

(a)

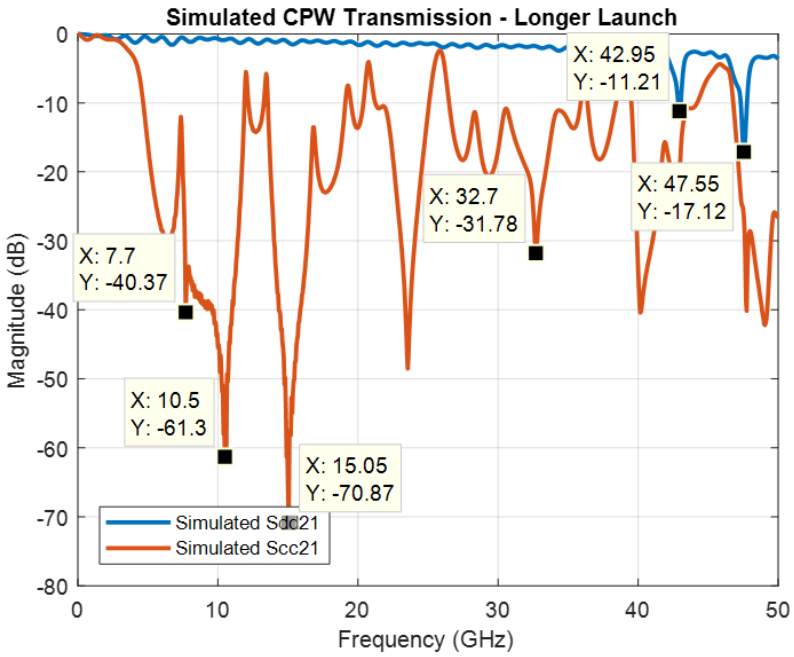

(b)

Figure 4.12 Simulated results of (a). a CPW structure with 8, 11, and 16 GHz filter with 1.5 mm launch taper and (b). a CPW structure with 8, 11, and 16 GHz filter with 13 mm launch taper.

However, results in Fig. 4.12 also introduced new challenges. The longer taper, as seen in Fig. 4.11, does not have a consistent taper to reference gap. The gap at the end of the launch is much larger than the gap at the signal pad. The small gap at the signal pad can lead to direct coupling between the pad and the reference at higher frequencies. This also resulted in the DM attenuation at 42.95 and 47.55 GHz shown in Fig 4.12. In the end, this approach, even though is proven to be able to mitigate the mismatching, was not adopted for the final production since the required length of the taper would be too long to eliminate the effect and since the initial design gave significant DM mismatches at higher frequencies.

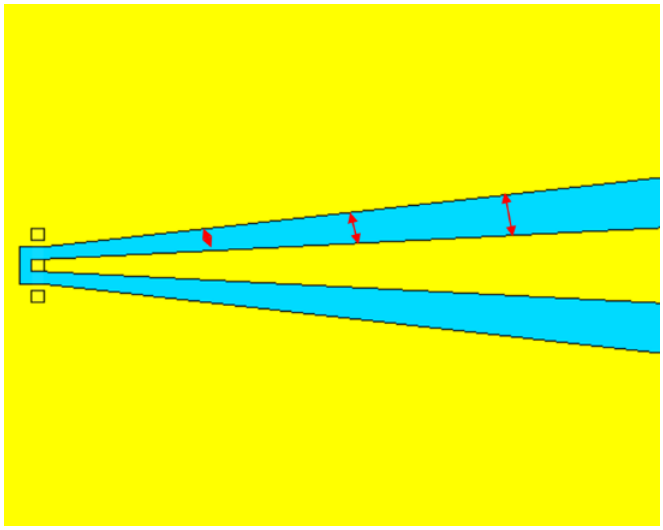

Figure 4.13 Close-up view of the RF launch model with long taper.

5. MEASUREMENT ANALYSIS

The final product, shown in Fig. 5.1 and 5.2, consists of eleven different traces in total. In addition to the six structures we mentioned in previous sections, the test board also includes two different transmission line models with no filter structure for dielectric characterization purpose: a cascaded 8, 11 and 16 GHz filter structure with narrower transmission line to reference gap, a cascaded 8, 11 and 16 GHz filter structure with smaller filter to filter spacing, and a double filter structure with one 16 GHz filter and one 32 GHz filter that have off-centered filter to reference stubs. A detailed layout and explanation can be found in Appendix A.

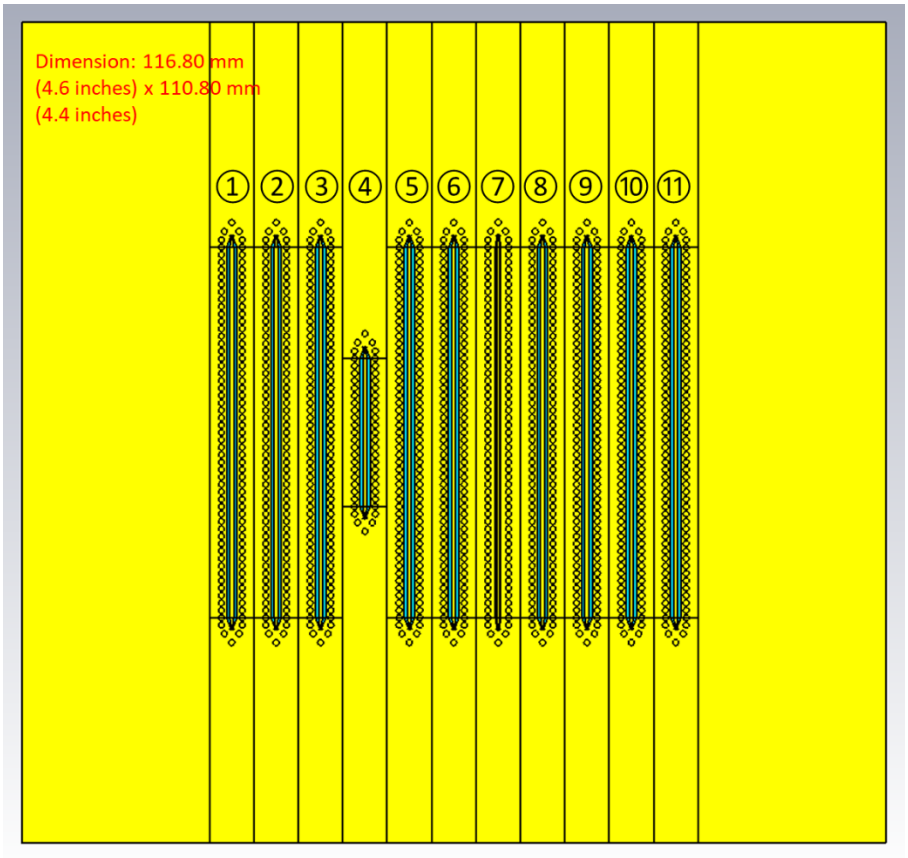

Figure 5.1 PCB model of the final product.

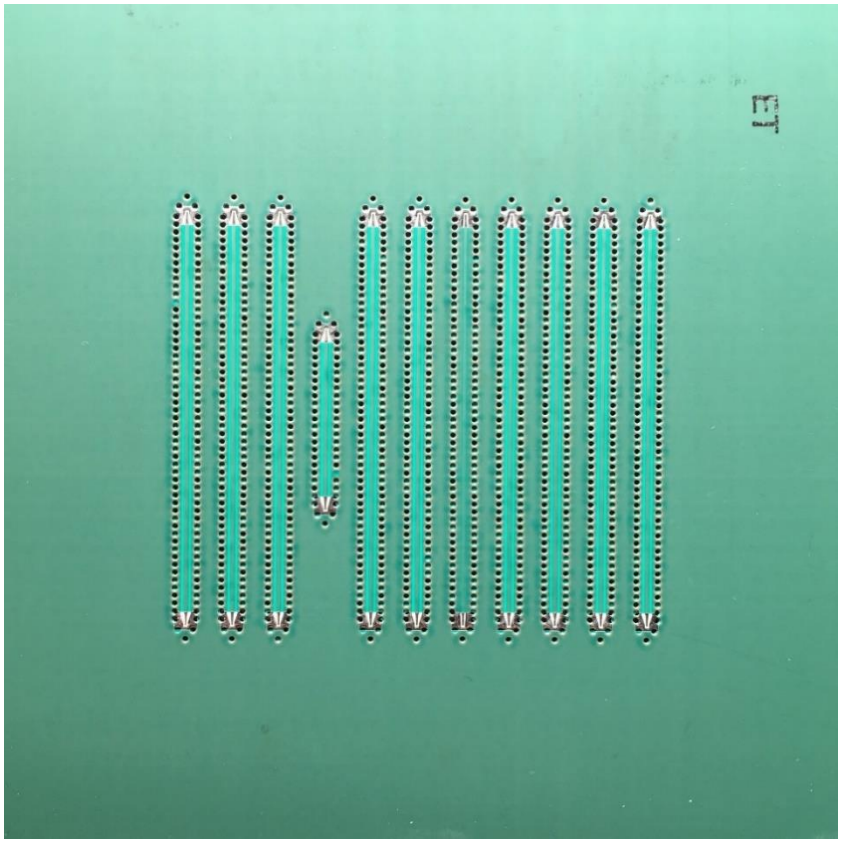

Figure 5.2 Manufactured PCB for testing.

5.1 Test Setup

The measurement testbed presented challenges since, unusually, our design for the RF signal launch does not allow measurement from one side of the board, does not allow single-sided probing – recall this choice eased the design of well-matched signal launches while avoiding the introduction of skew. The result is that the signal launch was made more feasible but made measurement more difficult as the design of the launch means that we have to land RF probes from both sides of the board at the same time. To accommodate for these constraints, a vertical testing solution was developed for our PCB testbed.

5.1.1. Equipment Setup

The test board is aligned vertically for measurement as shown in Fig. 5.3. A 3D printed plastic stand is designed and fabricated to hold the PCB in the proper position for measurement. Two 500 μm RF probes are connected to an Agilent (now Keysight) E8363B 40 GHz 2-port VNA with 2.92 mm cables. Another pair of the same type of RF probes with broadband 50 Ω loads is landed on the unused ports for matching purpose.

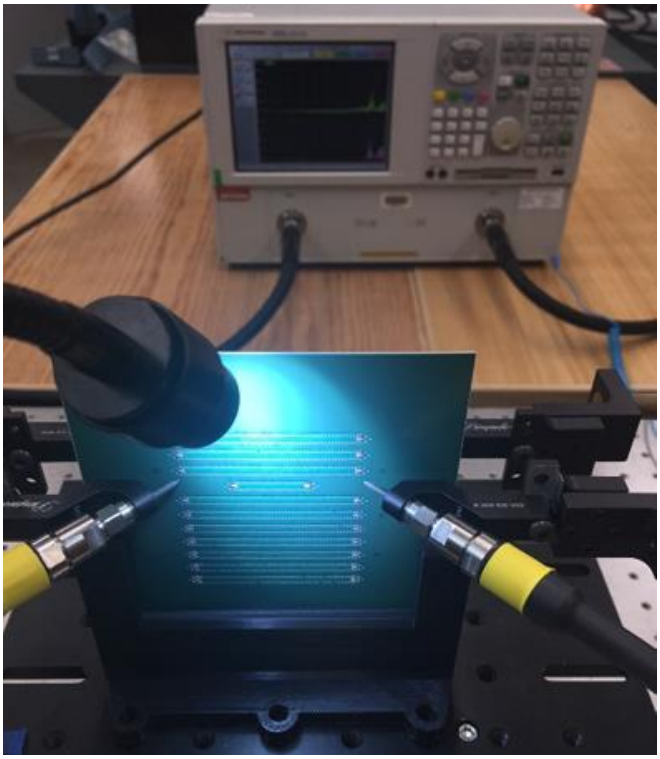

Figure 5.3 PCB measurement test setup with a 2-port VNA. The broadband loads are on the other side of the PCD, thus not showing.

To further validate our design, another test setup that utilizes an Agilent N5242A 4-port 26.5 GHz VNA with 2.92mm cables and RF probes are set at IBM Poughkeepsie and used for measurements. The setup is shown in Fig. 5.4.

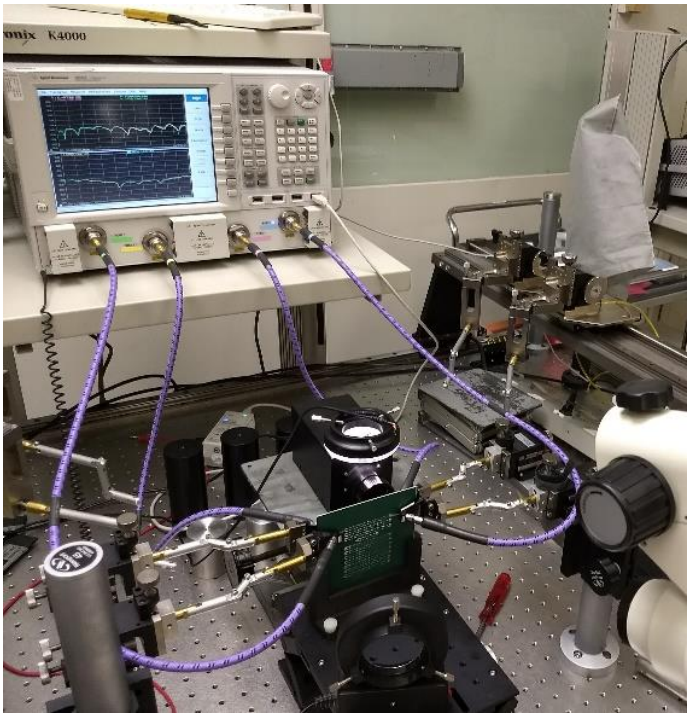

Figure 5.4 PCB measurement test setup with a 4-port VNA.

5.1.2. Calibration

Before testing, calibrations are needed to ensure accurate measurements. Two different calibration methods are performed and saved on the 2-port VNA in order to compare their results - the first method is a standard 2.92mm coaxial calibration kit and the second is an RF substrate calibration board. Both methods utilize SOLT standard, which is a calibration technique that uses defined short, open, load and thru standards in a kit at the reference plane to calibrate out potential sources of error in the VNA.

5.1.3. De-embedding Signal Launch Effects of the Structure

For our design, dielectric characterization of the manufactured PCB can be determined based on the measurements of scattering parameters of two transmission lines with no filtering element.

A shown in Fig. 6.5, a short and a long trace are used for the characterization. The lengths of the short and the long trace are 20 mm and 50 mm without the RF probe launch model, respectively. The shorter trace is used to de-embed the RF probe launch, and the longer trace is measured to give the proper reflection and transmission coefficients after de-embedding. This technique has been demonstrated in [10-14], where transmission measurements are used to determine the effective dielectric properties such as permittivity ε with the help of group and phase delay calculation.

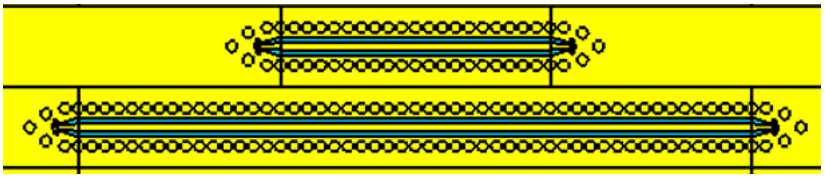

Figure 5.5 Structures used for de-embedding. No filtering element is placed in these structures.

Group delay measures the delay of the different frequency components in a signaling system. By applying the group delay method [16] to the difference of the transmission lines in fig. 5.5, we can find the change in phase of the traveling wave in a 30 mm transmission line and therefore calculate the dispersion of the dielectric material. Fig. 5.6 shows the wrapped and unwrapped phases of the traveling wave.

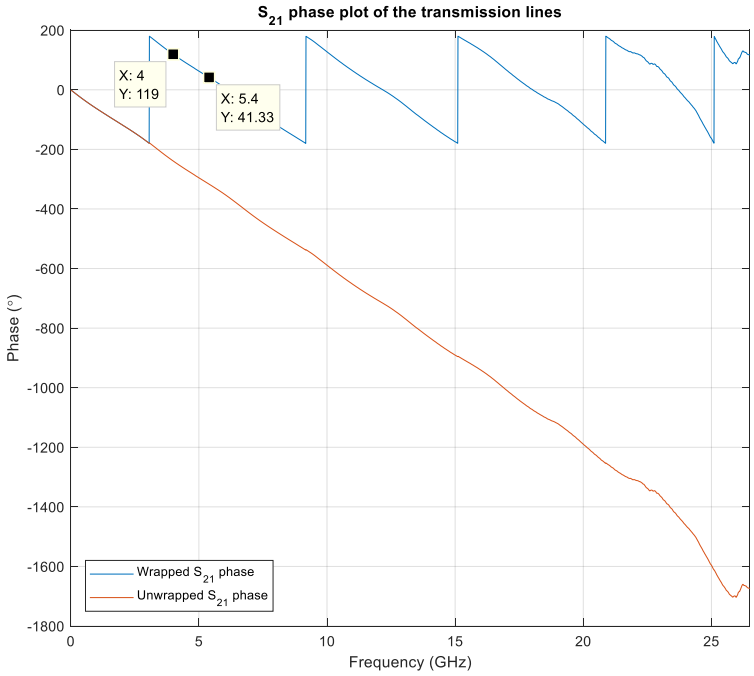

Figure 5.6 Phase plots of the difference of the transmission lines shown in Fig. 5.5.

The measured group delay τ_{gr} is the slope of this plot, and the linearity of the unwrapped phase indicates the device is non-dispersive. Therefore, the phase $\phi(f)$ is also a linear function of frequency

$$\phi(f) = \frac{-360^{\circ} f L\sqrt{\varepsilon_{eff}}}{c} \qquad \textit{(Equation 5-1)}$$

where f is the frequency in Hz, L is the length of the difference of the transmission line in meter, and c is the velocity of light in free space.

rearrange (Equation 5-1), we can get the effective permittivity

$$\varepsilon_{eff}(f) = \left(-\frac{\phi(f)c}{360^{\circ} f L}\right)^2 \qquad \textit{(Equation 5-2)}$$

and plot $\varepsilon_r(f)$ as seen in Fig. 5.7.

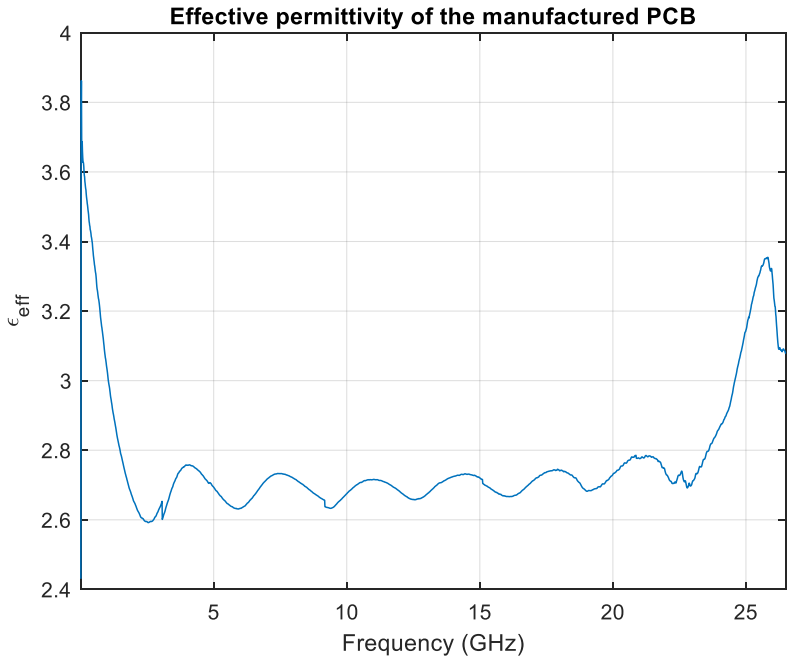

Figure 5.7 Calculated effective permittivity of the manufactured PCB.

Figure 5.7 shows that the effective permittivity of the manufactured PCB is lower than what we assumed in simulation models and may due to fabrication process variations. A smaller effective permittivity would also explain why the measured filtering frequencies are lower than expected as discussed in the next section. However, the behavior of the effective permittivity over the frequency range is hard to explain, since the effective permittivity should only increase or decrease as the frequency changes. The ripple effect shown in Fig. 5.7 could be caused by the uncertainties of the measurements. But further investigations should be conducted to verify this assumption.

5.2 Measurement Results and Analysis

5.2.1. Measurement Challenges

To measure the test board, it was set vertically on the RF station, an orientation which introduced many challenges during measurement. Due to the limitation of the 2-port VNA at Rose-Hulman, each structure requires six separate measurements to determine the complete mixed mode scattering matrix. Each measurement requires extreme care in the handling of cables and broadband loads, and adjustment of the metal arm of the probe station is often needed after each step.

In addition to the difficulties caused by the test setup, the test board itself is manufactured by an outside source, Advanced Circuits 4PCB, from Aurora, Colorado, the first time we used this vendor. A standard procedure that Advanced Circuits uses is to tin all exposed copper which caused the RF signal launches to have a finished surface which was not flat – making taking repeatable measurements of S-parameters with RF signal launches nearly impossible. The RF probes would either skate off the pads upon landing or land on a different location with a different profile, resulting in variations of signal launch due to inadequate contact or contacts which varied (since the RF probing could easily see different flex, etc. from measurement to measurement). Since the single-ended S parameter data collected was not repeatable, the mixed-mode S matrix calculated from them had was not physical showing non-reciprocal results (e.g., S_{dd21} not equal to S_{dd12}) and transmission S-parameters with a magnitude above 0 dB. Figure 5.8 shows the comparison between the simulated and measured data of the cascaded structure in section 3.5.2, where the DM transmission goes above 0 dB at several frequencies.

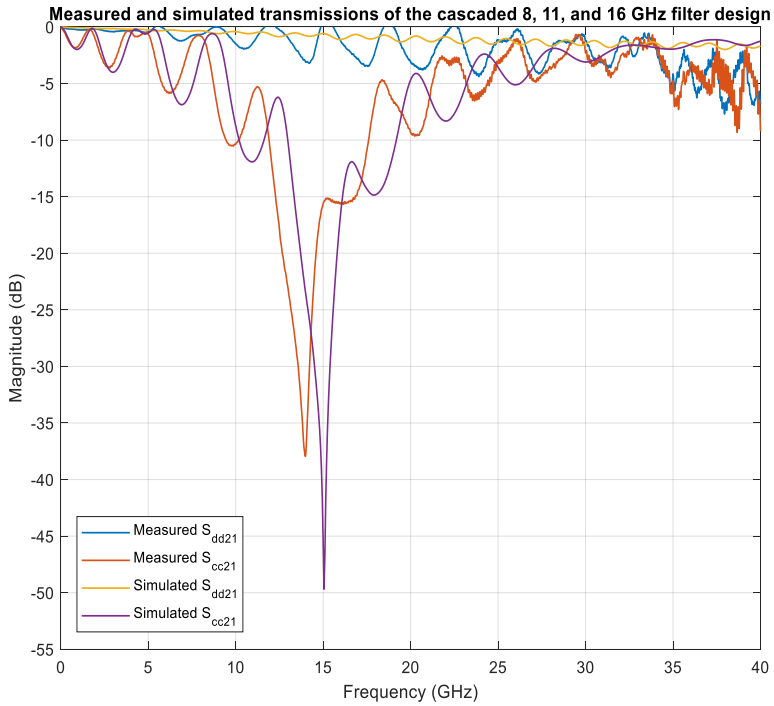

Figure 5.8 Physically impossible DM transmission results from the untreated PCB.

To fix this, Jack Shrader, one of the Rose-Hulman's ECE technicians, removed the unwanted solder from the signal pads. Figure 5.9 shows the before and after images of the signal pads. The flattened surface drastically improved our measurement repeatability. Comparisons between the simulation and measurements are shown below.

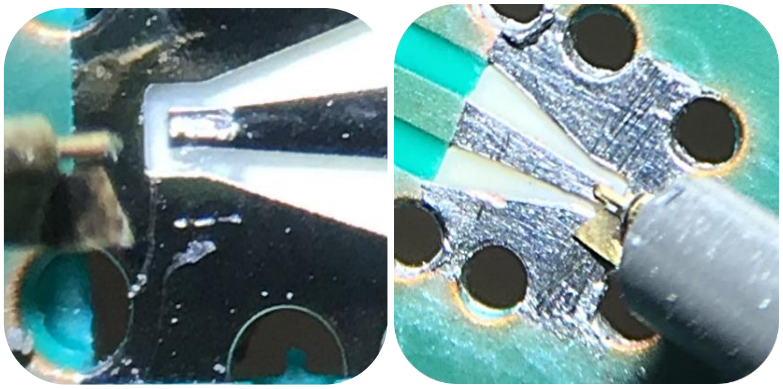

Figure 5.9 Uneven solder surface on the signal launch pad (left), and the flat pad surface after removal (right).

5.2.2. Single Filter Design at 16 GHz with 10 GHz 10-dB Bandwidth

Figures 5.10 provides comparisons between the simulated results and the direct measurements of the single filter structures we showcase in section 5.2.1. Therefore, the measured results still include the effects of the RF probe. To reduce the effect of the RF probes and signal launch pads, de-embedded measurements to 26.5 GHz using the 2-port VNA and auto fixture removal (AFR) technique are compared with simulations and shown in Fig. 5.11. The overall agreements between the simulated and measured CM and DM transmissions confirm these structures offer broadband CM filtering with excellent DM transmissions to 40 GHz. The ringing effect of DM signal using the direct measurement shown in each plot is expected (as mentioned in section 2D), since an impedance mismatch exists with the de-embedded results providing verification that the filter design is an effective solution in eliminating CM signals at a single frequency in differential CPW environments.

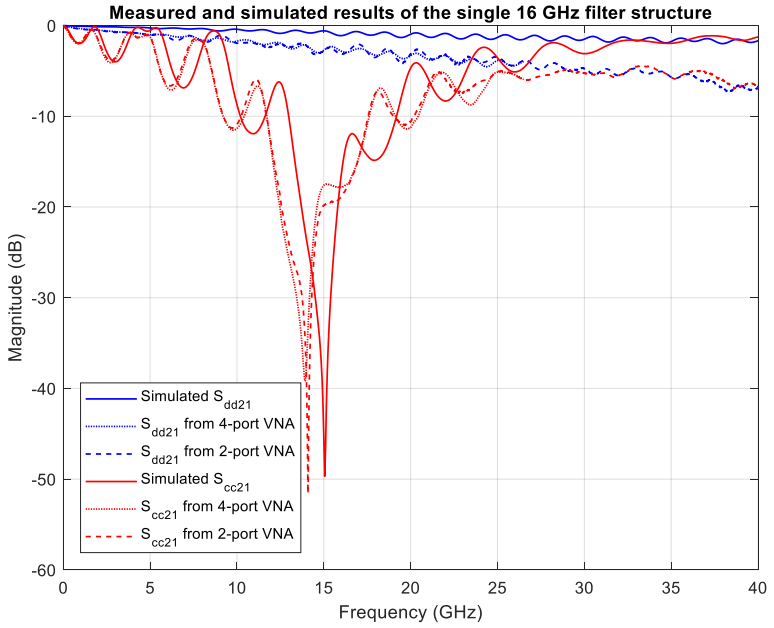

Figure 5.10 Measured and simulated transmission results of a differential CPW structure with a single 16 GHz filter.

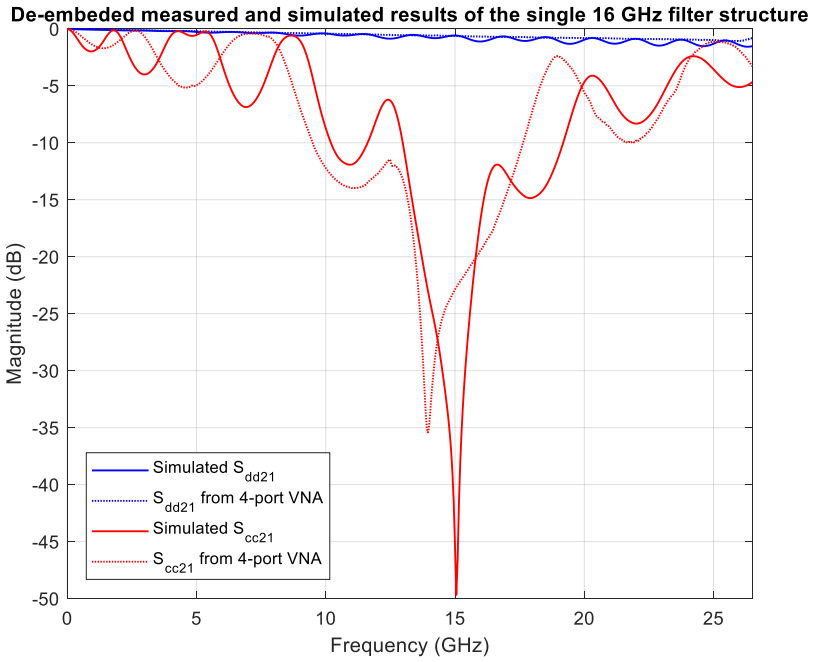

Figure 5.11 De-embedded results and simulated transmission of a differential CPW structure with a single 16 GHz filter.

5.2.3. Cascaded Filter Design at 8, 11, and 16 GHz with Multi-GHz 10-dB Bandwidths

Figures 5.12 provides comparisons between the simulated and measured results of the cascaded filter structures we showcase in section 4.2.2. The measured results include the effects from the RF probe. De-embedded measurements are shown in Fig. 5.13. Similar to the results in the previous section, the overall agreements between the simulated and measured transmissions confirm broadband CM filtering with excellent DM transmissions to 40 GHz can be achieved with our filter design. The de-embedded results solidify the fact that our filter concept can be a great solution to eliminate CM signals at multiple frequencies in differential CPW environments.

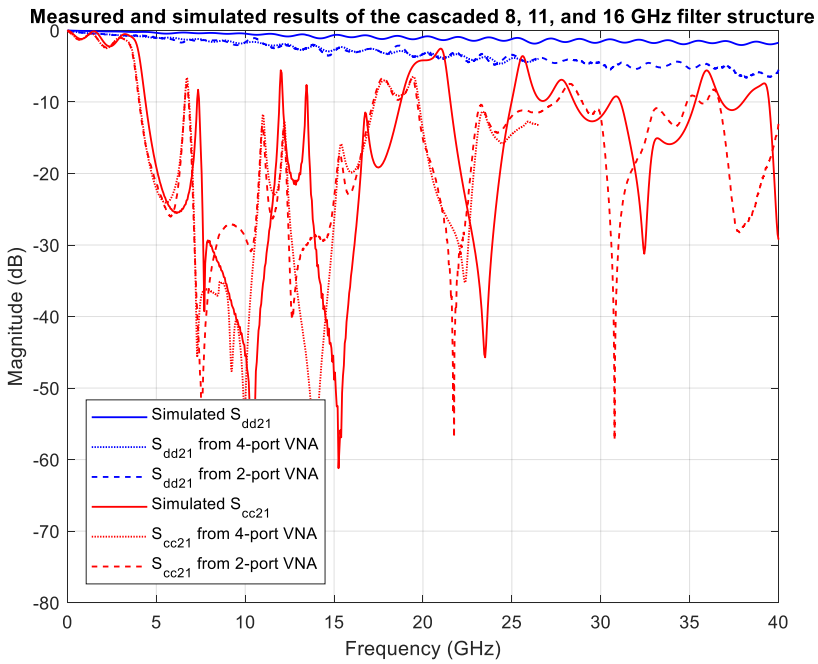

Figure 5.12 Measured and simulated transmission results of a differential CPW structure with the cascaded filters.

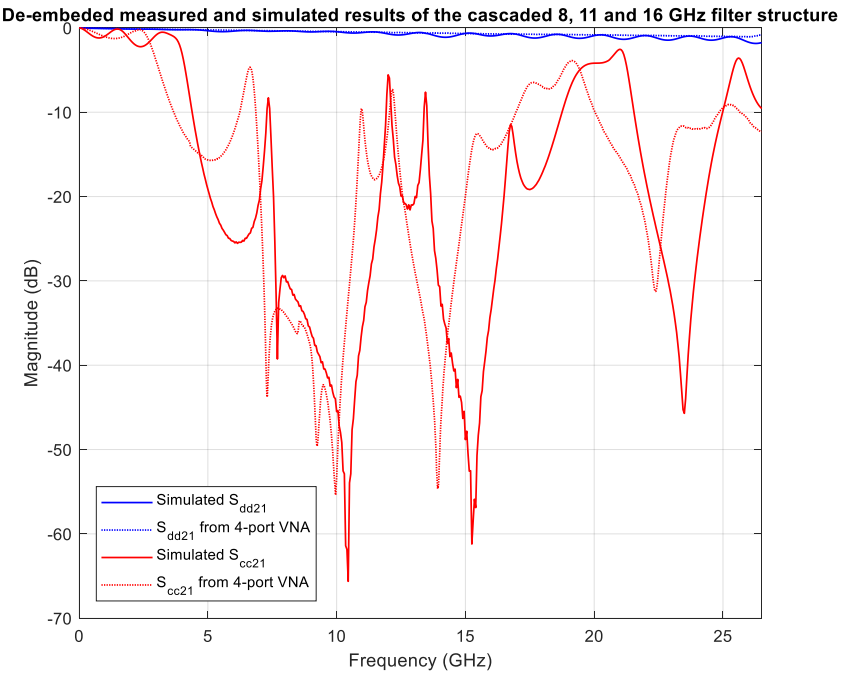

Figure 5.13 De-embedded results and simulated transmission of a differential CPW structure with the cascaded filters.

5.2.4. Centered and Off-centered Reference Stub Filter Design at 16 and 32 GHz with Multi-GHz 10-dB Bandwidths

Figures 5.14 and 5.15 provide comparisons between the simulated and measured results of the filter structures we showcase in section 5.2.3, where Fig. 5.14 shows filtering results for two half-wavelength filters with symmetric designs, and Fig. 5.15 shows filtering results for one filter that is a combination of two quarter-wavelength filters. De-embedded measurements are shown in Fig. 5.16 and 5.17. The overall agreements between the simulated and measured transmissions confirm that broadband CM filtering with excellent DM transmissions to 40 GHz can be achieved with our filter design. At the same time, results from Fig. 5.15 and 5.17 indicate that the

size of the filter structure can be greatly reduced by merging quarter-wavelength resonators together without sacrificing filtering results.

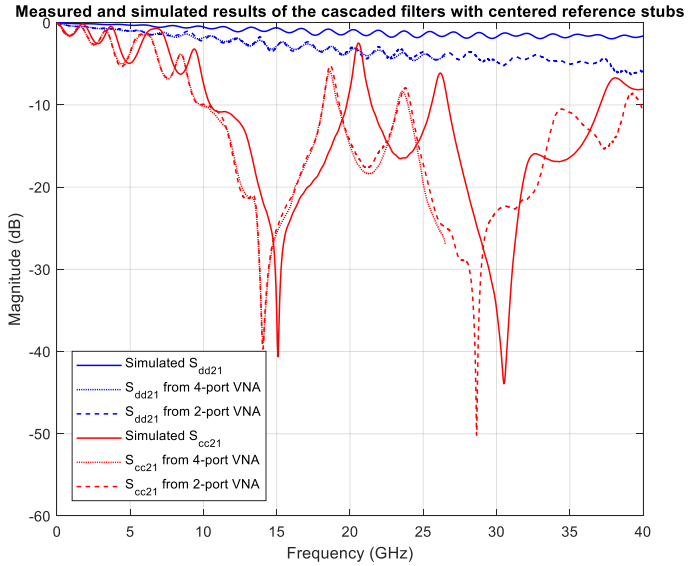

Figure 5.14 Measured and simulated transmission results for cascaded 16 GHz and 32 GHz filters with centered filter-to-reference stub.

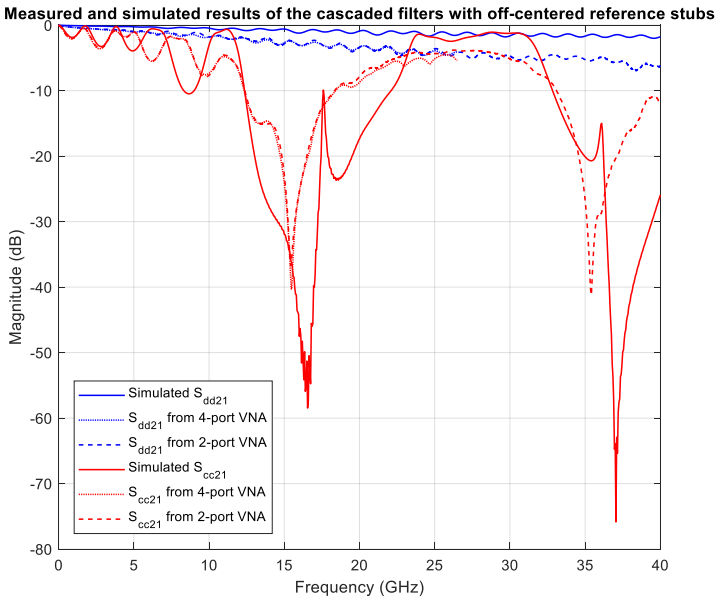

Figure 5.15 Measured and simulated transmission results for cascaded 16 GHz and 32 GHz filters with off-centered filter-to-reference stub.

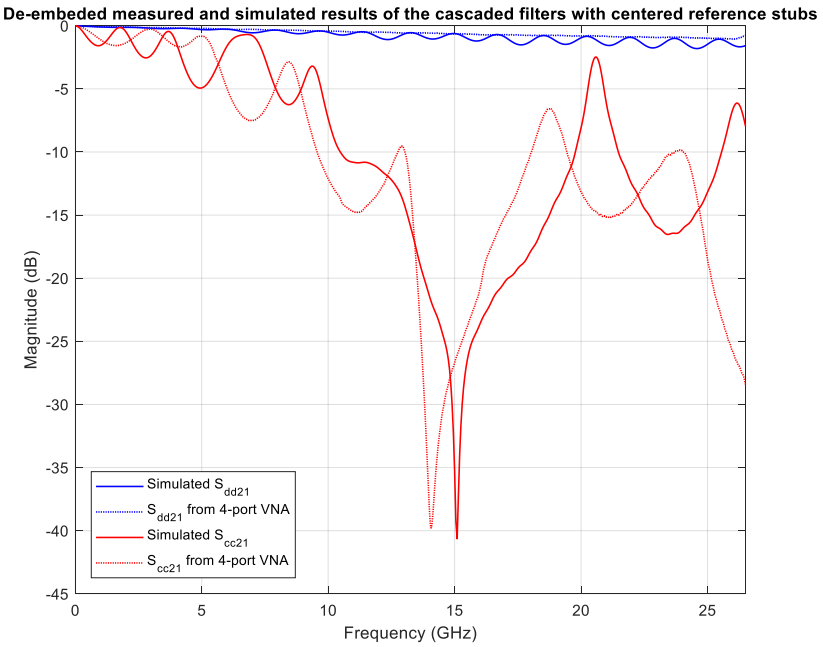

Figure 5.16 De-embedded measured and simulated results for the cascaded 16 GHz and 32 GHz filters with centered filter-to-reference stub.

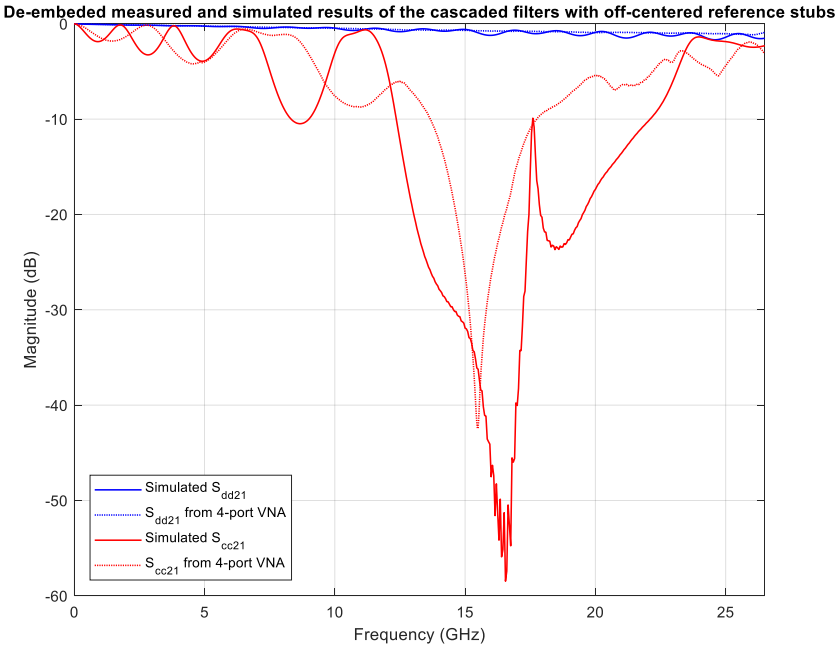

Figure 5.17 De-embedded measured and simulated results for the cascaded 16 GHz and 32 GHz filters with off-centered filter-to-reference stub.

5.2.5. Minimum Impact on DM and CM Transmissions with Different Trace to Reference Spacings

Figures 5.18 provides us insight on how the transmission line to reference spacing in a CPW structure impacts CM filtering. Measured results (Fig. 5.12) are compared with the measurement from the same structure with tighter trace to ground plane placement. With tighter spacing, the CM filtering effect is slightly reduced; However, the -10 dB bandwidth does not seem to be affected much. In fact, the filtering frequency is much closer to the frequency that we originally designed.

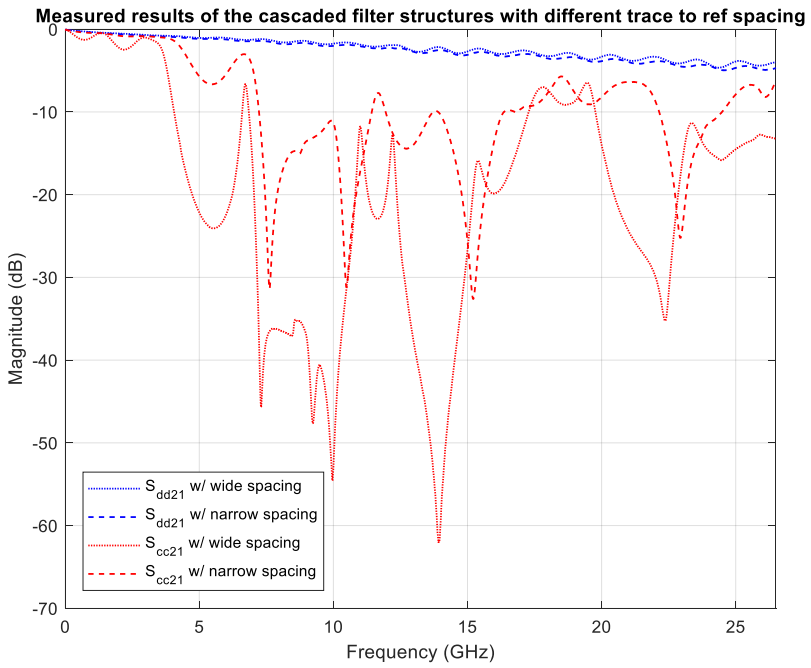

Figure 5.18 Comparison of measured results for the cascaded CM filtering structures with different transmission line to reference spacing.

5.2.6. Minimum Impact on DM and CM Transmissions with Different Filter to Filter Spacings

Figures 5.19 shows us how each individual filter affect each other on the filtering layer. Measured results (Fig. 5.12) are compared with the measurement from the same structure with a tighter filter to filter placement. The CM filtering effect does not seem to be affected to a significant degree with tighter spacing between filters. This suggests the size of our design can be further reduced, while still being able to maintain excellent CM filtering performance.

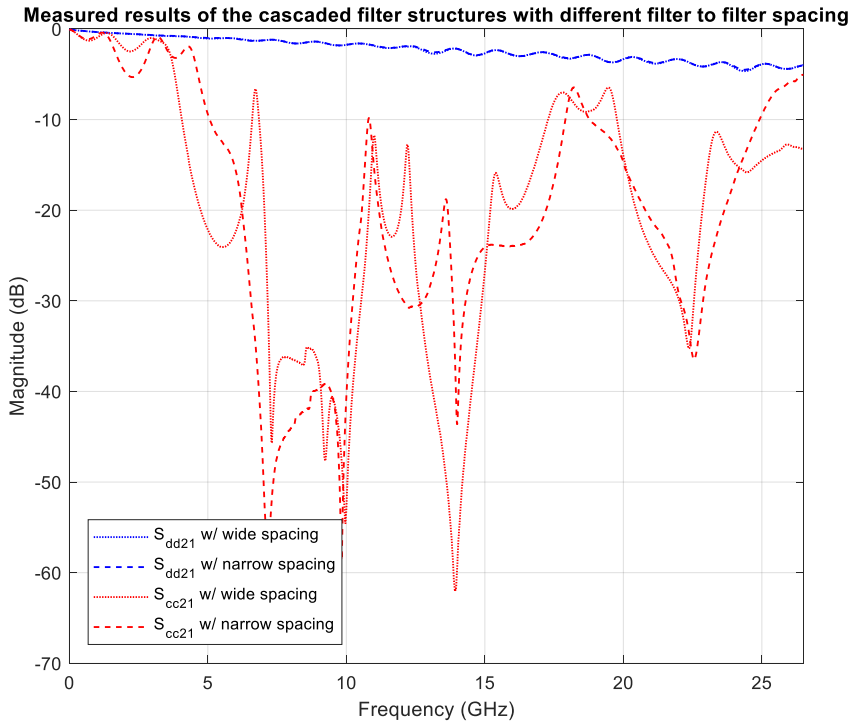

Figure 5.19 Comparison of measured results for the cascaded CM filtering structures with different filter to filter spacing.

6. CONCLUSIONS

The filtering structures introduced in this project all implement the same CM filter design concept, where a metallization layer acting as an electric wall to manipulate the CM electric flux is embedded in the horizontal plane of symmetry. The use of symmetric and asymmetric resonant structures is employed to offer broadband CM filtering in broadside coupled differential CPW structures. CM filtering is explored through modeling, simulations, and measurements. The CM filtering structures described in this work are demonstrated to offer broadband CM filtering together with effective DM transmission for high-speed signal transmission up to 40 GHz. For single filter structures, the 10-dB bandwidth is around 8 to 10 GHz and centered at desired frequencies. With cascaded designs, the 10-dB bandwidths can be expanded even further. At the same time, the de-embedded DM transmission of each structure shows less than 3 dB attenuation throughout the measured frequency range.

REFERENCES

[1] J. H. Dellinger, "The role of the ionosphere in radio wave propagation," in Electrical Engineering, vol. 58, no. 11, pp. 803-822, Nov. 1939.

[2] E. Sawyer, C. Kodama, C. O'Daniel, J. Cook and E. Wheeler, "Using common-mode filtering structures with microstrip differential lines in a multilayer printed circuit board environment," 2014 44th European Microwave Conference, Rome, 2014, pp. 1091-1094.

[3] S. G. Kang, G. Shaffer, C. Kodama, C. O'Daniel and E. Wheeler, "CSRR common-mode filtering structures in multilayer printed circuit boards," 2015 IEEE International Symposium on Electromagnetic Compatibility (EMC), Dresden, 2015, pp. 1300-1303.

[4] Y. He et al., "Common-mode filtering in multilayer printed circuit boards," 2017 IEEE International Symposium on Electromagnetic Compatibility & Signal/Power Integrity (EMCSI), Washington, DC, 2017, pp. 288-292.

[5] F. Fesharaki, T. Djerafi, M. Chaker, and Ke Wu, “Low-Loss and Low-Dispersion Transmission Line Over DC-to-THz Spectrum”, in IEEE Transactions on Terahertz Science and Technology, vol. 6, no. 4, pp. 611-618, July 2016.

[6] F. Fesharaki, T. Djerafi, M. Chaker and Ke Wu, "Mode-selective transmission line for DC-to-THz super-broadband operation," 2016 IEEE MTT-S International Microwave Symposium (IMS), San Francisco, CA, 2016, pp. 1-4.

[7] E. O. Hammerstad, Edited by F. Bekkadal, Microstrip Handbook, ELAB Report No. STF44 A74169, University of Trondheim, 1975.

[8] N. Simons, Rainee. (2002). Coplanar Waveguide Circuits, Components, and Systems.

[9] L. Shan, Y. Kwark, C. Baks and M. Ritter, "Layer misregistration in PCB and its effects on signal propagation," 2010 Proceedings 60th Electronic Components and Technology Conference (ECTC), Las Vegas, NV, USA, 2010, pp. 605-611.

[10] L. F. Chen, C. K. Ong, C. P. Neo, V. V.Varadan, and V. K. Varadan, Microwave Electronics: Measurement and Materials Characterization, England: John Wiley & Sons, Ltd, 2004.

[11] J. Baker-Jarvis, E. J. Vanzura, and W. A. Kissick, “Improved technique for determining complex permittivity with the transmission/reflection method” IEEE Trans. Microwave Theory & Tech., vol. 38, pp. 1096-1103, Aug. 1990.

[12] A. M. Nicolson, and G. F. Ross, “Measurement of intrinsic properties of materials by time domain techniques” IEEE Trans. Instrum. Meas., vol. IM-19, pp. 377382, November 1970.

[13] W. B. Weir, “Automatic measurement of complex dielectric constant and permeability at microwave frequencies” Proc. IEEE, vol. 62, pp. 3336, January 1974.

[14] J. Baker-Jarvis, M. D. Domich and R. G. Geyer, “Transmission/reflection and short-circuit line methods for measuring permittivity and permeability” NIST Technical Note 1355 (revised) National Institute of Standards and Technology, U.S. Department of Commerce, 1993.

APPENDIX A - Final Board Layout

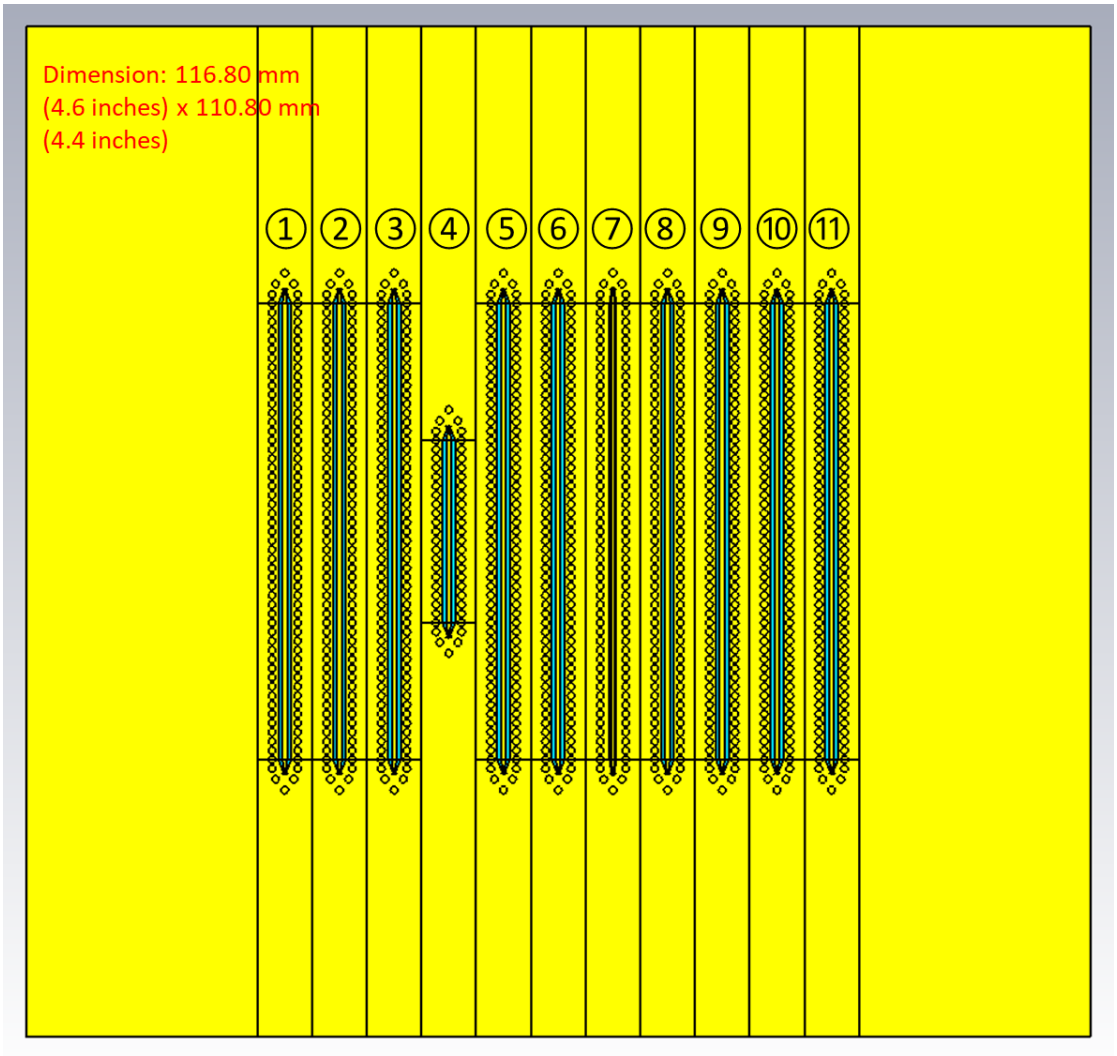

Fig. 1 PCB model of the final board.

Each numbering in Fig.1 represents a different structure:

①: Single Filter Structure: 8 GHz;

②: Single Filter Structure: 11 GHz;

③: Single Filter Structure: 16 GHz;

④: Zero filter Structure: 20 mm trans. line;

⑤: Zero filter Structure: 50 mm trans line;

⑥: Cascaded Structure: 8, 11, 16 GHz filters with wide transmission-GND(ref) gap;

⑦: Cascaded Structure: 8, 11, 16 GHz filters with narrow transmission-GND(ref) gap;

⑧: Cascaded Structure: 8, 11, 16 GHz filters with wide transmission-GND(ref) gap but smaller filter-filter spacing;

⑨: Double Filter Structure: 16 and 32 GHz filters with centered filter-GND(ref) stub;

⑩: Double Filter Structure: 16 and 32 GHz filters with off-centered filter-GND(ref) stub.

⑪: Single Filter Structure: 16 and 32 GHz filters with off-centered filter-GND(ref) stub.

APPENDIX B – MATLAB Code

Use codes shown below to plot DM and CM transmission from simulation and measurements

1. Code for DM and CM Transmissions

```
% This Script Plots both Common and Differential Modes in dB as functions
of frequency
% Ports structure and naming convention should be as follows:
%
% Port 1 <-------------------------> Port 2
% Port 3 <-------------------------> Port 4
% The S parameter files must be input as xxx.snp files in the same folder
% as this script as well as additional scripts needed to run this file.
clear;
close all;
clc
delim = ' ';
vna_header = 9;
cst_header = 11;
nfile_header = 1; % Newly generated s4p file header

%% measurement in s2p
% [VNA_f, VNA_Sdd1_dd2, VNA_Scc1_cc2] = ...
%     MixedMode_VNA('03-S21.s2p', '03-S41.s2p', '03-S23.s2p', '03-
S43.s2p', vna_header, 'MA');
% VNA_f = VNA_f./1e9;

%% Measurement in s4p
[f_n, Sdd1_dd2_n, Scc1_cc2_n, Sdd1_dd1_n, Scc1_cc1_n] = ...
    MixedMode_CST('trace11_sgf.s4p', nfile_header, 'DBA');
f_n = f_n/10^3;

 %% simulation in csv
DM = csvread('Offset_L_Sdd21.dat');
DMF = DM(:,1);
DMM = DM(:,2);

CM = csvread('Offset_L_Scc21.dat');
CMF = CM(:,1);
CMM = CM(:,2);


 %% plot DM & CM
figure;
```

```
plot(f_n,cplx2db(Sdd1_dd2_n),'b--',DMF, DMM,'b-
',f_n,cplx2db(Scc1_cc2_n),'r--', CMF,CMM,'r-');
title('Measured and simulated results of the single filter design with
off-centered reference stub');
xlabel 'Frequency (GHz)'
ylabel 'Magnitude (dB)'
legend('Measured S_d_d_2_1','Simulated S_d_d_2_1','Measured
S_c_c_2_1','Simulated S_c_c_2_1','location','southwest');
set( findobj(gca,'type','line'), 'LineWidth', 1);
grid on;
ylim([-70,0]);
xlim([0,50]);
%saveas(gcf,'Diff.png');
```

2. Code for Function MixedMode_CST

```
% Differential Mode and Common Mode S-Parameter Calculator with only the
% inputs needed for VNA Measurements in .s2p format
%
% Port 1 <------------------------> Port 2
% Port 3 <------------------------> Port 4
%
% Only S12, S14, S32, and S34 are needed as inputs.
function [f, Sdd12, Scc12, Sdd11, Scc11] = MixedMode_CST(Ss4p,
nheaderlines, sptype)
[f, S11, S12, S13, S14,~,~,~,~,S31,S32,S33,S34,~,~,~,~] = loadsNp(Ss4p,
nheaderlines, sptype, 0);
Sdd11 = 0.5*(S11-S13-S31+S33);
Scc11 = 0.5*(S11+S13+S31+S33);
Sdd12 = 0.5*(S12-S32-S14+S34);
Scc12 = 0.5*(S12+S32+S14+S34);
return
```

3. Code for Function cplx2db

```
function YDB = cplx2db(Y)
%    Converts the magnitude of complex data Y into dB values.
%    Useful for saving a step when plotting things like S-Parameters.
    YDB = mag2db(abs(Y));
end
```

4. Code for Function loadsNp

```
function [f, varargout] = loadsNp(fname, nheaderlines, sptype, freqPower,
N)
    %AUTHOR: CHRISTOPHER KODAMA christopher.kodama@gmail.com
    %Takes a touchstone (sNp) file and returns S-parameters in their
complex form.
    %nheaderlines should be the number of header lines in the sNp file.
    %For CST sNp file outputs, this is usually 4.  For the VNA, this value
    %is usually 6.
    %
    %sptype is the sNp file type. For sNp files, there are three different
file types:
    %Magnitude-angle 'MA',
    %dB-angle 'DBA', and
    %Real-Imaginary 'RI'.
    %You can check which file type your sNp file is by looking at the
header lines of your sNp file.
    %In this function, 'MA' is on by default.
    %
    %freqPower refers to the units of frequency in the sNp file.
    %If frequency is in GHz in the sNp file, freqPower should be set to 9.
The default value is 0.
    %
    %N refers to the N in sNp.  This is an optional argument; if your
    %filename has the proper extension (for example, for a 2-port
    %touchstone file (N=2), the extension should be .s2p), then this
function
    %will automatically determine N.  If you include this argument, it
    %won't read the file name and instead use the N provided.
    %
    %There are three different output methods:
    %Example 1: [f, S11, S12, S13, S1N, ... , SN1, SN2, SN3, ..., SNN] =
loadsNp('file.sNp', 4, 'RI', 9);
    %Example 2: [f, S1, S2, ... SN] = loadsNp('file.sNp', 4, 'RI', 9);
    %Where each SN is [S1N, S2N, S3N, ..., SNN], a [# frequency points]-
rows-by-[N]-columns matrix of S-parameters.
    %Example 3: [f, S] = loads2p('file.sNp', 4, 'RI', 9);
    %Where S is a [# frequency points]-rows-by-[N^2]-columns matrix of S-
parameters.
    %Example 4: [f, Sdd1_xxN, Scc1_xxN, Sdd2_xxN, Scc2_xxN] =
loadsNp('file.s4p', 4, 'MA', 9);
    %Where in CST, the differential mode was labeled as mode 1 and the
    %common mode was labeled as mode 2


    if (nargin <3)
        sptype = 'MA';
    end
    if (nargin <4)
        freqPower = 0;
    end
    if (nargin <5)
```

```
        N = str2double(fname(end-1));
        if (isempty(N))
            N = 2;
        end
    end

    file = importdata(fname,' ',nheaderlines);
    rawdata = file.data.';
    finitedata = rawdata(~isnan(rawdata));
    data = reshape(finitedata, 2.*N.^2+1, []).';

    rad = pi/180;
    f = data(:,1)*(10^(freqPower));
    S = zeros(length(data),N.^2);

    switch upper(sptype)
        case 'MA'
            for k=1:N^2
                S(:,k) = data(:,2*k).*exp(1i*data(:,2*k+1)*rad);
            end
        case 'DBA'
            for k=1:N^2
                S(:,k) = db2mag(data(:,2*k)).*exp(1i*data(:,2*k+1)*rad);
            end
        case 'RI'
            for k=1:N^2
                S(:,k) = complex(data(:,2*k), data(:,2*k+1));
            end
    end

    switch(nargout)
        case 2
            varargout{1} = S;
        case N+1
            varargout = mat2cell(S, size(S,1), ones(1,N)*N);
        otherwise
            varargout = mat2cell(S, size(S, 1), ones(1, size(S, 2)));
    end
end
```

APPENDIX C – Published Paper

Common-Mode Filtering in Multilayer Printed Circuit Boards

Yujie He[1], Zach Silva[1], Zach Bergstedt[1], Joseph Faia[1], Shelby Van Hoosier[1], Sang Goo Kang[*2], Garrett Shaffer[*3], Edward Wheeler[#1] and Michael Cracraft[+4]

[1]*Electrical and Computer Eng. Rose-Hulman Institute of Tech., 5500 Wabash Avenue, Terre Haute, IN 47803, USA*
[#]wheeler@rose-hulman.edu
[2]*Electrical Eng., Stanford University, Stanford, CA 94305, USA*
[3]*Electrical and Computer Eng, Purdue University, West Lafayette, IN 47907, USA*
[4]*IBM Systems and Technology Group, Poughkeepsie, NY 12603 USA*
+macracra@us.ibm.com

***Abstract*—Common mode (CM) conversion in differential communication links represents serious signal integrity (SI) and electromagnetic compatibility (EMC) hazards. Two types of common-mode filtering structures are investigated in this paper. The first employs complementary split ring resonator (CSRR) structures placed in the reference layer surrounded by via fences, and the second uses a composite right-/left-handed (CRLH) structure formed by placing metallic strips between the microstrip traces. Via fences were employed to surround the individual CSRR filtering structures, which allows cascading to either filter at multiple frequencies or else to broaden filtering bands. Via fences also prevent filtered CM energy from exciting parallel-plane waveguide (PPW) modes which would degrade the board's EMC and SI environments.**

Keywords*—*common mode filtering, signal integrity electromagnetic compatibility, defected ground structures differential signaling, complementary split ring resonators, composite right-/left-handed, via fencing

I. INTRODUCTION

Differential signaling paths carrying differential-mode (DM) signals support high-speed data transmission while limiting unwanted emissions since the currents on the two single-ended lines are directed oppositely. The opposing currents prevent effective radiation while offering some immunity to interference since electric and magnetic coupling usually effects both single-ended lines similarly, leaving the DM signal unaffected. Symmetry in the propagation environment is key for differential lines. Any asymmetry in the links – through either skew or unequal transmission parameters – can allow some differential-mode energy to be converted into common-mode signals which present EMC and SI hazards.

Past work has shown that CSRRs embedded in a reference plane can be used to suppress CM transmission while permitting propagation of DM signals. Cascading CSRRs of different sizes in a multilayer PCB environment can provide filtering at multiple frequencies and/or broadband filtering. CM filtering using CSRR structures has been demonstrated in 1 and 2 layer interfaces [1]-[3]. CM filtering based on 0.25λ resonators has been demonstrated and is related to the CRLH structures investigated herein [4]. CM filtering in a two-layer PCB using multiple CSRRs with varied sizes has been demonstrated from 4.5 to 7.5 GHz [5]. In multilayer printed circuit boards (PCB), crosstalk and unintended radiation can have major effects on performance. [6].

This paper will focus on the simulation and measurement of microstrip differential lines with CM filtering structures in a six-layer PCB. The designs use both top and edge launch connectors. A structure utilizing cascaded CSRRs with via fencing surrounding each CSRR structure has shown to be effective in filtering by both simulation and measurement. CM filtering structures formed by placing metallic strips between the microstrip traces can also be cascaded to realize broader band filtering or else to filter at multiple frequencies.

II. FILTERING STRUCTURES

A. *CSRR filtering structures*

CSRR structures with a variety of CM filtering frequencies were implemented on a six-layer PCB stack-up shown in Fig. 1. The CSRRs were cascaded along the signal path to increase bandwidth and filter multiple frequencies.

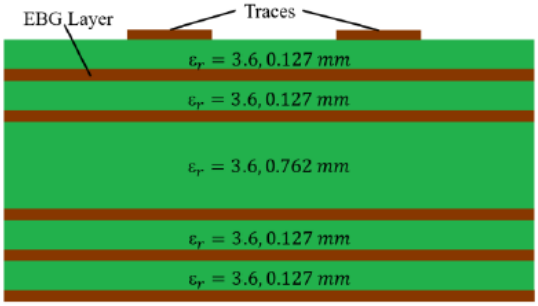

Fig. 1: Six-layer board stack up, 1 oz. copper, with 0.229 mm trace width and 0.453 mm trace separation.

The six-layer stack-up includes four CSRRs in the electromagnetic band gap (EBG) layer of the PCB, shown in Fig. 2. The EBG layer is the copper layer directly under the microstrip traces. Vias connect the EBG layer to the other reference layers in the PCB, including the layer immediately below the EBG layer.

One can gain an understanding of the mechanism for CM

filtering of the CSRR structure by first considering a split-ring resonator (SRR) – two nested conducting rings, each with a series gap. A time-varying magnetic field normal to an SRR will clearly induce a voltage about its perimeter via Faraday's law. Employing Babinet's principle, a time-varying electric field normal to a CSRR will excite the CSRR since it is the structure complementary to an SRR. Fig. 2(b) shows the electric flux patterns of DM and CM signals. Note there is a net electric flux to the reference plane for CM but not for DM. This results in a CM signal exciting the CSRR filter – resulting in CM filtering – while leaving the DM signal free to propagate relatively unaffected.

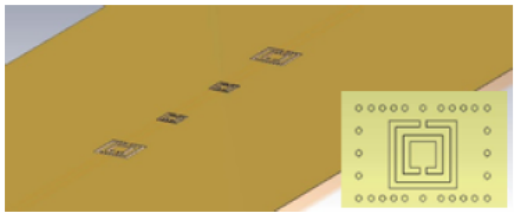

(a)

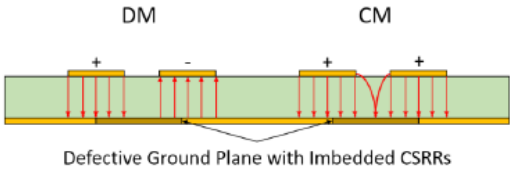

(b)

Fig. 2: (a) Cascaded CSRR in EBG layer with blow-up showing via fencing. (b) Differential microstrip pair showing electric flux line for CM and DM signals

The PCB using in this study was fabricated using Panasonic Megtron 6 which has a relative permittivity of approximately 3.6 and a loss tangent which varies from 0.005 at 1 GHz to 0.009 at 50 GHz. Via fencing placed around the CSRRs as shown in Fig. 2 isolates each filter and prevents filtered CM energy from exciting PPW modes. A diagram of a CSRR filtering structure is shown in Fig. 3. We used the parameter values in Table 1 to realize CM filtering at 6 and 12 GHz as discussed in part III.

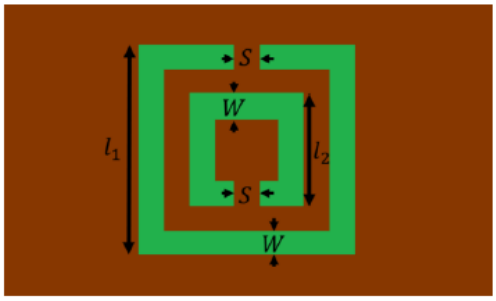

Fig. 3: Single CSRR with labeled design parameters

Table I: Design Parameters for CSRRs

	6 GHz Filtering	12 GHz Filter
l_1	2.60 mm	1.56 mm
l_2	1.50mm	1.26 mm
S	0.25 mm	0.15 mm
W	0.25 mm	0.15 mm

B. *CRLH filtering structures*

The complementary right-/left-handed filtering structures investigated here can provide broadband CM filtering or else CM filtering at multiple frequencies, depending the geometry of the CRLH structures employed.

The CRLH filter consists of a metal strip between the traces, the strip having a via to the reference layer at its center. The overall length of the strip is equal to half the effective wavelength of the target frequency ($\lambda_{eff}/2$). The strip acts as the filtering structure and is excited by a CM signal, which causes it to resonate while a DM signal does not excite the filtering structure.

Simulations were performed using the same six-layer stack-up as shown in Fig 1. The CRLH filtering structures are shown in Fig. 4.

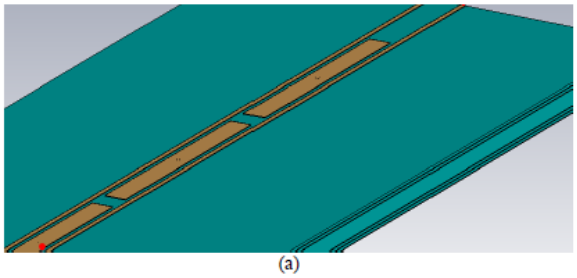

(a)

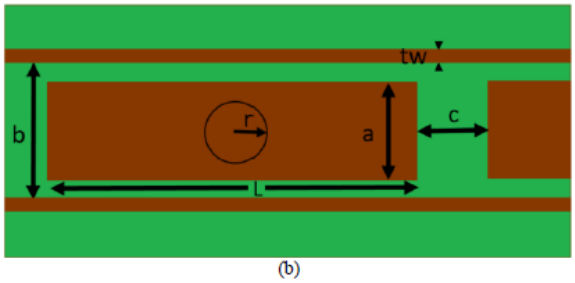

(b)

Fig 4: (a) Example metallic strip filters, (b) Parameterization of individual filter for design The following parameters were kept constant in each design: *b=1.235 mm, tw=0.233 mm, r=0.1 mm* while the other parameters were varied through simulation to vary filter performance.

III. CSRR FILTERING WITH LAUNCH CONNECTIONS

The signal launch designs are shown in Fig. 5. The edge launch is a bolt-on 2.92 mm coaxial connector. The top launch connector, shown in Fig. 5(b), was designed using a center via together with surrounding vias to realize the transition from coax to planar structure. In addition to the

vias, a small diving board structure was used on some intermediate layers to add needed capacitance and so improve the signal launch performance.

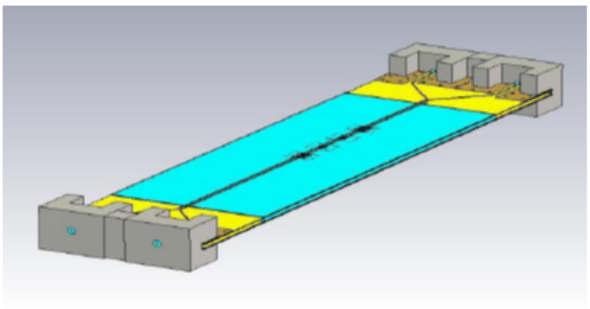

(a)

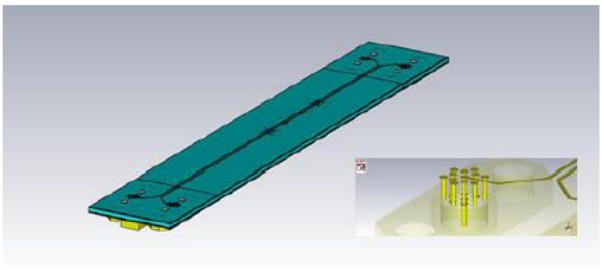

(b)

Fig. 5: (a) Edge launch CSRR CST model (b) Top launch CSRR CST model with launch design close up

Thru-reflect-line (TRL) calibration patterns were included for the top launch structures. Short-open-load-thru (SOLT) calibration was used with the end launch structures.

IV. Results

A. *CSRR Filtering Simulation & Measurement*

The cascaded CSRR filtering structures show filtering at 6, 12, and 18 GHz in measured data shown in Fig. 6(a) and the boards TRL patterns shown in Fig. 6(b).

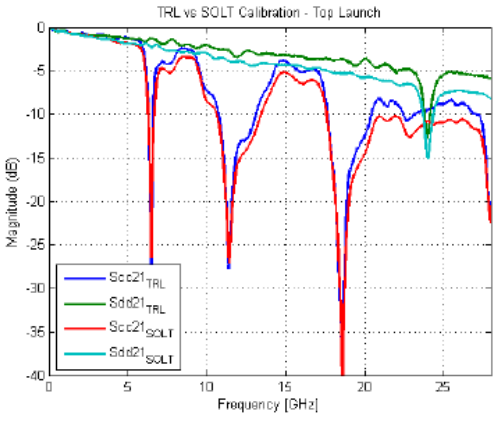

(a)

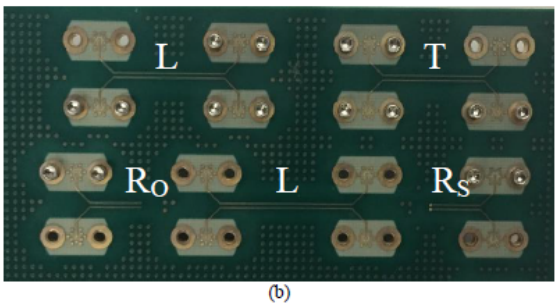

(b)

Fig. 6: (a) DM/CM results with different calibration methods (SOLT/TRL) for a CSRR filtered differential pair (b) Top launch TRL patterns on fabricated board

Comparing measurement between the TRL and SOLT calibration techniques in Fig. 6, the structure displays similar behavior for both, indicating that the launch contributes loss but adds no significant features or resonances.

The results in Fig. 7 show simulation and measurement for structures with both types of signal launch. Both provide filtering at 6, 12, 18 GHz with good agreement between simulation and measurement.

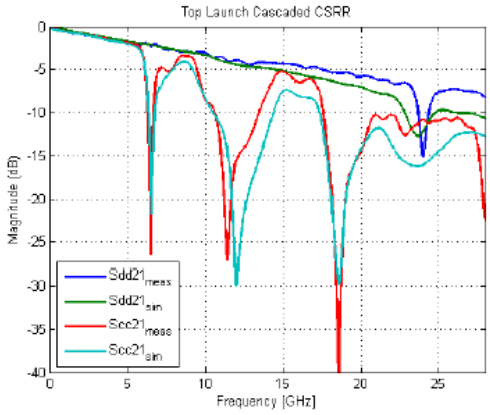

(a)

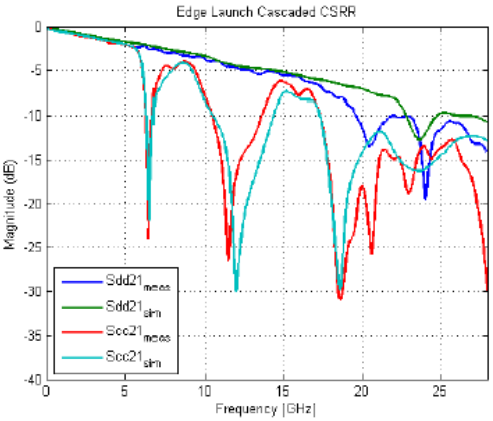

(b)

Fig. 7: (a) Simulated vs measurement for top launch CSRR structure, (b) Simulated vs measurement for edge launch CSRR structure

B. *Next Steps - CRLH Filtering*

Initial simulation results using CRLH structures suggest the feasibility of using CRLH structures for both broadband filtering and for filtering at multiple frequencies. To achieve broader band filtering, multiple structures are placed in cascade, each differing slightly in length. The initial results are shown in Fig 8. Adding two, three, and four filters in cascade with slightly varied lengths results in effective filtering over a broader band than one filter. It is important to note that differential transmission was unaffected. Sdd21 with the filter and without are shown to be on top of one another in Fig. 8. Since the filters are designed to operate at $\lambda_{eff}/2$ (which is approximately 11 mm at 7 GHz in Megtron 6), one can readily suppose that cascading filters of shorter lengths could increase the effective filtering bandwidth through the overlapping of the filtering effect of the individual structures.

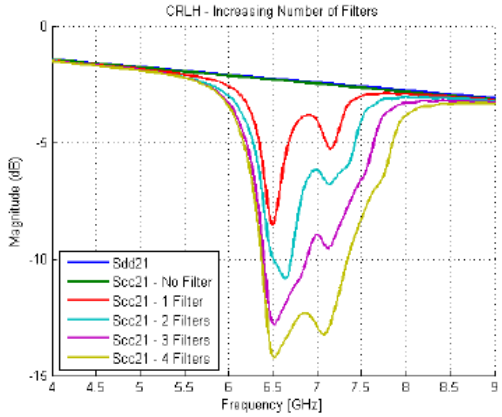

Fig 8: CM filtering with multiple filters in cascade with slightly varying lengths (L1=11.07 mm, L2=10.79 mm, L3=10.52 mm, L4=10.24 mm)

By using a cascade of filtering structures with larger differences in length, one can obtain filtering at multiple frequencies as shown in Fig. 9. The filters are designed to attenuate at 7 GHz (L = 11.07 mm) and at 14 GHz (L = 5.50 mm).

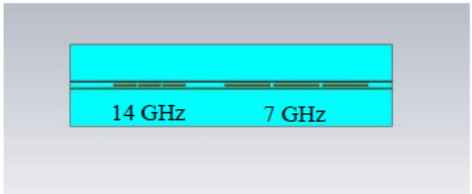

(a)

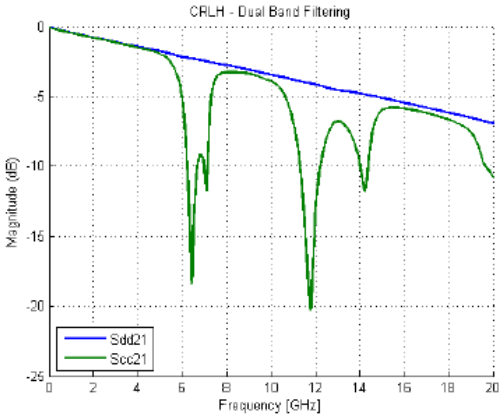

(b)

Fig. 9: (a) Top view of CRLH filtering structure with labeled filters to its targeted frequency, (b) Sdd21 and Scc21 showing dual band filtering at 7 GHz and 14 GHz

Three 7 GHz filters were cascaded with three 14 GHz filters, as shown in Fig. 9(a) but adding more filters of either length would increase the filtering at the respective target frequencies.

Surface current in the filters at the two filter frequencies provides a visual confirmation of the mechanism of CM filtering with CRLH structures. Fig. 10(a) shows surface current at 6.6 GHz. The higher surface current in the top three lower frequency filters shows that these structures are excited by the signal, versus the lower three structures which are unexcited. Fig. 10(b) shows surface current at 14 GHz which now illustrates higher current density in the lower structures with the upper ones now unexcited.

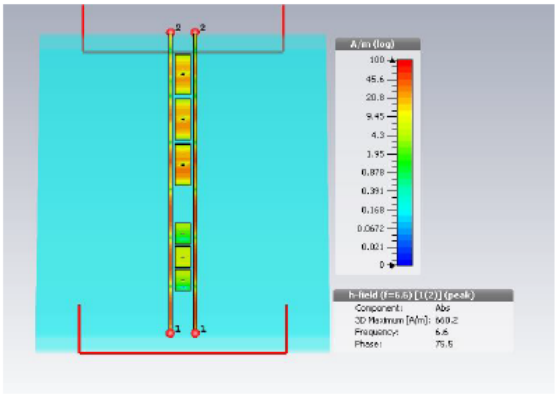

(a)

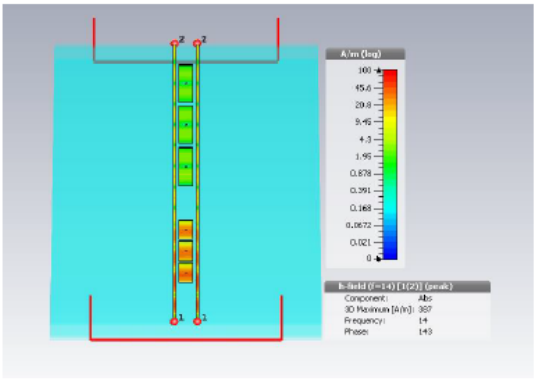

(b)

Fig. 10: (a) Surface current at 6.6 GHz, (b) Surface current at 14 GHz

We also carried out simulations for a range of values of the width of metallic strip between the traces (a) while keeping the trace separation constant, thus varying its coupling to the differential lines. The results of a parameter sweep of this width (a) are shown in Fig. 11.

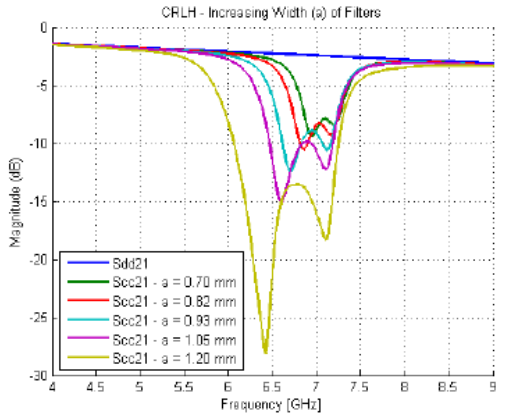

(a)

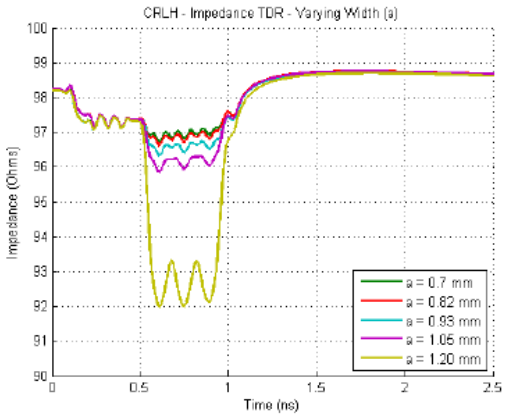

(b)

Fig. 11: (a) CM filtering obtained by varying the filter width (parameter 'a' in Fig. 3(b) from 0.7 to 1.2 mm (b) TDR Differential Impedance Simulation with the same width variation

With a=0.7 mm, common mode attenuation is less than 10 dB but, as the width increases, so does the CM filtering attenuation and bandwidth. At a=1.20 mm, the 10 dB attenuation bandwidth is approximately 1 GHz. Fig. 11(b) provides evidence that the DM impedance is more strongly affected as coupling increases with the filter element width is increased. As the width of the filter increases, the differential impedance drops. This effect is limited as long as the coupling is relatively week but, as the width increases, the differential impedance is affected more strongly as shown in Fig. 11(b). A tradeoff therefore exists between broadband CM filtering and effective DM transmission when using these CRLH structures for filtering.

V. CONCLUSION

This paper demonstrates effective CM filtering using CSRR structures. Measurement and simulation results for these structures employed in a six-layer PCB demonstrate effective CM filtering at multiple frequencies. Simulation results for CRLH filtering structures used in the same six-layer PCB also demonstrate its potential for broadband filtering or for filtering at multiple frequencies.

ACKNOWLEDGMENTS

The authors would like to thank Computer Simulation Technology (CST) and Rogers Corporation for the generous support offered through their University Programs.

REFERENCES

[1] T.-L. Wu, Chung-Hao Tsai, Tzong-Lin Wu, Itoh, T., "A Novel Wideband Common-Mode Suppression Filter for Gigahertz Differential Signals Using Coupled Patterned Ground Structure," IEEE Trans. Microw. Theory Tech., vol.57, no.4, pp.848-855, April 2009.

[2] E. Sawyer, C. Kodama, C. O'Daniel, J. Cook, and E. Wheeler, "Using Common-Mode Filtering Structures with Microstrip Differential Lines in a Multilayer Printed Circuit Board Environment," 2014 European Microwave Conference, October 5-10, Rome, Italy.

[3] J. Naqui, A. Fernández-Prieto, M. Durán-Sindreu, J. Selga, F. Mesa, J. Martel, F. Medina, and F. Martín "Common-Mode Suppression in Microstrip Differential Lines by Means of Complementary Split-Ring Resonators: Theory and Applications" IEEE Trans. Microw. Theory Tech., vol.60, no.10, pp.3023 -3034, October 2012.

[4] Q. Liu, G. Li, V. Khilkevich and D. Pommerenke, "Common-Mode Filters With Interdigital Fingers for Harmonics Suppression and Lossy Materials for Broadband Suppression" IEEE Trans. Electromagn. Compat., vol. 57, pp. 1740-1743 (2015).

[5] S. N. Khan, X. G. Liu, L. X. Shao and Y. Wang, "Complementary Split Ring Resonators of Large Stop Bandwidth," Prog. In Electromagn. Research Letters, vol. 14, pp. 127-132, 2010.

[6] S. Kang, G. Shaffer, C. Kodama, C. O'Daniel, E.Wheeler, "CSRR Common-Mode Filtering Structures in Multilayer Printed Circuit Boards," 2015 International EMC Symposium, Dresden, Germany.

APPENDIX D – Submitted Paper

Broadband Common-Mode Filtering in Differential Coplanar Waveguides

Yujie He, Joseph M. Faia, *Graduate Student Member, IEEE*, Michael Cracraft, *Senior Member, IEEE*, and Edward Wheeler, *Senior Member, IEEE*

***Abstract*— Coplanar waveguides can provide effective transmission with low dispersion into the millimeter-wave frequencies. Differential transmission lines carrying differential-mode signals display an enhanced immunity to outside interference when compared to single-ended transmission lines and are less likely to interfere with other signals through near-field electric or magnetic coupling or through unintentional electromagnetic radiations. Electromagnetic compatibility and signal integrity environments can be enhanced at the board level through the use of differential signaling. One hazard present in differential signaling is common-mode conversion, which describes the conversion of differential-mode signal energy to common-mode, which can then produce unintentional radiation as well as degrade electromagnetic compatibility and signal integrity environments. Due to the negative effects of common-mode signals, filtering structures are used to suppress the propagation of these common-mode signals. The common-mode filtering structures described herein are demonstrated to offer broadband common-mode filtering together with effective differential-mode transmission into millimeter wave frequencies. Design equations are presented to allow circuit designers to include filtering structures in which the common-mode filtering frequency has a straightforward and physics-based relationship to the structure's dimensions.**

***Index Terms*— Coplanar waveguide, common-mode filtering, electromagnetic compatibility, signal and power integrity**

I. Introduction

Since their introduction, coplanar waveguides (CPWs) have been used in printed circuit boards (PCBs) and in integrated circuits (ICs) [1-3]. A CPW structure can have effective transmission and low dispersion into the millimeter wave frequencies [4], making it a viable candidate in a range of microwave and millimeter-wave applications. Recent work has also shown that a conductor backed coplanar waveguide with sidewalls can provide transmission from DC to 0.5 THz, demonstrating the potential of CPW structures in high-speed and high-frequency applications [5-6].

A differential transmission line system comprises two single-ended transmission lines, with the common-mode (CM) voltage being the average of the two single-ended voltages and the difference between two single ended voltages being the differential-mode (DM) voltage and carries the data. Since the information of a differential signaling system is carried by the difference between a pair of closely placed traces, it displays an enhanced immunity to outside interference and is less likely to interfere with other signals whether through near-field electric or magnetic coupling or through unintentional electromagnetic radiation when compared to a single-ended transmission line. Therefore, the board-level electromagnetic compatibility (EMC) and signal integrity (SI) environments can be enhanced with the use of differential signaling.

In an ideal differential transmission system, the two single-ended transmission lines making up the differential link have identical lengths and environments. In this ideal DM transmission system, no DM mode energy will be converted to CM. In practice, however, this ideal differential transmission line often cannot be realized – routing requirements can lead to differences in effective length resulting in signal skew and brings one of the lines being closer to some circuits and farther from others, leading to differences in parasitic electric and magnetic couplings. Because CM currents, unlike DM currents, are in the same direction, they display much higher levels of unwanted radiation, resulting in serious EMC and SI hazards. Since CM conversion is always present in any practical PCB environment, CM filtering can play an important role in designs leading to good EMC and SI characteristics [7-11].

In this paper, broadside coupled differential CPW waveguides, comprising two single-ended CPWs, are investigated with vias connecting the references together. CM filtering elements can be placed in a metallization layer placed between the broadside coupled differential CPW waveguides. These CM filtering elements are dipole-like resonant structures, which are demonstrated, through simulation and measurement, to suppress CM transmission while allowing propagation of DM signals in multilayer PCBs from DC up to 40 GHz. Models are developed for the CM filtering elements, which allow the filtering frequencies to be predicted using simple design equations. A sensitivity analysis was also conducted which shows that the effectiveness of differential CPW waveguide's

Manuscript received -- ,----; This work was supported in part by the Lawrence J. Giacoletto Endowed Chair.

Y. He, J. M. Faia and E. Wheeler are with the Department of Electrical and Computer Engineering, Rose-Hulman Institute of Technology, Terre Haute, IN 47803 USA (corresponding author, E. Wheeler, wheeler@rose-hulman.edu).

M. Cracraft is with IBM Systems and Technology Group, Poughkeepsie, NY 12603 USA.

transmission and its CM filtering performance is maintained in the presence of moderate levels of layer to layer misregistration.

II. Board Design

The differential CPW waveguide structure modeled in this paper is constructed of two single-ended CPWs with broadside coupling. Each of the two single-ended CPWs consists of a center conductor with coplanar references as illustrated in Fig. 1a. Since the EM field's symmetry under differential mode excitation results in an effective electric wall midway between the center conductors, sections of metallization placed between the CPWs as shown in Fig. 1b have little effect on DM transmission through mm-wave frequencies but act as CM filters.

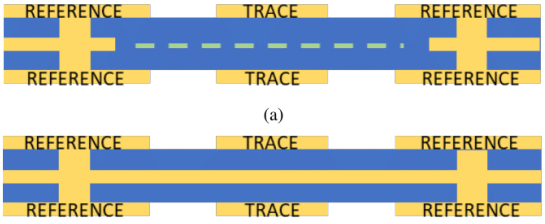

Fig. 1. (a) Cross-section of the broadside coupled differential CPW structure, where the dotted pale green line represents the effective electric wall of symmetry and (b) Cross-section of a broadside coupled differential CPW structure where metal patches exist for CM filtering.

A. *Filter Design*

In order for the CM filtering structures to be effective, they can either result in significant changes to CM electric or magnetic flux or else form resonant structures excited by net electric coupling. In order for filtering structures to be viable candidates for using in differential signaling, they should also have little effect on DM signals. The electric flux for the cross-section of a broadside coupled differential CPW under CM and DM signals is shown in Fig. 2, with Figs. 2a and 2b showing cross-sections with no CM filter present and Figs. 2c and 2d showing the cross-section with the CM filter present. Fig. 2 serves to illustrate these two factors. The first is that the proposed CM filter affects the electric flux pattern of CM signals to a greater extent than DM signals, and second that there is net flux to the filtering structure when a CM signal is present and no net flux when a DM signal is present. Net flux to the CM filtering structure excites resonances leading to effective filtering which can be predicted from filter's length as discussed below.

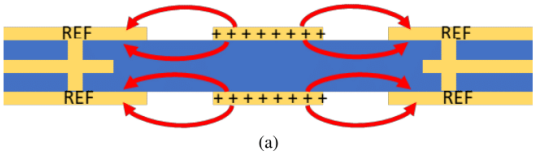

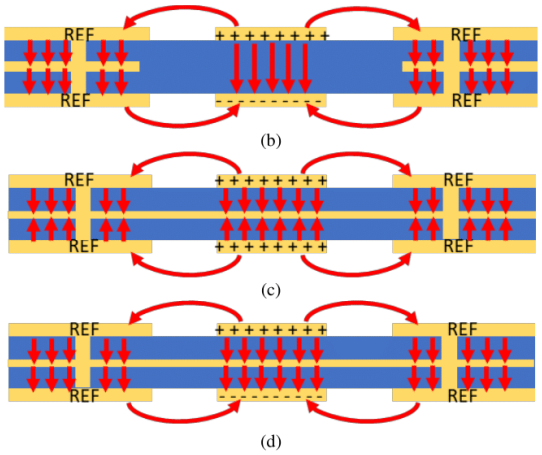

Fig. 2. Cross-section view of the electric field flux pattern of the differential CPW structure under (a) CM signal with no CM filter present, (b). DM signal with no filter, (c) CM signal with filter, and (d) DM signal with filter.

As an example, consider a design to filter CM signals at 16 GHz. The dielectric used is Rogers RO4350B with a relative permittivity of 3.48 at 10 GHz with a dissipation factor of 0.0037. A thin layer of Rogers RO4450F film, relative permittivity being 3.52 at 10 GHz with a dissipation factor of 0.004, is used for bonding and is included in simulation models as seen in Fig. 3b. In addition to providing a reference connection of the CM filters, via fences are placed along the CPW transmission line, which have an added benefit of preventing filtered CM energy from exciting parallel-plane waveguide modes [9].

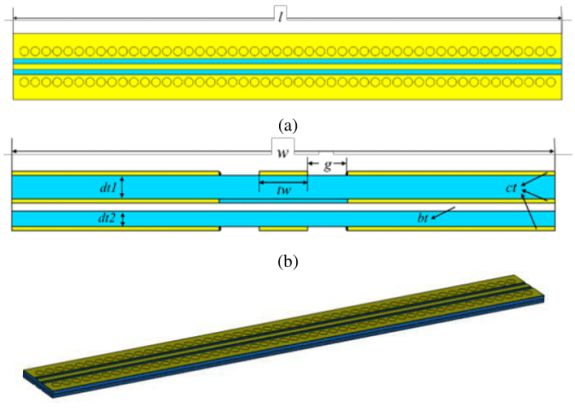

Fig. 3. (a). Top view which is identical to the bottom view; (b). cross-section view of the PCB, where the bonding film is shown in white; (c). perspective view showing overall structure.

The filter design consists of a metal patch with two stubs connecting the structure to the surrounding reference metallization. The filter resonates when the distance from a stub end to patch end is an odd number of quarter wavelengths.

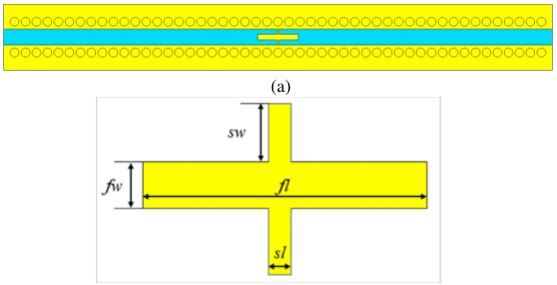

(a)

(b)

Fig. 4. (a). Filter layer view of the original single filter design; and (b). Close-up view of a single filter.

TABLE I
DIMENSIONS RESULTING IN CM FILTERING AT 16 GHZ

Parameters	Value (mm)	PARAMETERS	Value (mm)
ct	0.0432	*tw*	0.5360
dt1	0.2540	*g*	0.4432
dt2	0.1676	*fw*	0.5360
bt	0.0963	*fl*	3.6981
w	6.0000	*sw*	0.4432
l	50.000	*sl*	0.1250

Table 1 shows dimensions for this particular board design with *ct*, *dt1*, *bt*, and *dt2* representing the thickness of the metallization, top dielectric, bonding film and bottom dielectric, respectively. The filtering element acts as a half-wavelength resonator, where the effective filter length l_{eff} corresponds to the half-wavelength at the target filtering frequency and can be expressed as

$$l_{eff} = 2(\frac{fl}{2} + \frac{fw}{2} + sw) \quad (1)$$

Resonances occur at $l_{eff} = n\,\lambda/2$, where n = 1, 3…. With the geometries considered in this paper, the length extension due to fringing capacitance does not affect the filtering frequency to a significant degree and is neglected here.

B. RF Probe Launch Design

To provide a simple signal launch while avoiding skew, radio frequency (RF) probe launches were placed symmetrically on each side of the PCB, launches on one side connecting to the CPW on that side and launches on the other side connecting to the CPW there. The launch structure consists of 50 Ω CPW RF probe launch pads and a short taper for transmission line impedance matching. Vias are placed to achieve an adequate match. A close-up view of the launch with a 500 µm pitch from pad-to-pad pitch is shown in Fig. 5.

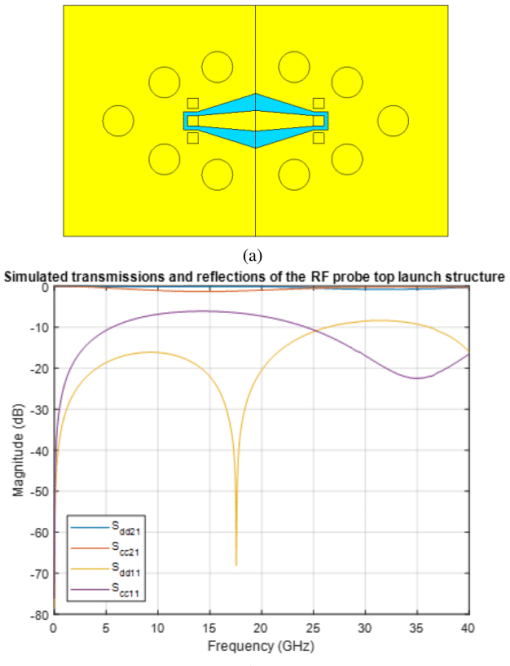

(a)

(b)

Fig. 5. (a). Top view of the RF probe launch THRU model. (b). Simulated transmission and reflection results of this proposed model.

III. MEASUREMENT AND RESULTS

Since the RF launch structure introduced in section 2 is a top launch structure, signal launches exist on both sides of the board for these differential transmission lines. In the following sections, we describe the test setups, illustrated in Figs. 6 and 7, for the PCB together with simulation and measurement results.

A. Measurement Facilities

Measurements were carried out at two facilities. At the first, shown in Fig. 6, two 500 µm GGB RF probes are connected to an Agilent (now Keysight) E8363B 40 GHZ 2-port VNA via 2.92 mm cables. Additional GGB RF probes with 50 Ω broadband loads are connected to unused ports for each 2-port measurement with SOLT calibration performed at the end of the cables.

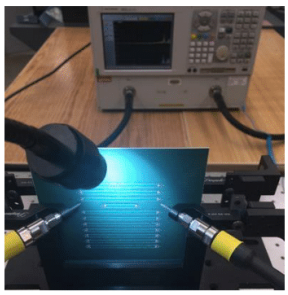

Fig. 6. PCB measurement setup with a 2-port VNA. The broadband 50 Ω loads are on the other side of the test board.

The second measurement facility, shown in Fig. 7, utilizes an Agilent N5242A 4-port 26.5 GHz VNA with 2.92mm cables and GGB RF probes. The same calibration technique is performed before measurements.

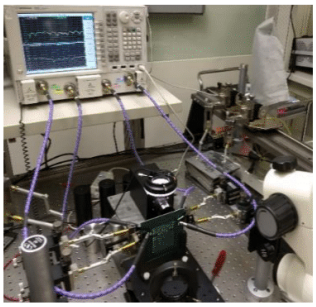

Fig. 7. PCB measurement setup with a 4-port VNA.

B. *Filtering at a Single Frequency*

A differential CPW structure with a single 16 GHz filter element, as described in section 2A, was considered first and was modeled, simulated and measured. Measurement results carried out at two facilities that are mentioned in the previous section are plotted with simulation results in Fig. 8 below. The simulated -10 dB bandwidth is 6.14 GHz and is centered at 15 GHz, demonstrating broadband CM filtering capability.

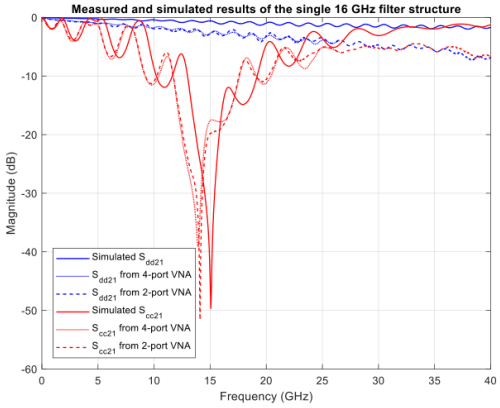

Fig. 8. Measured and simulated transmission results of a differential CPW structure with a single 16 GHz filter.

De-embedding using the auto fixture removal (AFR) technique is available for the 26.5 GHz measurements and is shown in Fig. 9 below [12-13]. This is included here in order to demonstrate that effective DM transmission is available in these differential CPW structures. In fact, the de-embedded DM transmission stays close to the simulation, indicating excellent DM transmission. As shown in Fig. 9, the measured -10 dB bandwidth is 8.13 GHz centered at 13.95 GHz.

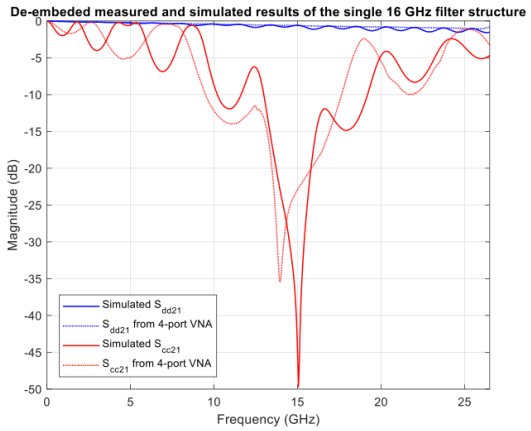

Fig.9. De-embedded measured and simulated results for a single 16 GHz filter (note different freq. range than in Fig. 8).

C. *Filtering at multiple frequencies*

The filters can be also cascaded to filter CM signals at multiple frequencies. A single filter, which can be considered as a half-wavelength resonator, may be viewed as a combination of two quarter-wavelength resonators for the same frequency. Therefore, in addition to cascading structures to filter at multiple frequencies, a single resonator structure can be used to filter at two different frequencies by varying the location of the patch-to-reference stub. Fig. 10a shows a cascade of two symmetric filters to filtering at 16 and 32 GHz, and Fig. 10b shows a single asymmetric filter also designed to filter at 16 and 32 GHz. As Fig. 10 shows, the single asymmetric filter design also requires less space in the filter layer than the cascaded symmetric filters.

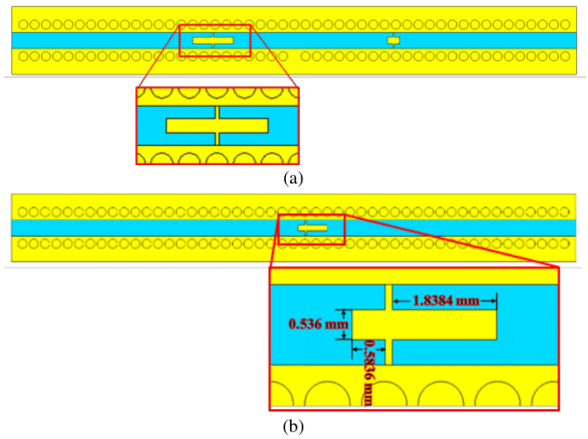

Fig. 10. Filter layer view of (a) symmetric cascaded half-wavelength filters (16 GHz and 32 GHz) with centered stubs, and (b) a single filter with off-centered stub designed for the same target frequencies, where each wing is a quarter-wavelength resonator.

Simulated and measured DM and CM transmission for the structures illustrated in Fig. 10a and 10b are shown in Figs. 11 and 12, respectively. Effective DM transmission is obtained for

both and similar CM filtering performance obtained in the two designs, with modest variation in CM filtering frequencies. For the cascaded symmetric filters, the filtering frequencies are centered at 15.1 GHz and 30.5 GHz in simulation with 10 dB bandwidths of 9.25 GHz and 10.3 GHz, respectively, while the center frequencies obtained in measurement are 14.07 GHz and 28.64 GHz with 10 dB bandwidths of 8.175 GHz and 14.61 GHz. For the single asymmetric filter design, the filtering frequencies are centered at 16.55 GHz and 37.15 GHz in simulation with 10 dB bandwidths of 5.26 GHz and 9.4 GHz, respectively, while the center frequencies obtained in measurement are 15.48 GHz and 35.42 GHz with 10 dB bandwidths of 5.94 GHz and 7.15 GHz. These results show filtering at two frequencies can be obtained by cascading two symmetric filters or by using a single asymmetric filter.

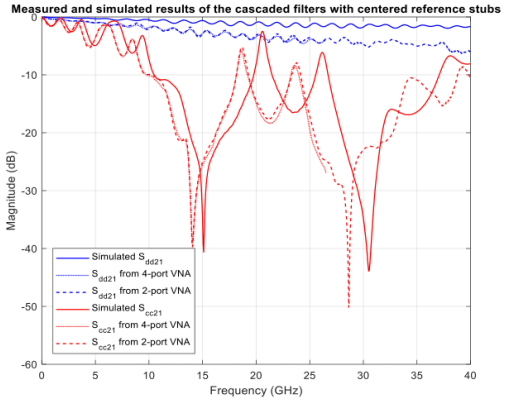

Fig.11. Measured and simulated transmission results for cascaded symmetric filters.

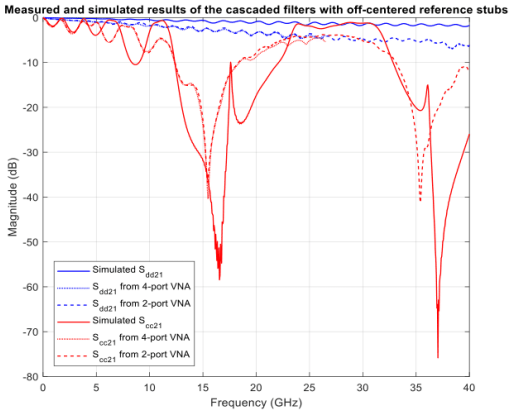

Fig. 12. Measured and simulated transmission results for a single filter with off-center filter-to-reference stub.

D. Registration Study

In multilayer PCB fabrication process, the degree of sensitivity to layer-to-layer misregistration is of vital importance since too high a sensitivity can result in system performance being compromised through manufacturing tolerances. Studies have also observed that misregistration can be a significant source of DM to CM conversion [14]. A registration study using simulated results was conducted to help understand the sensitivity of our structures to misalignment. The distance from the center of the transmission line to the vertical center axis of the board is parameterized as "*reg*" and swept from 0 to 5 mils. With each simulated value of *reg*, both top and bottom signal lines move away from the center in opposite directions. Thus, the actual trace-to-trace misregistration, or reg_{abs}, is twice the value of *reg*, as seen in Fig. 13. The plots in Fig. 14 show that these designs maintain nearly unaltered performance as the trace-to-trace misregistration reaches 10 mils or 0.254 mm.

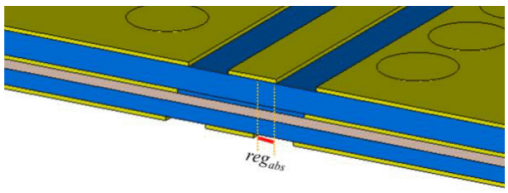

Fig.13. Side view of the differential pair with the trace-to-trace misregistration, reg_{abs}, labeled.

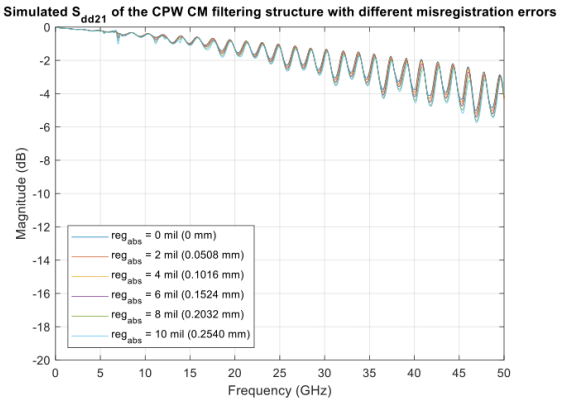

(a)

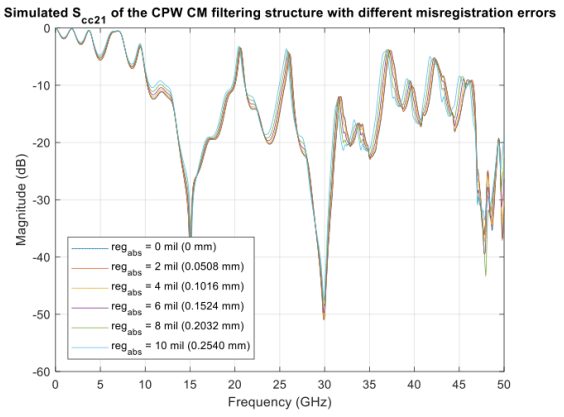

(b)

Fig. 14. Simulated results of the registration study: (a). differential mode signal transmission; (b). common mode signal transmission.

IV. Conclusions

In this work, the use of symmetric and asymmetric resonant structures is employed to offer broadband CM filtering in broadside coupled differential CPW structures. CM filtering is explored through modeling, simulation and measurement with simulated and measured results showing effective DM transmission and CM filtering up to 40 GHz. Design equations are developed to allow filtering structures to be designed where the desired CM filtering frequencies have a clear, physics-based relationship to the structure's dimensions. These filtering structures can be cascaded to filtering at multiple frequencies, or to broaden the frequencies at which filtering occurs.

References

[1] C. P. Wen, "Coplanar Waveguide: A Surface Strip Transmission Line Suitable for Nonreciprocal Gyromagnetic Device Applications," in *IEEE Trans. Microw. Theory Technol.*, vol. 17, no. 12, pp. 1087-1090, Dec 1969.

[2] J. L. B. Walker, "A survey of European activity on coplanar waveguide," 1993 *IEEE MTT-S International Microwave Symposium*, Atlanta, GA, USA, 1993, pp. 693-696 vol.2.

[3] T. Sporkmann, "The evolution of coplanar MMICs over the past 30 years." *Microwave Journal*. vol. 41, nNo. 7, pp. 96-111, July 1998.

[4] J. Coonrod, R. Rautio, "Comparing Microstrip and CPW Performance", *Microwave Journal*, vol. 55, no. 7, pp. 74-82, July 2012.

[5] F. Fesharaki, T. Djerafi, M. Chaker, and Ke Wu, "Low-Loss and Low-Dispersion Transmission Line Over DC-to-THz Spectrum", in *IEEE Trans. on Terahertz Science and Tech.*, vol. 6, no. 4, pp. 611-618, July 2016.

[6] F. Fesharaki, T. Djerafi, M. Chaker and Ke Wu, "Mode-selective transmission line for DC-to-THz super-broadband operation," *2016 IEEE MTT-S International Microwave Symposium, San Francisco, CA, 2016, pp. 1-4.*

[7] J. Naqui, M. Durán-Sindreu and F. Martín, "On the symmetry properties of coplanar waveguides loaded with symmetric resonators: Analysis and potential applications," *2012 IEEE/MTT-S International Microwave Symposium*, Montreal, QC, Canada, 2012, pp. 1-3.

[8] J. Naqui, A. Fernandez-Prieto, M. Duran-Sindreu, F. Mesa, J. Martel, F. Medina, and F. Martin, "Common-Mode Suppression in Microstrip Differential Lines by Means of Complementary Split Ring Resonators: Theory and Applications," *IEEE Trans. Microw. Theory Technol.*, vol. 60, no. 10, pp. 3023-3034, Oct. 2012.

[9] E. Sawyer, C. Kodama, C. O'Daniel, J. Cook and E. Wheeler, "Using common-mode filtering structures with microstrip differential lines in a multilayer printed circuit board environment," 2014 *European Microwave Conference*, Rome, 2014, pp. 1091-1094.

[10] S. G. Kang, G. Shaffer, C. Kodama, C. O'Daniel and E. Wheeler, "CSRR common-mode filtering structures in multilayer printed circuit boards," *2015 IEEE International Symposium on Electromagn. Compat.* (EMC), Dresden, 2015, pp. 1300-1303.

[11] Q. Liu, G. Li, V. Khilkevich and D. Pommerenke, "Common-Mode Filters With Interdigital Fingers for Harmonics Suppression and Lossy Materials for Broadband Suppression," *IEEE Trans. Electromagn. Compat.*, vol. 57, no. 6, pp. 1740-1743, Dec. 2015

[12] Keysight Technologies, Santa Rosa, CA, USA. Auto Fixture Removal (AFR). (2015) [Online]. Available: http://na.support.keysight.com /plts/help/WebHelp/VNACalAndMeas/Auto_Fixture_Removal.htm, Accessed on: Apr. 20, 2018.

[13] Keysight Technologies, Santa Rosa, CA, USA. Auto Fixture Removal (AFR). (2014) [Online]. Available: http://na.support.keysight.com /vna/help/latest/S3_Cals/Auto_Fixture_Removal.htm, Accessed on: Apr. 20, 2018.

[14] L. Shan, Y. Kwark, C. Baks and M. Ritter, "Layer misregistration in PCB and its effects on signal propagation," *2010 Proceedings 60th Electronic Components and Technology Conference* (ECTC), Las Vegas, NV, USA, 2010, pp. 605-611.

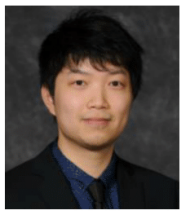

Yujie He received his B.S. in electrical engineering at Rose-Hulman Institute of Technology in 2015. He is currently working toward the M.S. degree in electrical engineering and research on signal integrity and electromagnetic compatibility for high-speed signal transmissions in the Electromagnetics and High-Speed Design Laboratory.

Joseph Faia received his B.S. in electrical engineering at Rose-Hulman Institute of Technology. He started his research as an undergraduate researcher in the Electromagnetics and High-Speed Design Laboratory where he continued to obtain his M.S.E.E in applied electromagnetics, working on topics including common mode filtering, metamaterials, and time-reversal radar.

Michael Cracraft (M'08-SM'17) received the B.S. (summa cum laude), M.S., and Ph.D. degrees in electrical engineering from the University of Missouri–Rolla in 2000, 2002, and 2007, respectively. He received the NSF IGERT fellowship while working with the Electromagnetic Compatibility Laboratory as a graduate student. Since 2007, he has been working in packaging and signal integrity on Z and Power systems for IBM Systems Group in Poughkeepsie, NY. He specializes in high-speed and high-frequency measurements, electromagnetic modeling, and model-to-hardware correlation.

Edward Wheeler (M'95—SM'97) received the M.S. and Ph.D. degrees in electrical engineering from the University of Missouri – Rolla. He is currently professor of electrical and computer engineering at Rose-Hulman Institute of Technology, holds the Lawrence J. Giacoletto Endowed Chair and is a member of the Electromagnetics and High-Speed Design Laboratory.